Regulation of Gene Transfection of Mesenchymal Stem Cells by Micropatterned Surfaces

Yongtao Wang

July 2021

Regulation of Gene Transfection of Mesenchymal Stem Cells by Micropatterned Surfaces

Yongtao Wang

Doctoral Program in Materials Science and Engineering

Submitted to the Graduate School of

Pure and Applied Sciences

in Partial Fulfillment of the Requirements

for the Degree of Doctor of Philosophy in

Engineering

at the

University of Tsukuba

Contents

List of abbreviations

ECM	Extracellular matrix
PEI	Polyethylenimine
AFM	Atomic force microscope
TCPS	Tissue culture polystyrene
DCC	Dicyclohexylcarbodiimide
DMSO	Dimethyl sulfoxide
AzPhPVA	Azidophenyl-derivatized poly(vinyl alcohol)
UV	Ultraviolet
$NaHCO_3$	Sodium bicarbonate
iPSCs	Induced pluripotent stem cells
hMSCs	Human bone marrow-derived mesenchymal stem cells
DMEM	Dulbecco’s modified Eagle’s medium
MSCGM	Mesenchymal Stem Cell Growth Medium BulletKit
BSA	Bovine serum albumin
PBS	Phosphate-buffered saline
FBS	Fetal bovine serum
GFP	Green fluorescence protein
Opti-MEM	Opti-MEM Reduced Serum Medium
pDNA	Plasmid deoxyribonucleic acid
FITC	Fluorescein isothiocyanate
Calcein-AM/PI	Calcein-acetoxymethyl ester/propidium iodide
Cyto D	Cytochalasin D
Bleb	Blebbistatin
BrdU	5-bromo-2'-deoxyuridine
HCl	Hydrogen chloride
FA	Focal adhesion
YAP	Yes-associated protein
TAZ	Transcriptional coactivator with PDZ-binding motif
ATP	Adenosine triphosphate
2D	Two dimension
3D	Three dimension
VSFs	Ventral stress fibers
DSFs	Dorsal stress fibers
TAs	Transverse arcs

Chapter 1

General introduction

1.1 Gene transfection

Gene transfection in mammalian cells is a process that introduces the exogenous genes into targeted cells to produce useful proteins [1-4]. It is a crucial technique to evaluate the desired genes and functional proteins. The exogenous genes are transferred into the cells by stable or transient transfection (Figure 1.1) [5]. Stable transfection is achieved by the integration of exogenous genes into host DNAs in targeted cells, which is called as transgenes [6]. This method can maintain continuous transgene expression in daughter cells. On the other hand, transient transfection cannot combine exogenous genes with host DNAs and may lose the targeted gene expression in the next few generations [7]. Viral-mediated gene carriers can conduct stable transfection due to the easy integration between viruses and host genes, while nonviral-mediated carriers lead to transient transfection [8]. Both transfection methods are available to play the potential role in gene therapy, which depends on the purpose of experiments. Therefore, gene transfection has attracted considerable attention in gene silencing, production of functional proteins and cell reprogramming [9-11].

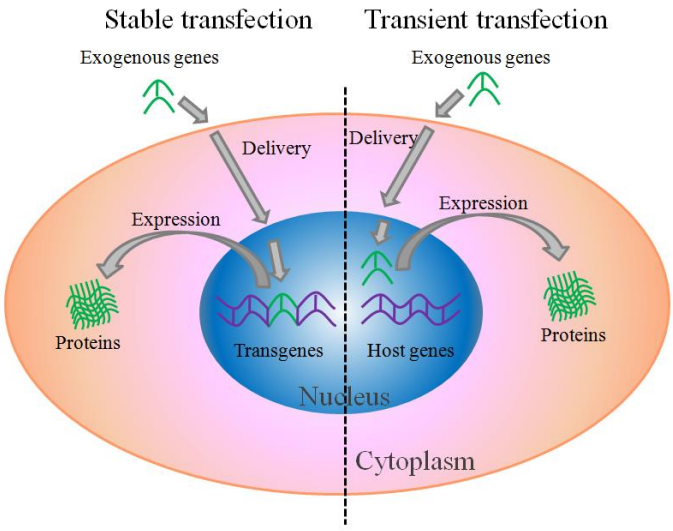

Figure 1.1 Illustration of stable and transient transfection. Exogenous genes (green color) are delivered into cells and express functional proteins by stable and transient gene expression.

1.1.1 Transmembrane delivery of gene transfection

Transmembrane delivery is the crucial procedure for efficient gene transfection. Cell plasma membrane serves as a natural boundary and the significant access to come in and go out in cells [12, 13]. Passive diffusion and active transport are two different internalization pathways to integrate exogenous molecules and particles into cells [14-17]. Small non-polar molecules (O_2, CO_2 and N_2) can cross over cell membrane by direct diffusion through lipid bilayer under the driving force of concentration difference or potential difference, while negative and positive ions go through cell membrane by ion pumps and ion channels, such as sodium/potassium (Na^+/K^+) pump [18]. However, lipids, DNAs, peptides and large particles entry the objected cells depending on the mechanism of energy-mediated endocytosis, such as clathrin, caveolae and macropinocytosis [19-22]. Recently, various methods of transmembrane delivery, which can be categorized in biological, physical and chemical methods, have been designed and developed to increase gene transfection efficiency (Figure 1.2) [5].

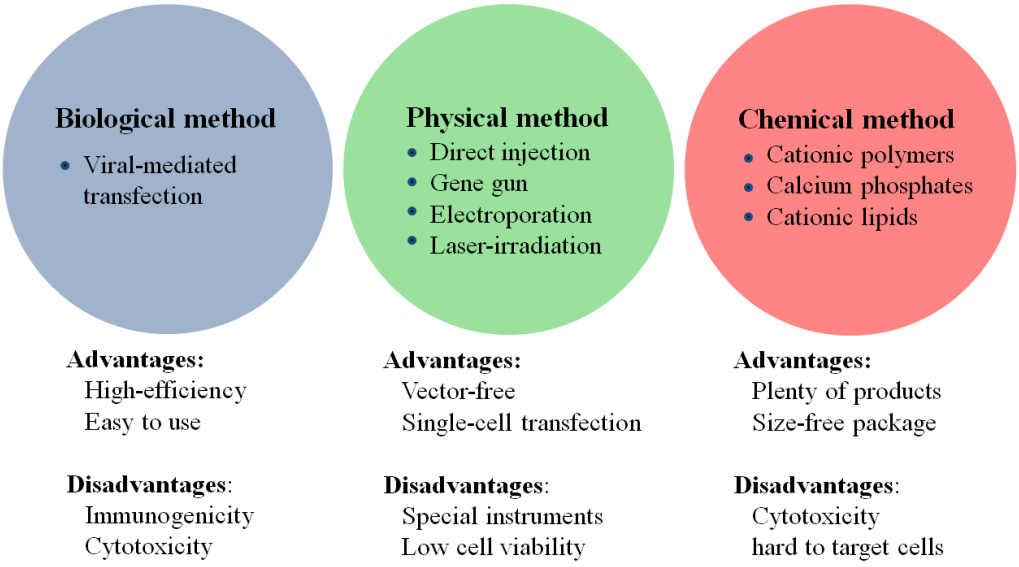

Figure 1.2 Gene transfection methods to deliver exogenous genes into cells. Biological, physical and chemical methods are presented to show the respective advantages and disadvantages.

1.1.1.1 Biological method for gene transfection

Viral-mediated transfection is a highly efficient technology to conduct stable transfection in cells due to the integration of exogenous genes and host DNAs [23-25]. Viral-mediated transfection is also called transduction, which is the most popular technique in clinical application [26]. For example, viral-mediated RNA interference (RNAi) enables local gene knockdown in the brain of adult mice and results in some behavioral changes [27]. A retrovirus carrier of murine leukemia virus is developed to create stable transgene expression in daughter cells [28, 29]. Agrobacterium tumefaciens-mediated transfection can deliver DNA precursors and establish gene amplification in different plant species [30]. Viral carriers may cause a nonspecific inflammatory reaction and inevitable immunogenicity in vivo, and even induce cancer incidence, which has the risk to trigger silent oncogenes [31]. In order to solve these drawbacks, the modified viruses are able to transfer a growth inhibitory or an exogenous gene that is sensitive to immune responses into targeted sick cells [32]. This is a very efficient and safe method against cancers.

1.1.1.2 Physical method for gene transfection

Physical method can directly deliver exogenous genes into the cells by some biophysical tools for efficient gene transfection [33]. These biophysical methods are composed of microinjection, electroporation, sonoporation, gene guns, laser-assisted penetration and so on [34-36]. Exogenous genes directly pass through plasm membrane by disturbing cell membrane [37]. This method can achieve precise gene modification in single-cell level and efficient transfection efficiency. However, it may lead to low cell viability due to the limited integrity of cell membrane [38]. In order to overcome these challenges, various biophysical techniques are designed and improved to enhance cell tolerance and cell activity [39]. Microinjection is one of the most useful methods to enhance gene transfection. An automated micropipette-based quantitative microinjection technology is used to deliver green/red fluorescent materials into human foreskin fibroblast cells [40]. Precise amount and volume of modified mRNA and plasmids are injected into a single cell. Colloidal systems including proteins, nucleic acids, lipids and nanoparticles are also injected into cells for gene therapy [41]. CRISPR/Cas9 gene editing method is combined with physical transfection method to increase gene transfection efficiency [42]. Electroporation is applied to CRISPR/Cas9 genome editing using ssODN (single stranded oligodeoxyribonucleotide) template in human iPSCs (induced pluripotent stem cells) and high homology-directed repair is observed in this system [43]. Gene guns are also used to regulate mitochondria transfection assisted with CRISPR/Cas9 gene editing and it can directly deliver human DNA mutations to the mitochondria by using heavy metal particles [44]. Instead of the gene editing-assisted method, direct sonoporation is used to administer naked plasmid DNA and nanobubbles in the peritoneal mesothelial cells [45]. Laser-assisted penetration is a very simple and convenient method to enhance transmembrane ability. 1064-nm Nd:YAG laser with a 17-nanosecond pulse is used to inject the pEGFP-N1 plasmid into human breast adenocarcinoma cells [46]. The cells present good cell membrane integrity and viability under this laser irradiation.

1.1.1.3 Chemical method for gene transfection

Chemical methods in regulation of gene transfection are the most popular techniques in recent studies [47-49]. The widely used chemical methods mainly include calcium phosphate, cationic polymers, cationic liposomes and their compounds [50]. In principle, exogenous particles are internalized in terms of fusion of plasma membrane and attraction of positive/negative charges in this method [5]. Calcium phosphate as gene vectors is the cheapest chemical method to enhance gene transfection [51]. This method will mix HEPES buffer solution with phosphate and calcium chloride solution with exogenous DNAs to form calcium phosphate complexes containing exogenous DNAs [52]. These nanoparticles are beneficial for cellular uptake. Lipids have the spherical monolayer structure, which can encapsulate exogenous genes. Lipids will fuse with cell plasma membrane to release exogenous genes into cells [53]. Dendrimers (dextran and polyethylenimine) are also used to increase the internalization of cells [54]. DNAs are combined with these cationic dendrimers and attracted on the cell membrane for efficient cell uptake. It is also well-known that gene transfection via cationic-based materials have some advantages, for example, easy DNA condensation, large package size (from 200 nm to 2 μm) and intrinsic endosomal capacity [55, 56]. This method also enables to avoid the problems of viral-based method, such as nonspecific inflammatory reaction and low safety [5]. However, this method usually leads to low gene transfection efficiency and limits transfected cell sources. Therefore, numerous studies have focused on the development of highly efficient cationic carriers and the invention of new cationic transfection techniques to enhance gene transfection efficiency [57].

1.1.2 Expression of exogenous genes in cells

Gene expression as the last process of gene transfection has the decisive influence on successful gene transfection [58]. Exogenous genes cannot directly pass through cell membrane due to size limitation and membrane separation [59]. Viruses can inject exogenous genes into cells by infecting cells and physical methods employ sophisticated equipment to release exogenous genes into cells for gene expression [60, 61]. Comparing with direct injection, endocytosis is an important uptake pathway to deliver exogenous genes [62]. Cellular uptake pathway includes clathrin-mediated, caveolae-mediated endocytosis, macropinocytosis and clathrin/caveolae-independent endocytosis. Intracellular trafficking of exogenous genes in various endocytosis is different to successfully express exogenous genes [63].

Gene expression in clathrin-mediated endocytosis depends on intracellular pH values [64]. First, the ligands of carriers are bonded with receptors of cell membrane to form the stable ligand-receptor complexes. The clathrin-coated pits will invaginate towards cells and then be pulled down from the membrane by intracellular driving force to develop the clathrin-coated vesicles. After the depolymerization of vesicles, the endosomes will form and further fuse with lysosomes. In this process, the pH of endosomes decreases to acidity (pH value ranging from 7 to 6 and further to 5) and low pH leads to the separation of receptors and ligands [65]. Ligands with exogenous genes are transported into different organelles, such as lysosome, Golgi apparatus and nucleus, while the vesicles with receptors return to cell membrane for recycling. Finally, exogenous genes are successfully expressed after transcription and translation (Figure 1.3).

Gene expression in macropinocytosis is related with the formation of heterogeneous macropinosomes, depending on cytoskeletal deformation on cell membrane [66]. This intracellular pathway is different in various cell types. Intracellular trafficking of caveolae refers to the formation of caveolin in cell membrane [67]. Exogenous genes are trapped in the caveolae and then encapsulated into caveosomes. Comparing with clathrin-mediated endocytosis, acid changes and lysosomal degradation were not involved in intracellular trafficking of caveolae [63].

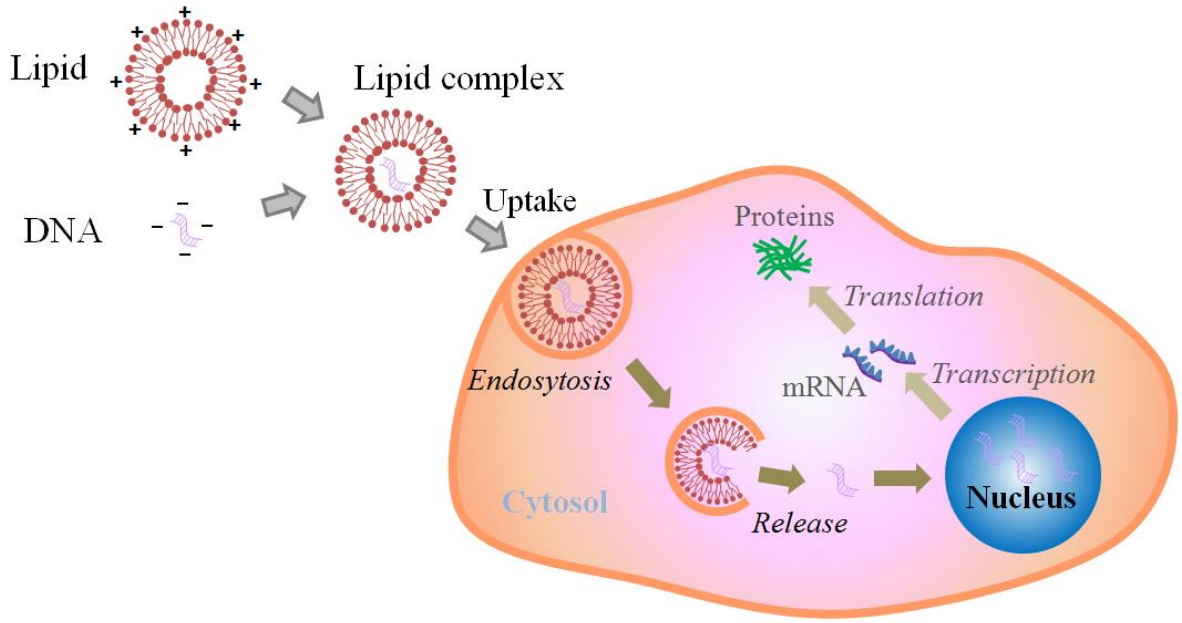

Figure 1.3 Gene expression of clathrin-mediated endocytosis in cells. The lipoplexes are internalized into cells and the exogenous genes are expressed in cells.

1.2 Current factors to regulate gene transfection

The controlled delivery of exogenous genes into the targeted cells or sick sites and highly efficient expression in cells are two important requirements to establish successful gene transfection [68]. The changes of some factors will influence gene transfection efficiency. Current factors, including different cell lines, various gene carrier materials and cellular microenvironment can affect cell uptake and gene expression to regulate gene transfection [69-71].

1.2.1 Different cell lines

Gene transfection can be affected by different cell lines, including somatic cells, stem cells, cancer cells and immune cells (Figure 1.4). Previous studies have reported that Chinese hamster ovary cells (CHO) and human embryonic kidney cells (HEK 293) are two predominant host cell lines for efficient gene transfection in clinical evaluation [72, 73]. These cell lines have the important ability to produce recombinant proteins in transient or stable expression [74]. Murine fibroblastic NIH 3T3 cells and neurons can be used to regulate gene transfection [73, 75]. Besides somatic cells, stem cells also play a very important role in regulating gene transfection. Mesenchymal stem cells (MSCs) are transfected to investigate gene transfection efficiency [76]. Although MSCs have low transfection efficiency, they have attracted considerable attention in gene therapy due to the ability to migrate into targeted sick sites [77]. In addition, gene transfection is conducted in different cancer cells, such as HeLa cells. HeLa is the most popular cell line in the regulation of gene transfection for cancer therapy [78]. In order to enhance the check-point ability of immune cells, exogenous genes are transferred into immune cells to identify the damaged and mutational cells [79]. This strategy is considered as an ideal method to treat most diseases, such as dysfunctional or dead cells, mutants, cancer cells. Dendritic cells (DCs) are transfected with CL22-DNA complexes including TAAs-encoded (tumor-associated antigens) genes for melanoma immunotherapy [80]. Autologous T cells are successfully activated with CL22-DNA (TAAs genes) DC cells to present the special antigen marker ($CD8^+$). Mesoporous silica microrods (MSRs) are developed to enhance the potency and immunogenicity of exogenous genes in DC cells [81]. The MSR scaffolds can stimulate antigen-specific $CD8^+$ T cell response. Therefore, exogenous genes are transferred into different cell lines for efficient gene transfection and gene therapy.

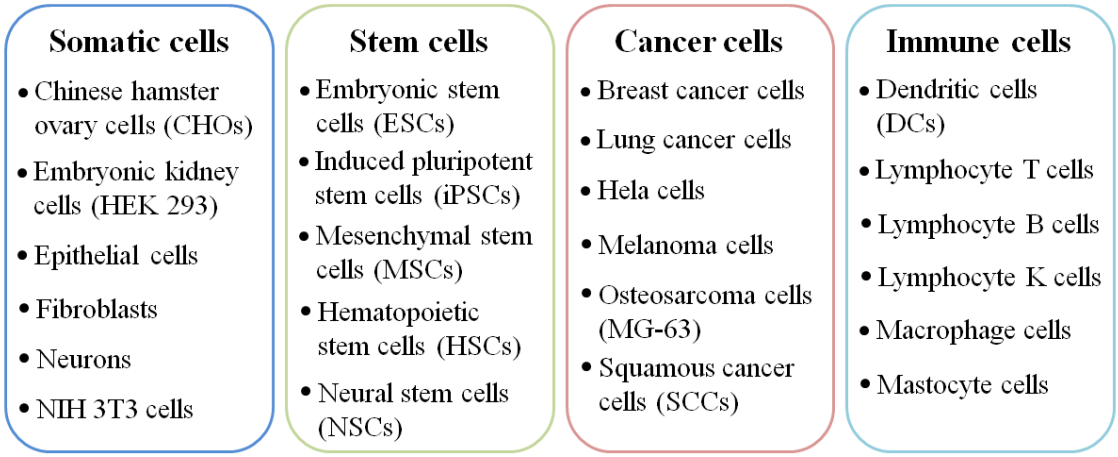

Figure 1.4 Cell lines used for gene transfection, including somatic cells, stem cells, cancer cells and immune cells.

1.2.2 Various gene carrier materials

Gene carrier materials play the crucial role in regulating gene transfection [82]. Various gene carrier materials have been well developed in recent years [83]. Gene carriers include viruses, cationic lipids (liposome DOTAP, DOPE and lipoplex), peptides and cationic polymers (PEI and polyplex) (Figure 1.5) [84-86]. Virus-based carriers are the most efficient gene carrier for gene transfection [87]. However, viruses are difficult to widely use in gene therapy due to low safety. Non-virus carriers have already become the most popular materials for applications in gene transfection [88]. Some current efforts about cationic-based materials are made for efficient gene transfection [89]. Cationic-modified fluorinated-core nano-micelles, polyethylenimine (PEI) and polymeric dendrimers have the advantages of strong DNA-binding ability and high internalization of exogenous genes [90, 91]. Cationic liposomes can enhance gene transfection efficiency by changing the nitrogen-phosphate ratio, liposome amount and surface potential difference [92]. Besides these cationic polymers and lipids, calcium phosphate and cationic amino acid are also good strategies to increase cellular uptake capacity in this method [93, 94].

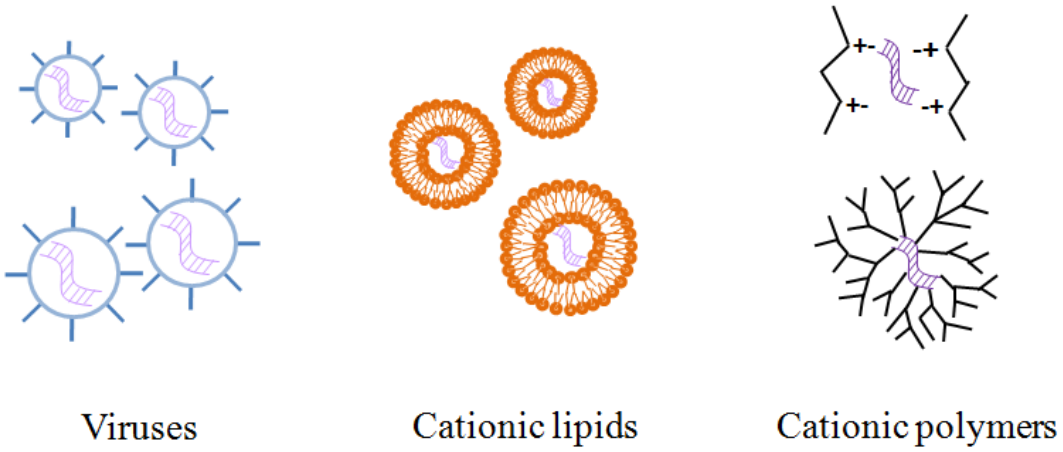

Figure 1.5 Various gene carrier materials including viruses, cationic lipids and cationic polymers.

1.2.3 Cellular microenvironment

Besides cell lines and gene carrier materials, cellular microenvironment also has a very important influence in regulating gene transfection [95]. Some components including biochemical components (ECM components, growth factors, O_2 concentration, nutrients, functional proteins and molecular cytokines) and biophysical components (cell mechanics and cell morphology) are important factors to affect cell functions, including cell adhesion, spreading, migration, fate and uptake [96-98]. Therefore, these factors also have a profound influence on gene transfection.

Biochemical components are reported to regulate cellular internalization of exogenous particles and gene transfection [99]. These factors mainly depend on different cell types and changes of chemical compositions [95]. ECM protein (collagen type *I*) is micropatterned on a glass substrate to regulate gene transfection of both HEK 293T and HepG2 cells [100]. After gene transfection with pmaxGFP plasmid vector, gene transfection efficiency is over 90%. The results show that ECM components can promote gene transfection. Oxygen plays a very important role in regulating cell functions. For example, when cells are in a state of hypoxia, cellular responses and cell-cell interactions (nutrients and biological cytokines) are

changed to adapt to the new environment [101]. Growth factors serve as the vital role for efficient gene transfection. It has been reported that hepatocyte growth factor (HGF) is beneficial for pulmonary emphysema by gene transfection with HGF in rats [102]. Therefore, these chemical factors can affect gene transfection *in vitro* and *in vivo*.

In order to investigate the influence of extracellular biophysical factors on gene transfection, substrate stiffness and cellular topography are varied to disclose the relationship between these factors and gene transfection [103-105]. Mechanical properties (viscosity and rigidity) have been studied to affect DNA uptake and gene transfection [106, 107]. High elastic moduli (110 kPa) present higher gene transfection efficiency than lower moduli (20 kPa) on cell-adhesive hydrogels [108]. Nano- to microtopographical patterns are also prepared to control cellular nanotopography. MSCs and COS7 cells are transfected with GFP-encoding plasmid to investigate the influence of cellular topography on gene transfection. These studies show that substrate mechanics and topography can affect gene transfection.

Cell morphology has been reported to regulate cell functions, such as cell spreading, migration, fate and uptake [109]. Micropatterns with larger sizes and elongation can enhance cellular uptake of gold nanoparticles and DNA synthesis activity [110, 111]. Some studies also disclose the influence of cell morphology on gene transfection [112-114]. For example, micropatterns with the 80-μm diameter and an 8:1 aspect ratio will increase transfection efficiency of exogenous genes in micropatterned hMSCs [115]. Microscale pitted surfaces (size, spacing and arrangement from 1 to 6 μm) are used to enhance gene transfection efficiency of normal human dermal fibroblasts [116]. Not only micropatterns, but also nanopatterns and their combination have been fabricated and used for gene transfection [117, 118]. Nano-groove structures (nanogroove width and height) are found to affect gene transfection efficiency of human lung fibroblasts [119]. A combination of 2-μm micropillars and 200-nm nanopillars is used to control cell morphology and this structure can enhance cell uptake capacity of fluorescence-labeled dextran in different cell lines (hMSCs and COS7 cells) [118]. Furthermore, biomolecules are adsorbed in the vertical alignment of nanostructures to investigate their influence on gene transfection [120]. Gene carriers are encapsulated in the hollow nanotubes to inject exogenous genes into cells for efficient gene transfection. These studies show that gene transfection can be affected by cell morphology. The reason is the reorganization of cytoskeletal structures in different cell morphologies, which can regulate cellular mechanics and may provide the driving force for endocytosis of exogenous genes (Figure 1.6) [121].

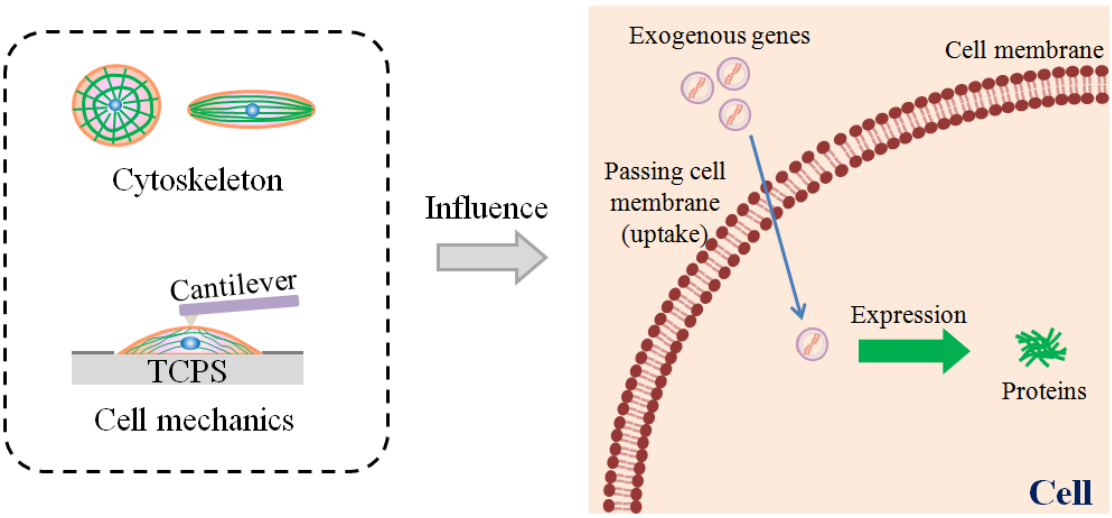

Figure 1.6 Reorganization of cytoskeletal structures and cell mechanics and their relationship with gene transfection.

1.3 Micropatterning strategies for gene transfection

Micropatterning techniques provide a feasible strategy for controlling cell morphology to investigate the influence of cell morphology on gene transfection [122]. These techniques include contact printing, photolithography, plasma treatment, laser ablation, electrospinning and stencil-assisted techniques [123]. Further, some studies have combined these methods together to precisely manipulate micro and nanoscale cell behaviors in cell biology [124].

1.3.1 Micropatterning methods

1.3.1.1 Contact printing technique

The establishment of non-fouling inks is the fundamental basis of contact printing technique to eliminate the non-specific interaction between protein-resistance surfaces and related biomolecules [125]. At first, biochemists find that some native molecules including agarose, albumin and mannitol show the ability to reduce the adsorption and aggregation of proteins on these surfaces [123]. However, for native molecules, the ability to resist proteins has limited efficiency and stability [126]. In order to solve these problems, a lot of synthetic polymers have been exploited rapidly. In particular, poly(ethylene glycol) (PEG) and PEG derivatives, such as poly-L-lysine-polyethylene glycol (PLL-g-PEG), PEG-polyphenylene oxiole (PPO)-PEG, poly(propylene sulfide (PPS)-PEG and PEG-diacrylate (DA), are the most popular biomaterials for anti-protein adsorption on surfaces [127, 128]. In addition, the stamps with desired geometric features are another key factor for contact printing method. For example, the micropatterns are fabricated by using polydimethylsiloxane (PDMS) elastomeric stamps and self-assembly monolayers (SAMs) (Figure 1.7) [129]. Fibronectin or octadecanethiol-coated PDMS stamp is placed onto tissue culture dishes or Au glass slides and then incubated in the non-adhesion SAMs of PLL-g-PEG or ethylene glycol-terminated material [130].

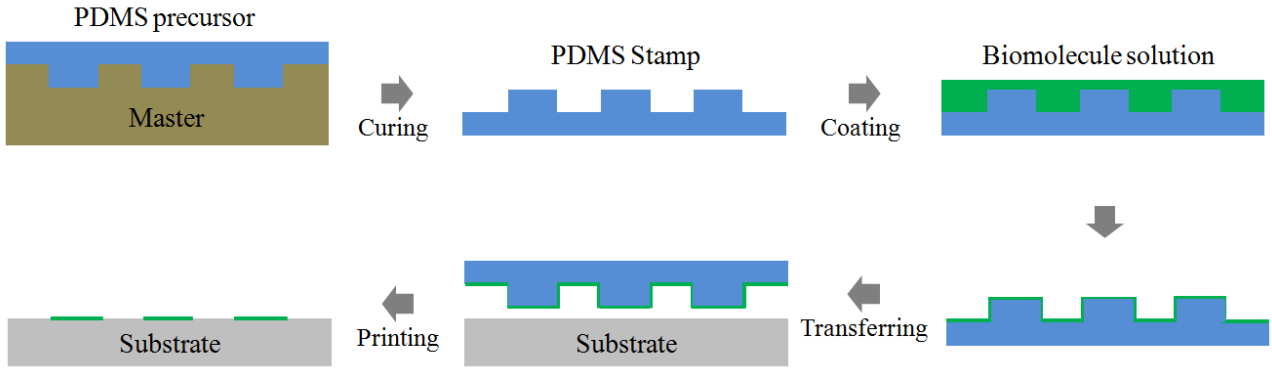

Figure 1.7 Illustration of contact printing process to prepare the micropatterns on substrate.

1.3.1.2 Photolithography technique

A photomask (glass and quartz) with designed geometric features is needed to produce various micropatterns for cell culture in photolithography process (Figure 1.8) [123]. Prior to transferring the geometric features of the photomask, UV sensitive materials (photo-reactive or photo-inert polymers) are coated on surfaces to form a thin layer with a thickness ranging from nano to micro meters. The photomask

is tightly placed onto the surfaces with photo-sensitive polymers. After UV irradiation, the desired micropatterns of photomasks are successfully delivered onto the coated surfaces. As previously reported, azidophenyl-derived photo-reactive poly(vinyl alcohol) (AzPhPVA) is synthesized and coated on the tissue culture polystyrene (TCPS) plates with a nanoscale thin layer for cell culture [131]. Micropatterns with different sizes, shapes and elongations are prepared by photolithography to regulate cell adhesion and spreading, proliferation, differentiation and uptake [132-134]. Furthermore, a thin layer of gold is sputtered onto the surfaces and then immersed in a solution of c(-RGDfK)-thiol peptide to modify arginine-glycine-aspartate (RGD) on the gold microstripes [135]. These microstripes can guide various cellular motilities in different cell lines.

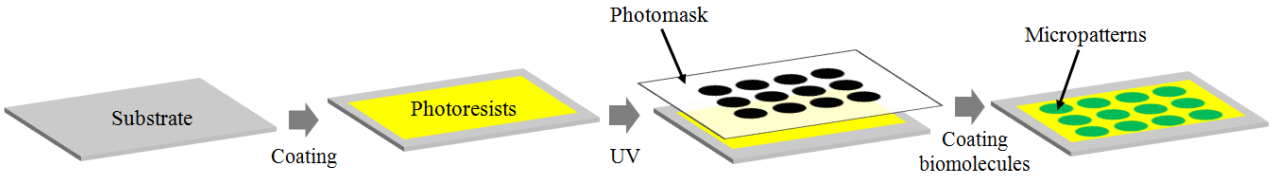

Figure 1.8 Illustration of photolithography process to prepare the micropatterns on substrates.

1.3.2 Application of micropatterning methods in gene transfection

Cells can interact with surrounding matrixes to sense extracellular stimuli [136]. The biophysical cues can affect cell functions. Micropatterning techniques are applied to investigate the relationship between physical cues and cell behaviors, such as endocytosis [137]. The influence of cell morphology and surface topography on exogenous gene transfection has been reported through micropatterning techniques. Micropatterns are prepared by photolithography to control cell size and aspect ratio [115]. The micropatterned cells are transfected to disclose the influence of cell morphology on gene transfection. Miniaturized droplet microarrays are occupied to enhance high-throughput screening of gene transfection in HEK293T cells [138]. Nanotextured silicon substrates are fabricated by electron beam lithography to regulate cytoskeletal structures and nuclear deformation. PEI-mediated gene transfection of skeletal myoblasts (C2C12 cell lines) is modulated [117]. Cell membrane curvature is manipulated by different structures using the same method [139]. Clathrin-mediated endocytosis is probed in living cells. Furthermore, carbon nanotube arrays are used to enhance gene transfection of tetramethylrhodamine (dextran) and quantum dots in HEK293 cells [120]. Therefore, Cell morphology can be controlled on the topographical surfaces and gene transfection is regulated by cell morphology.

1.4 Motivation, objectives and outline

1.4.1 Motivation

Gene transfection has become an urgently desired approach in science research and clinical application because of the increasing incidence of various gene-related diseases, such as mutants, genetic silencing and cancers [140-144]. Efficient delivery of exogenous genes into the dysfunctional cells and high expression level of exogenous genes in these cells are two vital proceedings to achieve the prosperous gene transfection [145, 146]. Because DNA chains possess the negative charges due to the existence of phosphate group,

naked DNA permeation through negatively charged cell membrane remains a great challenge [147]. Therefore, many cationic synthesized carriers including polyethylenimine (PEI), dendrimers, peptides and lipids have been rapidly developed to enhance gene transfection efficiency in recent years [148-152]. Comparing with viral-mediated vectors, cationically functionalized carriers present the typical characteristics of low immunogenicity and relative safety [153]. In addition, simple preparation, easy modification and high genetic loading capacity are extra advantages for these cationic carriers [154]. Nevertheless, cationic-carrier-mediated transfection is always accompanied with low gene transfection efficiency and limited cell types [147]. Currently, most efforts are concentrated to exploit novel polymeric carriers and transfection techniques.

Not only gene carriers and transfection methods, but also cellular morphology can affect the transfection of exogenous genes [115]. Cells show various morphologies that are dependent on the adhesion matrix and substrate [155]. Interaction between cells and the microenvironment is critical for the maintenance of cell activity and tissue metabolism [156]. Biological and physicochemical cues from the microenvironment provide various necessary signals to induce cellular responses [157]. In particular, physical cues, such as matrix viscoelasticity and cell morphology, have recently been found to play a crucial role in controlling cell functions [158]. Cells in tissues present various densities and morphologies to adapt to the microenvironment. Cell density, cell-cell interaction, cell size, cell geometry, cell elongation, cell adhesion/spreading area and cell chirality have been shown to regulate cell functions, including cell adhesion, migration, division, matrix secretion and differentiation [159-161]. These factors and cellular physical cues can be controlled through a variety of micropattern structures. Cells with different morphologies respond to microenvironmental signals by reorganizing their cytoskeletal structures and transducing the signals to the nucleus. The morphological features of cells not only directly affect cell functions but also have some influence on the uptake of extracellular vesicles and nanoparticles [110]. However, the influence of various cell morphologies on gene transfection remains unclear.

1.4.2 Objectives and outline

In this study, the photoreactive poly(vinyl alcohol) (PVA) was synthesized by introducing the azidophenyl group of 4-azidobenzoic acid into PVA. Micropatterns were prepared by micropatterning the photoreactive PVA through photolithography on TCPS surfaces. The prepared micropatterns were used to control stem cell morphology, including different cell density, cell size, cell shape, cell elongation, cell interaction, cell adhesion/spreading area and cell chirality. The influence of cell density and cell morphology on exogenous gene transfection of micropatterned hMSCs was investigated by transferring plasmid DNA (pAcGFP1-N1) into the hMSCs. The detailed outlines are listed as follows.

Chapter 2 describes the influence of cell density on gene transfection. The photoreactive PVA was synthesized to prepare the micropatterned surfaces. The micropatterned surfaces were used to control cell density. The hMSCs were cultured on the micropatterned surfaces and cell nuclei were stained to calculate cell density. Gene transfection efficiency increased with cell density at the low cell densities and decreased when cell density further increased. The different influence of cell density was correlated with its influence on cellular uptake capacity and DNA synthesis activity. Insufficient cell-cell interaction at a low cell density and too strong cell-cell interaction at a high cell density was not preferable for gene transfection. A moderate cell density had appropriate cell-cell interaction to facilitate gene transfection.

Chapter 3 describes the influence of cell size, shape and elongation on gene transfection of hMSCs. PVA-micropatterned surfaces were prepared and coated with fibronectin solution to precisely manipulate the size, shape and elongation of hMSCs. The influences of these factors on gene transfection were investigated on the micropatterns. Gene transfection was enhanced with increasing cell size and elongation, but not

affected by cell shape. Cytoskeletal structures played critical roles in regulating cellular uptake and the intercellular trafficking of exogenous genes. Cells with a large size and elongated morphology showed well-organized actin filaments with a high cellular modulus, therefore promoting cellular nanoparticle uptake, DNA synthesis and gene transfection.

Chapter 4 describes the influence of cell adhesion and spreading area on gene transfection. The hMSCs were seeded on the fibronectin-coated micropatterns to separately control cell adhesion and spreading area. Focal adhesion (FA) formation of hMSCs was confirmed for the cells cultured on all the micropatterns. The cells having large adhesion area assembled fiber-like FAs, while those having small adhesion area had little influence on FAs organization even though the cells had large spreading area. The cells with larger adhesion area showed higher transfection efficiency, while cell spreading area hardly affected gene transfection efficiency. The different influence of cell adhesion and spreading area was correlated with their influence on cellular uptake capacity, DNA synthesis, focal adhesion formation, cytoskeletal mechanics and mechano-signal activation.

Chapter 5 describes the influence of cell chirality and swirling angles on gene transfection. The micropatterns were coated with fibronectin solution to enhance cell attachment. The hMSCs adhered to the micropatterns and spread along the micropatterns. The chiral micropatterns induced the formation of chiral focal adhesions, chiral cytoskeletal structures and cell mechanics. Gene transfection was enhanced with increasing adhesion area, while hMSCs on left-handed and right-handed swirling micropatterns showed the same level. When swirling angle was changed from 0°, 30°, and 60° to 90°, gene transfection efficiency at a swirling angle of 60° was the lowest. After disturbance of actin filaments, transfection efficiency showed the same level in all micropatterned cells. Gene transfection was related with cytoskeletal structures.

Chapter 6 describes the conclusions of this dissertation.

1.5 References

[1] N. S. Orefice, Development of new strategies using extracellular vesicles loaded with exogenous nucleic acid, Pharmaceutics 12(8) (2020) 705.

[2] T. Frei, F. Cella, F. Tedeschi, J. Gutiérrez, G. B. Stan, M. Khammash, V. Siciliano, Characterization and mitigation of gene expression burden in mammalian cells, Nature Communications 11 (2020) 4641.

[3] A. Tay, The benefits of going small: nanostructures for mammalian cell transfection, ACS Nano 14(7) (2020) 7714-7721.

[4] S. Yamano, J. Dai, A. M. Moursi, Comparison of transfection efficiency of nonviral gene transfer reagents, Molecular Biotechnology 46 (2010) 287-300.

[5] T. K. Kim, J. H. Eberwine, Mammalian cell transfection: the present and the future, Analytical and Bioanalytical Chemistry 397 (2010) 3173-3178.

[6] D. J. Glover, H. J. Lipps, D. A. Jans, Towards safe, non-viral therapeutic gene expression in humans, Nature Reviews Genetics 6(4) (2005) 299-310.

[7] R. T. Félix, Multiple strategies for gene transfer, expression, knockdown, and chromatin influence in mammalian cell lines and transgenic animals, Molecular Biotechnology volume 34 (2006) 337-354.

[8] F. M. Wurm, Production of recombinant protein therapeutics in cultivated mammalian cells, Nature Biotechnology 22 (2004) 1393-1398

[9] D. Vetvicka, L. Sivak, C. M. Jogdeo, R. Kumar, R. Khan, Y. Hang, D. Oupický, Gene silencing delivery systems for the treatment of pancreatic cancer: where and what to target next? Journal of Controlled Release 331 (2021) 246-259.

[10] A. K. Patel, J. C. Kaczmarek, S. Bose, K. J. Kauffman, F. Mir, M. W. Heartlein, F. DeRosa, R. Langer, D. G. Anderson, Inhaled nanoformulated mRNA polyplexes for protein production in lung epithelium, Advanced Materials 31(8) (2019) 1805116.
[11] L. Warren, C. Lin, mRNA-based genetic reprogramming, Molecular Therapy 27(4) (2019) 729-734.
[12] G. J. Doherty, H. T. McMahon, Mechanisms of endocytosis, Annual Review of Biochemistry 78 (2009) 857-902.
[13] J. M. Besterman, R. B. Low, Endocytosis: a review of mechanisms and plasma membrane dynamics, Biochemical Journal 210(1) (1983) 1-13.
[14] I. Neri, N. Kern, A. Parmeggiani, Modeling cytoskeletal traffic: an interplay between passive diffusion and active transport, Physical Review Letters 110 (2013) 098102.
[15] K. Sugano, M. Kansy, P. Artursson, A. Avdeef, S. Bendels, L. Di, G. F. Ecker, B. Faller, H. Fischer, G. Gerebtzoff, H. Lennernaes, F. Senner, Coexistence of passive and carrier-mediated processes in drug transport, Nature Reviews Drug Discovery 9 (2010) 597-614.
[16] M. Drechsler, F. Giavazzi, R. Cerbino, I. M. Palacios, Active diffusion and advection in drosophila oocytes result from the interplay of actin and microtubules, Nature Communications 8 (2017) 1520.
[17] M. Mittasch, P. Gross, M. Nestler, A. W. Fritsch, C. Iserman, M. Kar, M. Munder, A. Voigt, S. Alberti, S. W. Grill, M. Kreysing, Non-invasive perturbations of intracellular flow reveal physical principles of cell organization, Nature Cell Biology 20 (2018) 344-351.
[18] T. M. Fyles, Synthetic ion channels in bilayer membranes, Chemical Society Reviews 36 (2007) 335-347.
[19] E. Yuba, Y. Nakajima, K. Tsukamoto, S. Iwashita, C. Kojima, A. Harada, K. Kono, Effect of unsaturated alkyl chains on transfection activity of poly(amidoamine) dendron-bearing lipids, Journal of Controlled Release 160(3) (2012) 552-560.
[20] S. Huang, J. Li, L. Han, S. Liu, H. Ma, R. Huang, C. Jiang, Dual targeting effect of Angiopep-2-modified, DNA-loaded nanoparticles for glioma, Biomaterials 32(28) (2011) 6832-6838.
[21] K. Sandvig, S. Pust, T. Skotland, B. Deurs, Clathrin-independent endocytosis: mechanisms and function, Current Opinion in Cell Biology 23(4) (2011) 413-420.
[22] J. S. Wadia, R. V. Stan, S. F. Dowdy, Transducible TAT-HA fusogenic peptide enhances escape of TAT-fusion proteins after lipid raft macropinocytosis, Nature Medicine 10 (2004) 310-315.
[23] W. A. Carlezon Jr., V. A. Boundy, C. N. Haile, S. B. Lane, R. G. Kalb, R. L. Neve, E. J. Nestler, Sensitization to morphine induced by viral-mediated gene transfer, Science 277(5327) (1997) 812-815.
[24] G. L. Odom, P. Gregorevic, J. S. Chamberlain, Viral-mediated gene therapy for the muscular dystrophies: successes, limitations and recent advances, Biochimica et Biophysica Acta-Molecular Basis of Disease 1772(2) (2007) 243-262.
[25] P. D. Robbins, S. C. Ghivizzani, Viral vectors for gene therapy, Pharmacology & Therapeutics 80(1) (1998) 35-47.
[26] A. Pfeifer, I. M. Verma, Gene therapy: promises and problems, Annual Review of Genomics and Human Genetics 2 (2001) 177-211.
[27] J. D. Hommel, R. M. Sears, D. Georgescu, D. L. Simmons, R. J. D. Leone, Local gene knockdown in the brain using viral-mediated RNA interference, Nature Medicine 9 (2003) 1539-1544.
[28] S. H. B. Abina, F. L. Deist, F. Carlier, C. Bouneaud, C. Hue, J. P. D. Villartay, A. J. Thrasher, N. Wulffraat, R. Sorensen, S. D. Girod, A. Fischer, E. G. Davies, W. Kuis, L. Leiva, M. C. Calvo, Sustained correction of X-linked severe combined immunodeficiency by ex vivo gene therapy, The New England Journal of Medicine 346 (2002) 1185-1193.
[29] J. Roesler, S. Brenner, A. A. Bukovsky, N. W. Theobald, T. Dull, M. Kelly, C. I. Civin, H. L. Malech,

Third-generation, self-inactivating gp91phoxlentivector corrects the oxidase defect in NOD/SCID mouse-repopulating peripheral blood-mobilized CD34+ cells from patients with X-linked chronic granulomatous disease, Blood 100(13) (2002) 4381-4390.
[30] S. Marillonnet, C. Thoeringer, R. Kandzia, V. Klimyuk, Y. Gleba, Systemic agrobacterium tumefaciens-mediated transfection of viral replicons for efficient transient expression in plants, Nature Biotechnology 23 (2005) 718-723.
[31] L. Boto, Horizontal gene transfer in evolution: facts and challenges, Proceedings of the Royal Society 277(1683) (2021) 819-827.
[32] D. R. Wilson, Viral-mediated gene transfer for cancer treatment, Current Pharmaceutical Biotechnology 3(2) (2002) 151-164.
[33] J. M. Escoffre, J. Teissié, M. P. Rols, Gene transfer: how can the biological barriers be overcome? The Journal of Membrane Biology 236 (2010) 61-74.
[34] S. M. Humbert, R. H. Guy, Physical methods for gene transfer: improving the kinetics of gene delivery into cells, Advanced Drug Delivery Reviews 57(5) (2005) 733-753.
[35] Z. Fei, S. Wang, Y. Xie, B. E. Henslee, C. G. Koh, L. J. Lee, Gene transfection of mammalian cells using membrane sandwich electroporation, Analytical Chemistry 79(15) (2007) 5719-5722.
[36] L. B. Feril Jr., R. Ogawa, K. Tachibana, T. Kondo, Optimized ultrasound-mediated gene transfection in cancer cells, Cancer Science 97(10) (2006) 1111-1114.
[37] T. Nozaki, R. Ogawa, L. B. Feril Jr., G. Kagiya, H. Fuse, T. Kondo, Enhancement of ultrasound-mediated gene transfection by membrane modification, The Journal of Gene Medicine 5(12) (2003) 1046-1055.
[38] T. Azzam, A. J. Domb, Current developments in gene transfection agents, Current Drug Delivery 1 (2004) 165-193.
[39] X. Du, J. Wang, Q. Zhou, L. Zhang, S. Wang, Z. Zhang, C. Yao, Advanced physical techniques for gene delivery based on membrane perforation, Drug Delivery 25(1) (2018) 1516-1525.
[40] Y. T. Chow, S. Chen, R. Wang, C. Liu, C. Kong, R. A. Li, S. H. Cheng, D. Sun, Single cell transfection through precise microinjection with quantitatively controlled injection volumes, Scientific Reports 6 (2016) 24127.
[41] P. Tiefenboeck, J. A. Kim, J. C. Leroux, Intracellular delivery of colloids: past and future contributions from microinjection, Advanced Drug Delivery Reviews 132 (2018) 3-15.
[42] A. K. Fajrial, Q. Q. He, N. I. Wirusanti, J. E. Slansky, X. Ding, A review of emerging physical transfection methods for CRISPR/Cas9-mediated gene editing, Theranostics 10(12) (2020) 5532-5549.
[43] X. Xu, D. Gao, P. Wang, J. Chen, J. Ruan, J. Xu, X. Xia, Efficient homology-directed gene editing by CRISPR/Cas9 in human stem and primary cells using tube electroporation, Scientific Reports 8 (2018) 11649.
[44] M. A. Sazonova, A. I. Ryzhkova, V. V. Sinyov, M. D. Sazonova, Z. B. Khasanova, N. A. Nikitina, V. P. Karagodin, A. N. Orekhov, I. A. Sobenin, Creation of cultures containing mutations linked with cardiovascular diseases using transfection and genome editing, Current Pharmaceutical Design 25(6) (2019) 693-699.
[45] K. Nishimura, K. Yonezawa, S. Fumoto, Y. Miura, M. Hagimori, K. Nishida, S. Kawakami, Application of direct sonoporation from a defined surface area of the peritoneum: evaluation of transfection characteristics in mice, Pharmaceutics 11(5) (2019) 244.
[46] S. K. Mohanty, M. Sharma, P. K. Gupta, Laser-assisted microinjection into targeted animal cells, Biotechnology Letters 25 (2003) 895-899.
[47] L. Jin, X. Zeng, M. Liu, Y. Deng, N. He, Current progress in gene delivery technology based on

chemical methods and nano-carriers, Theranostics 4(3) (2014) 240-255.
[48] A. Hamm, N. Krott, I. Breibach, R. Blindt, A. K. Bosserhoff, Efficient transfection method for primary cells, Tissue Engineering 8(2) (2002) 235-245.
[49] M. Jinno, Y. Ikeda, H. Motomura, Y. Kido, S. Satoh, Investigation of plasma induced electrical and chemical factors and their contribution processes to plasma gene transfection, Archives of Biochemistry and Biophysics 605 (2016) 59-66.
[50] Z. X. Chong, S. K. Yeap, W. Y. Ho, Transfection types, methods and strategies: a technical review, PeerJ 9 (2021) e11165.
[51] V. V. Sokolova, I. Radtke, R. Heumann, M. Epple, Effective transfection of cells with multi-shell calcium phosphate-DNA nanoparticles, Biomaterials 27(16) (2006) 3147-3153.
[52] A. Kovtun, R. Heumann, M. Epple, Calcium phosphate nanoparticles for the transfection of cells, Bio-Medical Materials and Engineering 19(2-3) (2009) 241-247.
[53] B. Ruozi, F. Forni, R. Battini, M. A. Vandelli, Cationic liposomes for gene transfection, Journal of Drug Targeting 11(7) (2003) 407-414.
[54] C. Dufès, I. F. Uchegbu, A. G. Schätzlein, Dendrimers in gene delivery, Advanced Drug Delivery Reviews 57(15) (2005) 2177-2202.
[55] T. Montier, T. Benvegnu, P. A. Jaffres, J. J. Yaouanc, P. Lehn, Progress in cationic lipid-mediated gene transfection: a series of bio- inspired lipids as an example, Current Gene Therapy 8(5) (2008) 296-312.
[56] B. Ma, S. Zhang, H. Jiang, B. Zhao, H. Lv, Lipoplex morphologies and their influences on transfection efficiency in gene delivery, Journal of Controlled Release 123(3) (2007) 184-194.
[57] S. Chernousova, M. Epple, Live-cell imaging to compare the transfection and gene silencing efficiency of calcium phosphate nanoparticles and a liposomal transfection agent, Gene Therapy 24 (2017) 282-289.
[58] R. Ra, S. Alwani, I. Badea, Polymeric nanoparticles in gene therapy: new avenues of design and optimization for delivery applications, Polymers 11(4) (2019) 745.
[59] J. Buck, P. Grossen, P. R. Cullis, J. Huwyler, D. Witzigmann, Lipid-based DNA therapeutics: hallmarks of non-viral gene delivery, ACS Nano 13(4) (2019) 3754-3782.
[60] P. Y. P. Law, Y. M. Liu, H. Geng, K. H. Kwan, M. M. Y. Waye, Y. Y. Ho, Expression and functional characterization of the putative protein 8b of the severe acute respiratory syndrome-associated coronavirus, FEBS Letters 580(15) (2006) 3643-3648.
[61] M. Tan, H. T. A. van Tol, M. Mokry, T. A. E. Stout, B. A. J. Roelen, Microinjection induces changes in the transcriptome of bovine oocytes, Scientific Reports 10 (2020) 11211.
[62] I. S. Zuhorn, R. Kalicharan, D. Hoekstra, Lipoplex-mediated transfection of mammalian cells occurs through the cholesterol-dependent clathrin-mediated pathway of endocytosis, Journal of Biological Chemistry 277(20) (2002) 18021-18028.
[63] I. A. Khalil, K. Kogure, H. Akita, H. Harashima, Uptake pathways and subsequent intracellular trafficking in nonviral gene delivery, Pharmacological Reviews 58(1) (2006) 32-45.
[64] K. Takei, V. Haucke, Clathrin-mediated endocytosis: membrane factors pull the trigger, Trends in Cell Biology 11(9) (2001) 385-391.
[65] F. R. Maxfield, T. E. McGraw, Endocytic recycling, Nature Reviews Molecular Cell Biology 5 (2004) 121-132.
[66] M. Amyere, M. Mettlen, P. V. D. Smissen, A. Platek, B. Payrastre, A. Veithen, P. J. Courtoy, Origin, originality, functions, subversions and molecular signalling of macropinocytosis, International Journal of Medical Microbiology 291(6-7) (2001) 487-494.
[67] S. D. Conner, S. L. Schmid, Regulated portals of entry into the cell, Nature 422 (2003) 37-44.
[68] Y. Wang, Y. Nie, Z. Ding, M. Yao, R. Du, L. Zhang, S. Wang, D. Li, Y. Wang, M. Cao, An amphiphilic

peptide with cell penetrating sequence for highly efficient gene transfection, Colloids and Surfaces A: Physicochemical and Engineering Aspects 590 (2020) 124529.
[69] X. Xie, T. Zheng, W. Li, Recent progress in ionic coassembly of cationic peptides and anionic species, Macromolecular Rapid Communications 41(24) (2020) 2000534.
[70] K. Liu, Y. Sun, M. Cao, J. Wang, J. R. Lu, H. Xu, Rational design, properties, and applications of biosurfactants: a short review of recent advances, Current Opinion in Colloid & Interface Science 45 (2020) 57-67.
[71] R. M. Visalakshan, M. N. MacGregor, A. A. Cavallaro, S. Sasidharan, A. Bachhuka, A. M. M. Vasilev, J. D. Hayball, K. Vasilev, Creating nano-engineered biomaterials with well-defined surface descriptors, ACS Applied Nano Materials 1(6) (2018) 2796-2807.
[72] M. Stuible, A. Burlacu, S. Perret, D. Brochu, B. P. Roc, J. Baardsnes, M. Loignon, E. Grazzini, Y. Durocher, Optimization of a high-cell-density polyethylenimine transfection method for rapid protein production in CHO-EBNA1 cells, Journal of Biotechnology 281 (2018) 39-47.
[73] Y. Tang, K. Garson, L. Li, B. C. Vanderhyden, Optimization of lentiviral vector production using polyethylenimine‐mediated transfection, Oncology Letters 9(1) (2015) 55-62.
[74] J. Ye, V. Kober, M. Tellers, Z. Naji, P. Salmon, J. F. Markusen, High-level protein expression in scalable CHO transient transfection, Biotechnology and Bioengineering 103(3) (2009) 542-551.
[75] M. Jiang, G. Chen, High Ca2+-phosphate transfection efficiency in low-density neuronal cultures, Nature Protocols 1 (2006) 695-700.
[76] M. Paidikondala, S. Kadekar, O. P. Varghese, Innovative strategy for 3D transfection of primary human stem cells with BMP-2 expressing plasmid DNA: a clinically translatable strategy for ex vivo gene therapy, International Journal of Molecular Sciences 20(1) (2019) 56.
[77] L. T. Wang, C. H. Ting, M. L. Yen, K. J. Liu, H. K. Sytwu, K. K. Wu, B. L. Yen, Human mesenchymal stem cells (MSCs) for treatment towards immune- and inflammation-mediated diseases: review of current clinical trials, Journal of Biomedical Science 23 (2016) 76.
[78] T. K. Jie, W. H. W. Lim, K. W. Leong, The effect of the degree of chitosan deacetylation on the efficiency of gene transfection, Biomaterials 25(22) (2004) 5293-5301.
[79] N. Shang, M. Figini, J. Shangguan, B. Wang, C. Sun, L. Pan, Q. Ma, Z. Zhang, Dendritic cells based immunotherapy, American Journal of Cancer Research 7(10) (2017) 2091-2102.
[80] A. Irvine, P. Trinder, D. Laughton, H. Ketteringham, R. H. McDermott, S. C. H. Reid, A. M. R. Haines, A. Amir, R. Husain, R. Doshi, L. S. Young, A. Mountain, Efficient nonviral transfection of dendritic cells and their use for in vivo immunization, Nature Biotechnology 18 (2000) 1273-1278.
[81] T. L. Nguyen, Y. Yin, Y. Choi, J. H. Jeong, J. H. Jeong, J. Kim, Enhanced cancer DNA vaccine via direct transfection to host dendritic cells recruited in injectable scaffolds, ACS Nano 14(9) (2020) 11623-11636.
[82] T. Gonzalez-Fernandez, B. N. Sathy, C. Hobbs, G. M. Cunniffe, H. O. McCarthy, N. J. Dunne, V. Nicolosi, F. J. O'Brien, D. J. Kelly, Mesenchymal stem cell fate following non-viral gene transfection strongly depends on the choice of delivery vector, Acta Biomaterialia 55 (2017) 226-238.
[83] W. Khan, H. Hosseinkhani, D. Ickowicz, P. D. Hong, D. S. Yu, A. J. Domb, Polysaccharide gene transfection agents, Acta Biomaterialia 8(12) (2012) 4224-4232.
[84] M. A. Hunt, M. J. Currie, B. A. Robinson, G. U. Dachs, Optimizing transfection of primary human umbilical vein endothelial cells using commercially available chemical transfection reagents, Journal of Biomolecular Techniques 21(2) (2010) 66-72.
[85] I. I. Slowing, J. L. Vivero-Escoto, C. W. Wu, V. S. Y. Lin, Mesoporous silica nanoparticles as controlled release drug delivery and gene transfection carriers, Advanced Drug Delivery Reviews 60(11) (2008) 1278-1288.

[86] A. Aied, U. Greiser, A. Pandit, W. Wang, Polymer gene delivery: overcoming the obstacles, Drug Discovery Today 18(21-22) (2013) 1090-1098.
[87] J. E. Phillips, C. A. Gersbach, A. J. García, Virus-based gene therapy strategies for bone regeneration, Biomaterials 28(2) (2007) 211-229.
[88] R. Saha, S. Bhayye, S. Ghosh, A. Saha, K. Sarkar, Supramolecular assembly of amino acid based cationic polymer for efficient gene transfection efficiency in triple negative breast cancer, ACS Applied Bio Materials 2(12) (2019) 5349-5365.
[89] Y. Cao, Y. F. Tan, Y. S. Wong, M. W. J. Liew, S. Venkatraman, Recent advances in chitosan-based carriers for gene delivery, Marine Drugs 17(6) (2019) 381.
[90] L. H. Wang, D. C. Wu, H. X. Xu, Y. Z. You, High DNA-binding affinity and gene-transfection efficacy of bioreducible cationic nanomicelles with a fluorinated core, Angewandte Chemie International Edition 128(2) (2016) 765-769.
[91] M. Wang, H. Liu, L. Li, Y. Cheng, A fluorinated dendrimer achieves excellent gene transfection efficacy at extremely low nitrogen to phosphorus ratios, Nature Communications 5(1) (2014) 3053.
[92] J. Lee, Y. J. Cho, J. W. Lee, H. J. Ahn, KSP siRNA/paclitaxel-loaded PEGylated cationic liposomes for overcoming resistance to KSP inhibitors: synergistic antitumor effects in drug-resistant ovarian cancer, Journal of Controlled Release 321(10) (2020) 184-197.
[93] J. E. Lee, Y. Yin, S. Y. Lim, E. S. Kim, J. Jung, D. Kim, J. W. Park, M. S. Lee, J. H. Jeong, Enhanced transfection of human mesenchymal stem cells using a hyaluronic acid/calcium phosphate hybrid gene delivery system, Polymers 11(5) (2019) 798.
[94] Y. Aoshima, R. Hokama, K. Sou, S. R. Sarker, K. Iida, H. Nakamura, T. Inoue, S. Takeoka, Cationic amino acid based lipids as effective nonviral gene delivery vectors for primary cultured neurons, ACS Chemical Neuroscience 4(12) (2013) 1514-1519.
[95] H. J. Kong, D. J. Mooney, Microenvironmental regulation of biomacromolecular therapies, Nature Reviews Drug Discovery 6 (2007) 455-463.
[96] D. Mirska, K. Schirmer, S. S. Funari, A. Langner, B. Dobner, G. Brezesinski, Biophysical and biochemical properties of a binary lipid mixture for DNA transfection, Colloids and Surfaces B: Biointerfaces 40(1) (2005) 51-59.
[97] M. C. de Lima, S. Neves, A. Filipe, N. Duzgunes, S. Simoes, Cationic liposomes for gene delivery: from biophysics to biological applications, Current Medicinal Chemistry 10(14) (2003) 1221-1231.
[98] A. M. Ledo, K. H. Vining, M. J. Alonso, M. Garcia-Fuentes, D. J. Mooney, Extracellular matrix mechanics regulate transfection and SOX9-directed differentiation of mesenchymal stem cells, Acta Biomaterialia 110 (2020) 153-163.
[99] B. R. Olden, Y. Cheng, J. L. Yu, S. H. Pun, Cationic polymers for non-viral gene delivery to human T cells, Journal of Controlled Release 282 (2018) 140-147.
[100] O. G. Alamdari, E. Seyedjafari, M. Soleimani, N. Ghaemi, Micropatterning of ECM proteins on glass substrates to regulate cell attachment and proliferation, Avicenna Journal of Medical Biotechnology 5(4) (2013) 234-240.
[101] S. Kourembanas, T. Morita, Y. Liu, H. Christou, Mechanisms by which oxygen regulates gene expression and cell-cell interaction in the vasculature, Kidney International 51(2) (1997) 438-443.
[102] N. Shigemura, Y. Sawa, S. Mizuno, M. Ono, M. Ohta, T. Nakamura, Y. Kaneda, H. Matsuda, Amelioration of pulmonary emphysema by in vivo gene transfection with hepatocyte growth factor in rats, Circulation 111 (2005) 1407-1414.
[103] C. Chu, H. Kong, Interplay of cell adhesion matrix stiffness and cell type for non-viral gene delivery, Acta Biomaterialia 8(7) (2012) 2612-2619.

[104] R. L. Mauck, B. A. Byers, X. Yuan, R. S. Tuan, Regulation of cartilaginous ECM gene transcription by chondrocytes and MSCs in 3D culture in response to dynamic loading, Biomechanics and Modeling in Mechanobiology 6 (2007) 113-125.
[105] M. C. Coen, R. Lehmann, P. Groening, L. Schlapbach, Modification of the micro- and nanotopography of several polymers by plasma treatments, Applied Surface Science 207(1-4) (2003) 276-286.
[106] S. Modaresi, S. Pacelli, J. Whitlow, A. Paul, Deciphering the role of substrate stiffness in enhancing the internalization efficiency of plasmid DNA in stem cells using lipid-based nanocarriers, Nanoscale 10 (2018) 8947-8952.
[107] P. Garg, S. Kumar, S. Pandey, H. Seonwoo, P. H. Choung, J. Koh, J. H. Chung, Triphenylamine coupled chitosan with high buffering capacity and low viscosity for enhanced transfection in mammalian cells, in vitro and in vivo, Journal of Materials Chemistry B 1 (2013) 6053-6065.
[108] H. J. Kong, J. Liu, K. Riddle, T. Matsumoto, K. Leach, D. J. Mooney, Non-viral gene delivery regulated by stiffness of cell adhesion substrates, Nature Materials 4 (2005) 460-464.
[109] V. Vogel, M. Sheetz, Local force and geometry sensing regulate cell functions, Nature Reviews Molecular Cell Biology 7 (2006) 265-275.
[110] X. Wang, X. Hu, J. Li, A. C. M. Russe, N. Kawazoe, Y. Yang, G. Chen, Influence of cell size on cellular uptake of gold nanoparticles, Biomaterials Science 4(6) (2016) 970-978.
[111] X. Wang, T. Nakamoto, I. Dulińska-Molak, N. Kawazoe, G. Chen, Regulating the stemness of mesenchymal stem cells by tuning micropattern features, Journal of Materials Chemistry B 4(1) (2016) 37-45.
[112] S. R. Ryoo, Y. K. Kim, M. H. Kim, D. H. Min, Behaviors of NIH-3T3 fibroblasts on graphene/carbon nanotubes: proliferation, focal adhesion, and gene transfection studies, ACS Nano 4(11) (2010) 6587-6598.
[113] C. Galli, G. Passeri, F. Ravanetti, E. Elezi, M. Pedrazzoni, G. M. Macaluso, Rough surface topography enhances the activation of Wnt/β-catenin signaling in mesenchymal cells, Journal of Biomedical Materials Research Part A 95A(3) (2010) 682-690.
[114] R. J. McMurray, A. K. T. Wann, C. L. Thompson, J. T. Connelly, M. M. Knight, Surface topography regulates wnt signaling through control of primary cilia structure in mesenchymal stem cells, Scientific Reports 3 (2013) 3545.
[115] Y. Yang, X. Wang, X. Hu, N. Kawazoe, Y. Yang, G. Chen, Influence of cell morphology on mesenchymal stem cell transfection, ACS Applied Materials & Interfaces 11 (2018) 1932-1941.
[116] A. F. Adler, A. T. Speidel, N. Christoforou, K. Kolind, M. Foss, K. W. Leong, High-throughput screening of microscale pitted substrate topographies for enhanced nonviral transfection efficiency in primary human fibroblasts, Biomaterials 32(14) (2011) 3611-3619.
[117] P. Y. Wang, Y. S. Lian, R. Chang, W. H. Liao, W. S. Chen, W. B. Tsai, Modulation of PEI-mediated gene transfection through controlling cytoskeleton organization and nuclear morphology via nanogrooved topographies, ACS Biomaterials Science & Engineering 3(12) (2017) 3283-3291.
[118] B. K. K. Teo, S. H. Goh, T. S. Kustandi, W. W. Loh, H. Y. Low, E. K. F. Yim, The effect of micro and nanotopography on endocytosis in drug and gene delivery systems, Biomaterials 32(36) (2011) 9866-9875.
[119] K. Wang, A. Bruce, R. Mezan, A. Kadiyala, L. Wang, J. Dawson, Y. Rojanasakul, Y. Yang, Nanotopographical modulation of cell function through nuclear deformation, ACS Applied Materials & Interfaces 8 (2016) 5082-5092.
[120] M. Golshadi, L. K. Wright, I. M. Dickerson, M. G. Schrlau, High-efficiency gene transfection of cells through carbon nanotube arrays, Small 12(22) (2016) 3014-3020.
[121] X. Wang, X. Hu, N. Kawazoe, Y. Yang, G. Chen, Manipulating cell nanomechanics using micropatterns, Advanced Functional Materials 26(42) (2016) 7634-7643.

[122] S. Mattiassi, M. Rizwan, C. L. Grigsby, A. M. Zawa, K. W. Leong, E. K. F. Yim, Enhanced efficiency of nonviral direct neuronal reprogramming on topographical patterns, Biomaterials Science 9(15) (2021) 5175-5191.
[123] D. Falconnet, G. Csucs, H. M. Grandin, M. Textor, Surface engineering approaches to micropattern surfaces for cell-based assays, Biomaterials 27(16) (2006) 3044-3063.
[124] W. Wang, G. Li, J. Wang, W. Song, J. Luo, F. Meng, Y. Zhang, Involvement of Rac1 in the micro/nano-topography sensing and osteogenic differentiation in bone marrow mesenchymal stem cells, Materials & Design 157 (2018) 402-411.
[125] C. M. Nelson, S. Raghavan, J. L. Tan, C. S. Chen, Degradation of micropatterned surfaces by cell-dependent and -independent processes, Langmuir 19(5) (2003) 1493-1499.
[126] B. D. Ratner, S. J. Bryant, Biomaterials: where we have been and where we are going, Annual Review of Biomedical Engineering 6 (2004) 41-75.
[127] S. Pasche, S. M. D. Paul, J. Vörös, N. D. Spencer, M. Textor, Poly(l-lysine)-graft-poly(ethylene glycol) assembled monolayers on niobium oxide surfaces: a quantitative study of the influence of polymer interfacial architecture on resistance to protein adsorption by ToF-SIMS and in situ OWLS, Langmuir 19(22) (2003) 9216-9225.
[128] G. L. Kenausis, J. Vörös, D. L. Elbert, N. Huang, R. Hofer, L. Ruiz-Taylor, M. Textor, J. A. Hubbell, N. D. Spencer, Poly(l-lysine)-g-poly(ethylene glycol) layers on metal oxide surfaces: attachment mechanism and effects of polymer architecture on resistance to protein adsorption, The Journal of Physical Chemistry B 104(14) (2000) 3298-3309.
[129] Y. B. Lee, E. M. Kim, H. Byun, H. Chang, K. Jeong, Z. M. Aman, Y. S. Choi, J. Park, H. Shin, Engineering spheroids potentiating cell-cell and cell-ECM interactions by self-assembly of stem cell microlayer, Biomaterials 165 (2018) 105-120.
[130] A. M. C. Egea, E. Trévisiol, C. Vieu, Direct patterning of probe proteins on an antifouling PLL-g-dextran coating for reducing the background signal of fluorescent immunoassays, Biointerphases 8 (2013) 37.
[131] Y. Yang, X. Wang, T. C. Huang, X. Hu, N. Kawazoe, W. B. Tsai, Y. Yang, G. Chen, Regulation of mesenchymal stem cell functions by micro-nano hybrid patterned surfaces, Journal of Materials Chemistry B 6 (2018) 5424-5434.
[132] X. Wang, X. Hu, I. Dulińska-Molak, N. Kawazoe, Y. Yang, G. Chen, Discriminating the independent influence of cell adhesion and spreading area on stem cell fate determination using micropatterned surfaces, Scientific reports 6(1) (2016) 1-13.
[133] T. Nakamoto, X. Wang, N. Kawazoe, G. Chen, Influence of micropattern width on differentiation of human mesenchymal stem cells to vascular smooth muscle cells, Colloids and Surfaces B: Biointerfaces 122 (2014) 316-323.
[134] X. Wang, W. Song, N. Kawazoe, G. Chen, Influence of cell protrusion and spreading on adipogenic differentiation of mesenchymal stem cells on micropatterned surfaces, Soft Matter 9(16) (2013) 4160-4166.
[135] X. Yao, X. Wang, J. Ding, Exploration of possible cell chirality using material techniques of surface patterning, Acta Biomaterialia 126 (2021) 92-108.
[136] R. O. Hynes, Integrins: bidirectional, allosteric signaling machines, Cell 110(6) (2002) 673-687.
[137] X. Tan, J. Heureaux, A. P. Liu, Cell spreading area regulates clathrin-coated pit dynamics on micropatterned substrate, Integrative Biology 7(9) (2015) 1033-1043.
[138] W. Lei, K. Demir, J. Overhage, M. Grunze, T. Schwartz, P. A. Levkin, Droplet-microarray: miniaturized platform for high-throughput screening of antimicrobial compounds, Advanced Biosystems, 4(10) (2020) 2000073.

[139] W. Zhao, L. Hanson, H. Y. Lou, M. Akamatsu, P. D. Chowdary, F. Santoro, J. R. Marks, A. Grassart, D. G. Drubin, Y. Cui, B. Cui, Nanoscale manipulation of membrane curvature for probing endocytosis in live cells, Nature Nanotechnology 12 (2017) 750-756.
[140] C. E. Dunbar, K. A. High, J. K. Joung, D. B. Kohn, K. Ozawa, M. Sadelain, Gene therapy comes of age, Science 359(6372) (2018) eaan4672.
[141] J. Slone, T. Huang, The special considerations of gene therapy for mitochondrial diseases, NPJ Genomic Medicine 7 (2020) 7.
[142] C. M. Blakely, T. B. K. Watkins, W. Wu, B. Gini, J. J. Chabon, C. E. McCoach, N. McGranahan, G. A. Wilson, N. J. Birkbak, V. R. Olivas, J. Rotow, A. Maynard, V. Wang, M. A. Gubens, K. C. Banks, R. B. Lanman, A. F. Caulin, J. S. John, A. R. Cordero, P. Giannikopoulos, A. D. Simmons, P. C. Mack, D. R. Gandara, H. Husain, R. C. Doebele, J. W. Riess, M. Diehn, C. Swanton, T. G. Bivona, Evolution and clinical impact of co-occurring genetic alterations in advanced-stage EGFR-mutant lung cancers, Nature Genetics 49 (2017) 1693-1704.
[143] S. Y. Alhaji, S. C. Ngai, S. Abdullah, Silencing of transgene expression in mammalian cells by DNA methylation and histone modifications in gene therapy perspective, Biotechnology and Genetic Engineering Reviews 35(1) (2018) 1-25.
[144] S. L. Ginn, I. E. Alexander, M. L. Edelstein, M. R. Abedi, J. Wixon, Gene therapy clinical trials worldwide to 2012-an update, Journal of Gene Medicine 15(2) (2013) 65-77.
[145] G. Shim, D. Kim, Q. V. Le, G. T. Park, T. Kwon, Y. K. Oh, Nonviral delivery systems for cancer gene therapy: strategies and challenges, Current Gene Therapy 18(1) (2018) 3-20.
[146] Y. Wang, Y. Yang, X. Wang, N. Kawazoe, Y. Yang, G. Chen, The varied influences of cell adhesion and spreading on gene transfection of mesenchymal stem cells on a micropatterned substrate, Acta Biomaterialia 125 (2021) 100-111.
[147] M. S. Al-Dosari, X. Gao, Nonviral gene delivery: principle, limitations, and recent progress, The AAPS Journal 11 (2009) 671.
[148] N. P. Gabrielson, D. W. Pack, Acetylation of polyethylenimine enhances gene delivery via weakened polymer/DNA interactions, Biomacromolecules 7(8) (2006) 2427-2435.
[149] J. Yang, Q. Zhang, H. Chang, Y. Cheng, Surface-engineered dendrimers in gene delivery, Chemical Reviews 115(11) (2015) 5274-5300.
[150] J. P. Gratton, J. Yu, J. W. Griffith, R. W. Babbitt, R. S. Scotland, R. Hickey, F. J. Giordano, W. C. Sessa, Cell-permeable peptides improve cellular uptake and therapeutic gene delivery of replication-deficient viruses in cells and in vivo, Nature Medicine 9 (2003) 357-362.
[151] Y. Wang, Y. Yang, X. Wang, T. Yoshitomi, N. Kawazoe, Y. Yang, G. Chen, Micropattern-controlled chirality of focal adhesions regulates the cytoskeletal arrangement and gene transfection of mesenchymal stem cells, Biomaterials 271 (2021) 120751.
[152] C. Liu, Q. Feng, J. Sun, Lipid nanovesicles by microfluidics: manipulation, synthesis, and drug delivery, Advanced Materials 31(45) (2019) 1804788.
[153] M. A. Mintzer, E. E. Simanek, Nonviral vectors for gene delivery, Chemical Reviews 109(2) (2009) 259-302.
[154] T. Niidome, L. Huang, Gene therapy progress and prospects: nonviral vectors, Gene Therapy 9 (2002) 1647-1652.
[155] M. R. Salick, B. N. Napiwocki, J. Sha, G. T. Knight, S. A. Chindhy, T. J. Kamp, R. S. Ashton, W. C. Crone, Micropattern width dependent sarcomere development in human ESC-derived cardiomyocytes, Biomaterials 35(15) (2014) 4454-4464.
[156] A. Higuchi, Q. D. Ling, Y. Chang, S. T. Hsu, A. Umezawa, Physical cues of biomaterials guide stem

cell differentiation fate, Chemical Reviews 113(5) (2013) 3297-3328.
[157] M. Rahmati, E. A. Silva, J. E. Reseland, C. A. Heyward, H. J. Haugen, Biological responses to physicochemical properties of biomaterial surface, Chemical Society Reviews 49 (2020) 5178-5224.
[158] K. Lee, Y. Chen, X. Li, Y. Wang, N. Kawazoe, Y. Yang, G. Chen, Solution viscosity regulates chondrocyte proliferation and phenotype during 3D culture, Journal of Materials Chemistry B 7 (2019) 7713-7722.
[159] Y. Chen, K. Lee, Y. Yang, N. Kawazoe, G. Chen, PLGA-collagen-ECM hybrid meshes mimicking stepwise osteogenesis and their influence on the osteogenic differentiation of hMSCs, Biofabrication 12 (2020) 025027.
[160] K. Lee, Y. Chen, T. Yoshitomi, N. Kawazoe, Y. Yang, G. Chen, Osteogenic and adipogenic differentiation of mesenchymal stem cells in gelatin solutions of different viscosities, Advanced Healthcare Materials 9(23) (2020) 2000617.
[161] T. Vignaud, C. Copos, C. Leterrier, M. T. Nahuelpan, Q. Tseng, J. Mahamid, L. Blanchoin, A. Mogilner, M. Théry, L. Kurzawa, Stress fibres are embedded in a contractile cortical network, Nature Materials 20 (2021) 410-420.

Chapter 2

Cell density and interaction controlled by micropatterned surfaces and their influences on gene transfection of mesenchymal stem cells

2.1 Abstract

Although cell density can affect gene transfection, its reason remains elusive. In this study, micropatterns were used to control cell density and investigate how and why cell density could affect gene transfection of hMSCs. Micropatterned surfaces with various square densities were prepared by photo-grafting AzPhPVA onto TCPS surfaces through the designed photomask to control cell density. After cell seeding, cell density was calculated to be 2.5 ± 0.7 - $112.6 \pm 9.6 \times 10^3$ cells/cm^2 by nucleus staining. Cell density could be well controlled by adjusting the ratio of non-adhesive area to cell adhesive area on micropatterned surfaces. Transfection experiment was performed to disclose the influence of cell density on gene transfection efficiency. The percentage of GFP positive cells in all checked cells was compared. The results showed that transfection efficiency showed a first-increasing and then-decreasing tendency with increasing cell density. The cells on 4:1 micropattern showed the highest transfection efficiency. The different influence of cell density on transfection efficiency was strongly correlated with its influence on cellular uptake capacity and DNA synthesis. Insufficient cell-cell interaction at a low cell density and too strong cell-cell interaction at a high cell density was not preferable for gene transfection. A moderate cell density had appropriate cell-cell interaction to facilitate high transfection efficiency. This hypothesis was confirmed by controlling cell size, cell-cell interaction and cell protrusion on differently designed micropatterns.

2.2 Introduction

Gene therapy has become an urgently desired approach in science research and clinical application because of the increasing incidence of various gene-related diseases, such as mutants, genetic silencing and cancers [1-5]. Efficient delivery of exogenous genes into the dysfunctional cells and high expression level of exogenous genes in these cells are two vital proceedings to achieve prosperous gene therapy [6, 7]. Because DNA chains possess negative charges due to the existence of phosphate group, naked DNA permeation through negatively charged cell membrane remains a great challenge [8]. Therefore, many cationic synthesized carriers including polyethylenimine (PEI), dendrimers, peptides and lipids have been rapidly

developed to enhance gene transfection efficiency in recent years [9-13]. Comparing with viral-mediated vectors, cationically functionalized carriers present the typical characteristics of low immunogenicity and relative safety [14]. In addition, simple preparation, easy modification and high genetic loading capacity are extra advantages for these cationic carriers [15]. Nevertheless, cationic-carrier-mediated transfection is always accompanied with low gene transfection efficiency and limited cell types [8, 16]. Currently, most efforts are concentrated to exploit novel polymeric carriers and transfection techniques.

Apart from efficient gene carriers and advanced transfection methods, cellular microenvironment can also affect gene transfection efficiency but is always overlooked [17]. Cells in organisms are enveloped in the neighboring cells and extracellular matrixes (ECMs) [18]. In addition of cell-ECMs interaction, cell density is regarded as one of the key factors to evaluate cell size and cell-cell interaction [19]. Cell-density-dependent cell size and cell-cell interaction play the crucial role in regulating cellular functions, such as cell spreading, adhesion, migration, proliferation, differentiation and uptake [20-25]. However, it is difficult to control different cell density on the same cell culture surface by the conventional cell culture methods. Therefore, microfabrication technique is a very useful tool to manipulate cell density on the same culture substrate [26].

Cell density can control cell morphology to determine intracellular signaling pathways. Some studies have been reported that cell density enables to mediate cell fates [27, 28]. For example, high cell density stimulates chondrogenic differentiation while low cell density induces faster cell proliferation [29]. Although the influence of cell density on cellular proliferation and differentiation is widely investigated, how cell-density-dependent cell size and interaction affects cellular uptake of exogenous genes and gene transfection was rarely reported. Exploration of cell density on the uptake pathway and subsequent intracellular trafficking is necessary through the micropatterned surfaces. In this study, various micropatterns were prepared by UV-grafting poly(vinyl alcohol) on the tissue culture plates through designed photomasks to control cell density, cell size, cell-cell interaction and cell protrusion. The influence of these factors on gene transfection of hMSCs was investigated.

2.3 Materials and methods

2.3.1 Synthesis and characterization of photo-reactive PVA

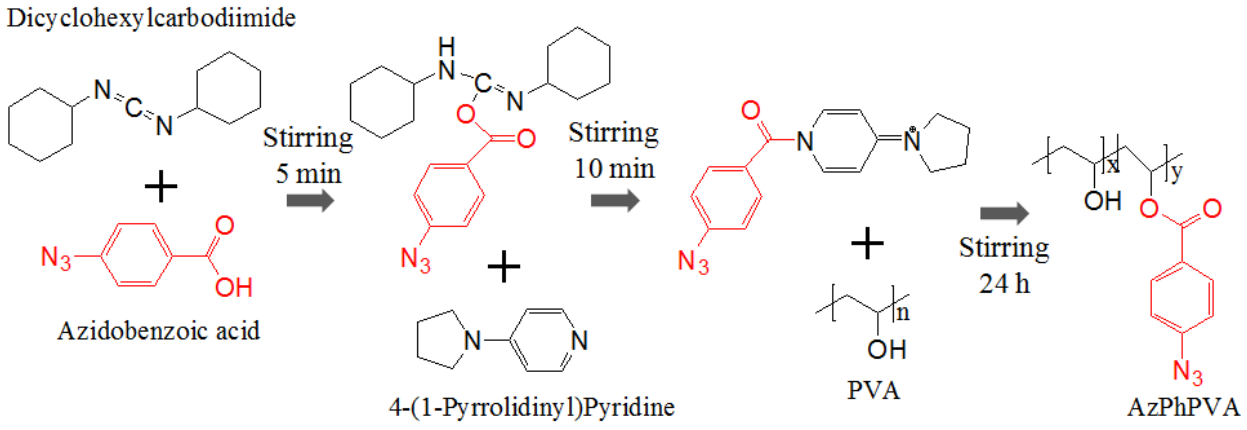

Figure 2.1 Synthesis process of photo-reactive PVA by Steglich esterification.

Photo-reactive poly(vinyl alcohol) (PVA) was synthesized by introducing azidophenyl group of 4-azidobenzoic acid into PVA (Figure 2.1) [30]. In brief, 1850 mg 4-azidobenzoic acid (Wako Pure Chemical Industries, Ltd., Japan) was dissolved in 25 mL dimethyl sulfoxide (DMSO, Wako Pure Chemical Industries, Japan) under stirring at room temperature in the dark. 234 mg/mL dicyclohexylcarbodiimide (DCC, Watanabe Chemical Industries, Ltd., Japan) and 16.8 mg/mL 4-(1-pyrrolidinyl) pyridine (Wako Pure Chemical Industries, Ltd., Japan) in 10 mL DMSO were dropped into 4-azidobenzoic acid solution under stirring in the dark, respectively. After 10 min, 40 mL DMSO containing 12.5 mg/mL PVA (Wako Pure Chemical Industries, Ltd., Japan) was dropped into above mixture solution under stirring in the dark. The reaction was continued at room temperature in the dark for 24 h. After the reaction mixture was dialyzed against Milli-Q water, azidophenyl-derived photo-reactive PVA (AzPhPVA) was successfully synthesized. Azidobenzoic acid, PVA, a mixture of PVA and azidobenzoic acid, and AzPhPVA solution was characterized by ultraviolet-visible (UV-Vis) absorbance analysis (JASCO V-660 Spectrophotometer). AzPhPVA solution was freeze-dried and re-dissolved in deuterium oxide (D_2O, Sigma-Aldrich Co. LLC., USA). AzPhPVA D_2O solution was characterized by ^{1}H-NMR.

2.3.2 Micropatterning of photo-reactive PVA

Tissue culture polystyrene (TCPS) plates were cut from cell culture flasks and coated with an aqueous solution of 0.3 mg/mL AzPhPVA in the central region (1.5 × 1.5 cm^2). After air-drying at room temperature in the dark, AzPhPVA-coated TCPS plates were covered with the photomask containing micropatterns with gradient square density and irradiated with 0.25 J/cm UV light (FS-1500, Tokyo Rikakai, Japan) at the fixed distance of 15 cm. The photomask was composed of micro-squares with the side length of 200 μm. Four-type square densities were designed on photomask and the ratio of non-adhesive area (AzPhPVA area) to adhesive area (TCPS area) was 4:1, 9:1, 25:1 and 50:1, respectively. After complete washing in Milli-Q water bath, the micropatterned surfaces were obtained. The microdots with different diameters (30 and 60 μm), different numbers of connecting lines (0, 1, 2, 4, and 6 short lines) and different numbers of protrusion lines (0, 1, 2, 4, and 6 short lines) were prepared in the same way. The width of short lines was set at 2.5 μm. The images of micropatterns were captured by a phase-contrast microscope (Olympus, Japan).

The topography of micropatterns was measured by an atomic force microscope (MFP-3D-BIO AFM, Asylum Research Corporation, USA). A commercially available DNP cantilever with a spring constant of 0.06 N/m and oscillation frequency of 12-14 kHz was purchased from American Bruker Corporation. The cantilever was equipped with a silicon nitride tip to scan the micropatterns in Milli-Q water in contact mode. Section view was used to analyze the height of PVA-grafted layer and diameters of microdots. Three independent micropatterns were used to calculate the mean and standard deviation (SD). In order to enhance cell adhesion on micropatterns, fibronectin (20 μg/mL in $NaHCO_3$, Sigma-Aldrich, USA) was coated on the micropatterned surfaces at 37℃ in a 5% CO_2 incubator for 1 h. The fibronectin-coated micropatterns were incubated with anti-fibronectin primary antibody (1:200 in BSA, Santa Cruz Biotechnology, USA) overnight and stained with Alexa Fluor-488 labeled secondary antibody (1:1000 in PBS, Invitrogen, USA) in the dark.

2.3.3 Cell culture

Human bone marrow-derived mesenchymal stem cells (hMSCs, Passage 2) were obtained from Lonza Walkersville of America. The cells were seeded in 25 cm^2 tissue culture flasks and subcultured twice in mesenchymal stem cell growth BulletKit medium (Lonza, USA) at 37℃ in a 5% CO_2 incubator [35]. The

cells at passage 4 were harvested by treatment with trypsin/EDTA solution and suspended in Dulbecco's modified Eagle's medium (DMEM, Sigma-Aldrich, USA) containing 10% fetal bovine serum (FBS, Gibco™, USA). The sterilized plates were put into cell culture dishes and supplemented with 3 mL DMEM medium. Glass rings were covered onto the micropatterned surfaces to prevent hMSCs leaking during cell seeding. After that, cell suspension solution was added onto the micropatterned surfaces in each glass ring. Cell seeding density was 2.5×10^3 cells/cm^2. After cell culture for 6 h, glass rings were removed and hMSCs were further cultured for 18 h. The same procedure was executed on micropatterns with different protrusions. For cell seeding on the micropatterns with different contact lines, cell seeding density was 1.5×10^3 cells/cm^2. After 1 h cell culture, glass rings were removed and cell culture plates were gently shaken to remove non-adhered cells. Glass rings were replaced on the micropatterns to repeat this step 3 times to enhance cell seeding efficiency. In addition, hMSCs were seeded on the bare TCPS plates as a comparison under the same conditions. Cell morphology was observed by a phase-contrast microscope with a DP-70 CCD camera (Olympus, Japan). In order to calculate cell number in each micro-square, the nuclei were stained with Hoechst 33258 (1:1000 in PBS, Wako Pure Chemical Industries, Ltd., Japan) for 10 min and followed with PBS washing. Five independent experiments (≥ 200 cells) were used to calculate the mean and SD.

2.3.4 Amplification and purification of plasmid

The pAcGFP1-N1 plasmid expressing green fluorescence proteins (GFP) was bought from Clontech Laboratories in America. The plasmid was amplified in *Escherichia coli* DH5*α* (*E. coli*, Takara Bio, Inc., Japan) and purified according to the previous report [32]. In brief, pAcGFP1-N1 plasmid was transferred into *E. coli* under the heat shock mode and further incubated at 37℃ for 1 h. The transformed *E. coli* was seeded on the Agar-LB plates containing 30 μg/mL kanamycin (Sigma-Aldrich, USA) and cultured at 37℃ overnight. The colony on Agar-LB plates were selected and re-suspended in 25 mg/mL LB Broth Miller (Nacalai Tesque, Japan) with 30 μg/mL kanamycin. The suspension solution was incubated at 37℃ under shaking for 18 h. After that, the amplified plasmid was obtained and further purified with a Plasmid Mini Kit (Qiagen, USA) according to the company's protocol. The concentration of pAcGFP1-N1 was measured at 260 nm by Nanodrop spectrophotometry (Thermo Fisher, USA).

2.3.5 Gene transfection

A commercially available Lipofectamine™ 2000 transfection reagent (Invitrogen, USA) was applied to enhance gene transfection efficiency of pAcGFP1-N1 plasmid in the micropatterned cells. In order to prepare the cationic Lipofectamine™ 2000/GFP-plasmid complexes, 1 μL Lipofectamine™ 2000 solution and 500 ng pAcGFP1-N1 were separately diluted in 100 μL Opti-MEM medium (Life Technologies, USA). After incubation at room temperature for 5 min, pAcGFP1-N1 solution was incorporated into Lipofectamine™ 2000 solution and further incubated in Opti-MEM medium for 30 min to obtain the cationic liposome/plasmid complexes. In principle, positive charges of Lipofectamine™ 2000 could be attracted with negatively charged phosphate groups of pAcGFP1-N1 plasmid to form the stable lipoplexes. Before the addition of cationic lipoplexes, hMSCs were seeded on micropatterns and further cultured at 37℃ in a CO_2 incubator for 24 h. DMEM growth medium was changed to Opti-MEM medium and cultured for 2 h. Then, glass rings were placed on the micropatterned surfaces to prevent the lipoplexes leaking. A 200 μL aliquot of the cationic lipoplexes was added into each glass ring for gene transfection. After incubation for 6 h, glass rings were removed and Opti-MEM medium was changed to DMEM medium and cultured for another 18 h

to express green fluorescence proteins. After that, the samples were fixed with 4% paraformaldehyde (Wako Pure Chemical Industries, Ltd., Japan) for 10 min and treated with 1% Triton™ X-100 (Sigma-Aldrich, USA) for 10 min. After PBS washing, the cells were blocked with 2% bovine serum albumin (BSA, Wako Pure Chemical Industries, Ltd., Japan, Japan) for 30 min and followed with PBS washing. Nuclei and actin filaments were stained with Hoechst 33258 (1:1000 in PBS) and Alexa Fluor-594 phalloidin (1:40 in PBS, Invitrogen, USA), respectively. The fluorescent images of stained samples were captured by a fluorescence microscope. ImageJ software was used to analyze the fluorescent images to evaluate the GFP positive cells according to the previous report [32, 33]. The equation $CFY=TFY-(A\times AFY)$ was used to analyze the fluorescence images of the transfected cells, where *CFY* is the corrected fluorescence yield of transfected cells and untreated cells, *A* and *TFY* are the spreading area and total fluorescence yield of the cells of interest, and *AFY* is the average autofluorescence yield of the micropatterns. A *CFY* proportion (≥ 50 times) relative to the untreated cells was used to define the transfected cells. The percentage of GFP-positive cells in all checked cells was defined as the transfection efficiency. Five independent experiments (≥ 200 cells) were carried out to calculate the mean and SD.

2.3.6 Cellular uptake of cationic microspheres

Fluoresbrite carboxylate microspheres having a diameter of 500 nm (Funakoshi Co., Ltd., Japan) were used to evaluate cellular uptake capacity of micropatterned hMSCs. Uptake experiment was performed in a similar way with transfection experiment. Firstly, 1 μL Lipofectamine™ 2000 solution and 0.1 μL microspheres solution were separately diluted in 100 μL Opti-MEM medium. After incubation at room temperature for 5 min, microspheres solution was incorporated into Lipofectamine™ 2000 solution and incubated for 30 min to obtain cationic microspheres complexes. The next experiments were the same as mentioned above. After 24 h culture, the samples were washed by PBS for 3 times and a 200 μL aliquot of 0.4% trypan blue solution (Sigma-Aldrich, USA) was applied to quench the extracellular green fluorescence of microspheres. The samples were fixed with 4% paraformaldehyde solution for 10 min and followed with PBS washing. The cells were treated with Triton™ X-100 for 10 min and blocked with 2% BSA for 30 min. Nuclei and actin filaments were stained with Hoechst 33258 for 10 min and Alexa Fluor-594 phalloidin for 20 min, respectively. The stained cells were observed by an Olympus fluorescence microscope. Total and average fluorescence yields of FITC per cell were calculated by an ImageJ software. Five independent experiments and more than 25 cells were performed to calculate the mean and SD.

2.3.7 Evaluation of DNA synthesis by BrdU staining

5-bromo-2'-deoxyuridine (BrdU, Thermo Fisher, USA) was used to investigate DNA synthesis of micropatterned hMSCs. Before the cells were seeded on micropatterned TCPS plates, hMSCs were cultured in FBS-free DMEM growth medium including 4500 mg/L glucose, 584 mg/L glutamine, 100 U/mL penicillin, 100 μg/mL streptomycin, 0.1 mM nonessential amino acid, 0.4 mM proline and 50 mg/L ascorbic acid for 24 h to keep the cells in G0 state. After the starved cells were seeded on micropatterns for 24 h, transfection experiment was executed and incubated in Opti-MEM medium at 37℃ in a 5% CO_2 incubator for 6 h. Opti-MEM medium was changed to DMEM growth medium containing 1% BrdU labeling reagent and further cultured for 18 h. For BrdU staining, hMSCs were fixed with 70% ethanol for 30 min and denatured with 2 M HCl for 30 min. After PBS washing, the cells were permeabilized with 1% Triton™ X-100 for 10 min and washed with PBS. 2% BSA was used to block the cells for 30 min and rinsed with

PBS. The cells were stained with monoclonal mouse anti-BrdU primary antibody (1: 200 in BSA, Abcam, USA) for 1.5 h and Alexa Fluor-488 donkey anti-mouse IgG antibody (1:1000 in PBS, Thermo Fisher, USA) in the dark for 1 h. Finally, nuclei were stained with Hoechst 33258 in the dark for 10 min. Fluorescent images of the stained cells were captured by a fluorescence microscope. Number of BrdU positive cells was counted according to nuclei staining. The percentage of BrdU positive cells in all checked cells was defined as DNA synthesis activity. Five independent samples (≥ 200 cells) were used to calculate the mean and SD.

2.3.8 Cell membrane staining

After the cells were seeded on the micropatterns for 24 h, the hMSCs were washed with PBS for 3 times. The samples were fixed with 4% paraformaldehyde solution for 10 min and followed with 3 PBS washing. Cell membrane of micropatterned hMSCs was stained with PlasMem bright green (1:200 in PBS, Dojindo Laboratories, Japan) for 15 min and followed with 3 PBS washing. The samples were stained with Hoechst 33258 in the dark for 10 min. The fluorescent images were captured by a fluorescence microscope.

2.3.9 Statistical analysis

All quantitative data were presented as the mean ± SD. Statistical significance of the results was evaluated by using one-way ANOVAs with a Tukey's post-test for comparison between multiple conditions ($n \geq 5$) and $p < 0.05$ was considered as significant.

2.4 Results

2.4.1 Characterization of synthesized photo-reactive PVA

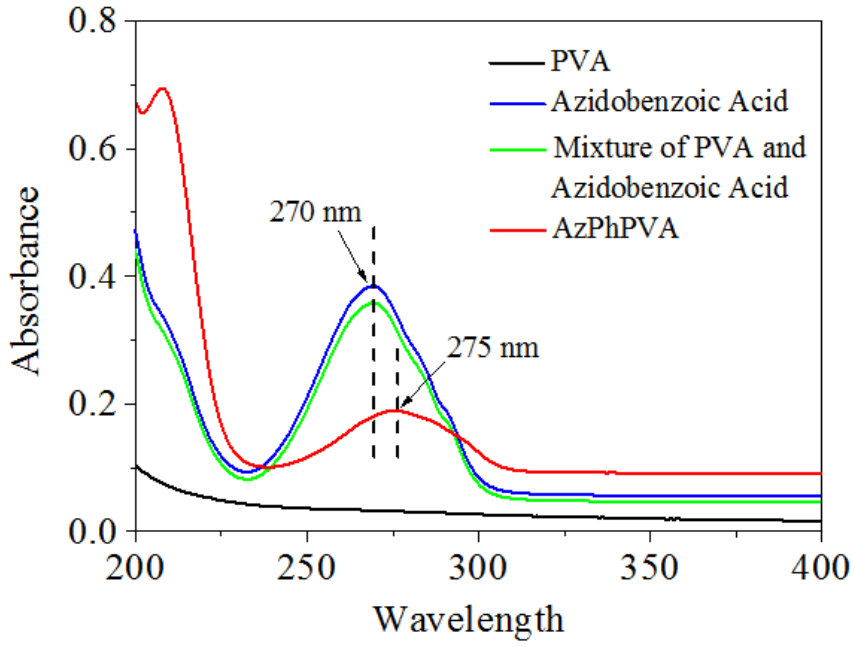

Figure 2.2 UV spectra of PVA, azidobenzoic acid, mixture of PVA and azidobenzoic acid, and AzPhPVA.

The photo-reactive PVA was synthesized as previously reported [30]. Azidophenyl group of 4-azidobenzoic acid was introduced into PVA by the reaction of carboxyl group of 4-azidobenzoic acid and hydroxyl group of PVA. In order to confirm the formation of photo-reactive AzPhPVA, the synthesized AzPhPVA solution was characterized by using UV-Vis absorbance analysis and ^{1}H-NMR. Firstly, the absorbance peak (275 nm) of AzPhPVA showed that the benzenoid structure was introduced in AzPhPVA (Figure 2.2). PVA, azidobenzoic acid, and the mixture of PVA and azidobenzoic acid were also measured. Absorbance peak of benzenoid structure in unreacted azidobenzoic acid appeared at approximately 270 nm. Configuration change of azidobenzoic acid induced the bathochromic shift of benzenoid absorbance peak of AzPhPVA. Further, the percentage of azidophenyl group in PVA chains was calculated according to ^{1}H-NMR spectrum (Figure 2.3). The peaks between 7 and 8 ppm were the protons of benzenoid structures. The peaks at around 1.4 and 3.8 ppm were the methylene and methylidyne protons on AzPhPVA, respectively. The grafting degree was calculated through the integration of each peak in ^{1}H-NMR spectrum. The results showed that the photo-reactive AzPhPVA solution was successfully synthesized.

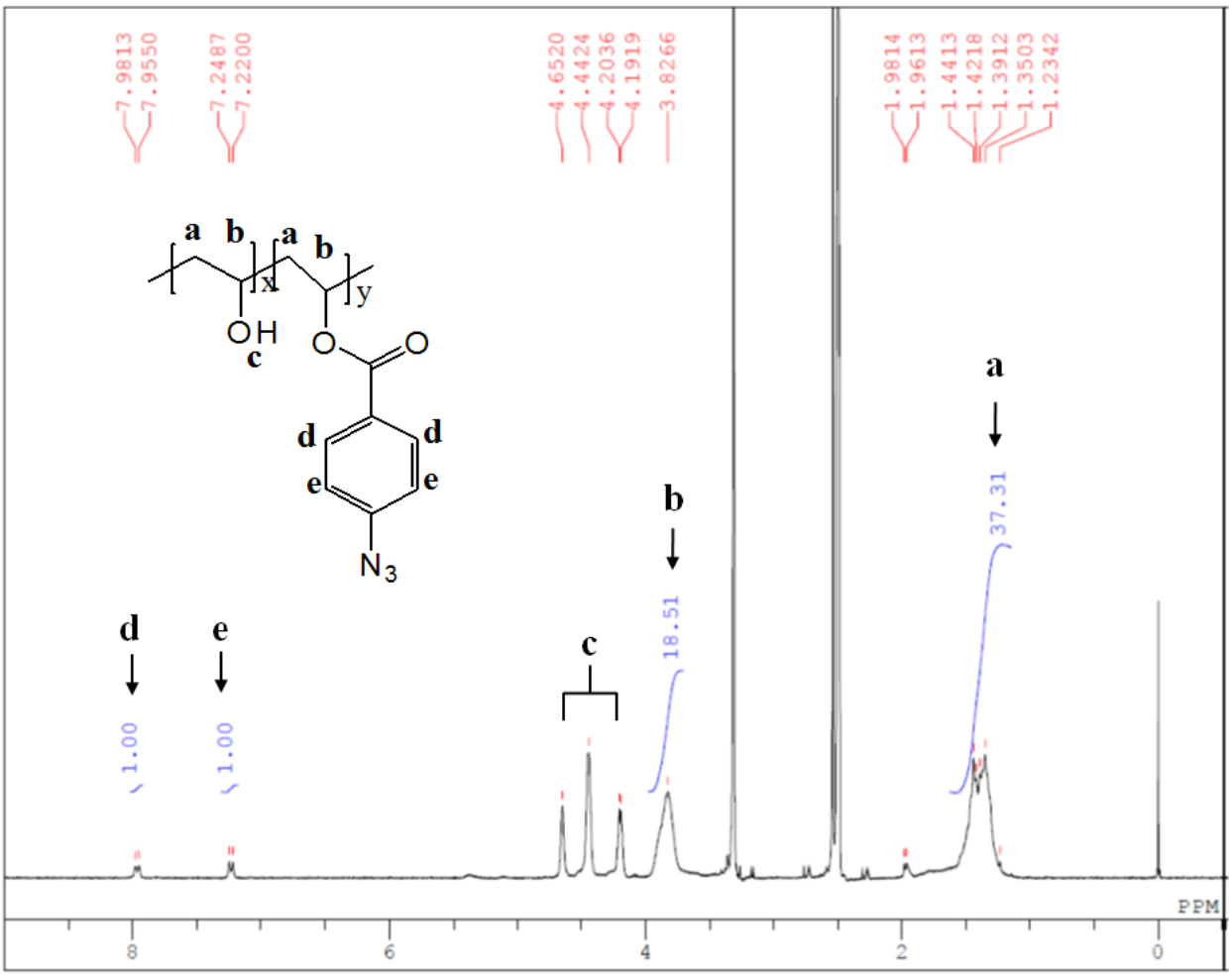

Figure 2.3 ^{1}H-NMR spectrum of synthesized photo-reactive PVA. The peaks between 7 and 8 ppm were the protons of benzenoid structures. The peaks at around 1.4 and 3.8 ppm were the methylene and methylidyne protons of PVA, respectively. The structure of photo-reactive AzPhPVA was showed and the corresponding peaks were marked by a-d.

2.4.2 Preparation and characterization of micropatterns

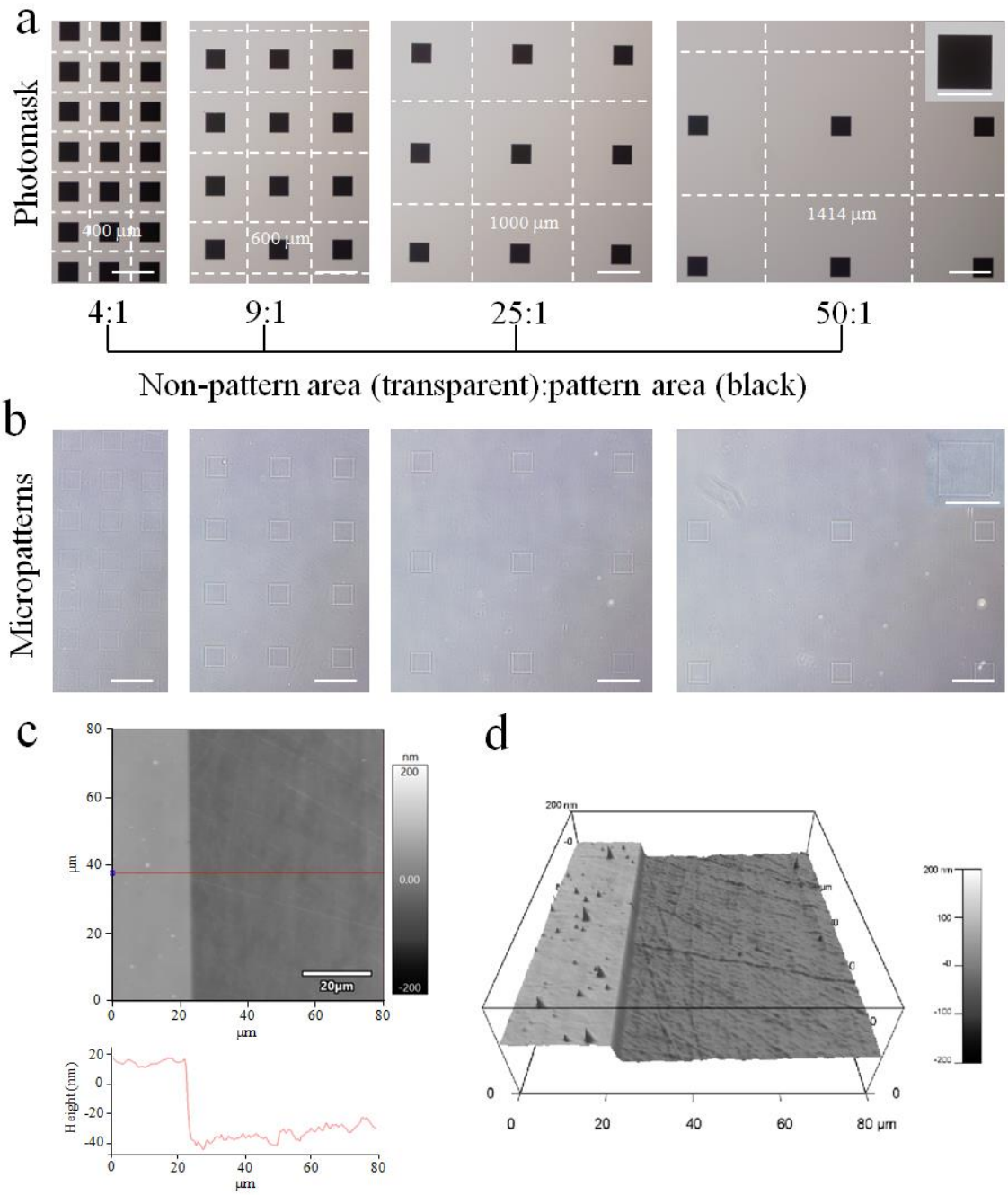

Figure 2.4 Characterization of micropatterned surfaces with gradient square density. (a) Phase-contrast images of the designed photomask. Four-type square density was designed on photomask. Dark squares represented cell adhesion regions and side length was fixed as 200 μm. The dashed white squares indicated cell non-adhesion area. Area ratio of non-pattern region to pattern region was defined as 4:1, 9:1, 25:1 and 50:1, respectively. Scale bar: 500 μm. Insert was high magnification. Scale bar: 200 μm. (b) Phase-contrast images of the prepared micropatterns on TCPS plates. Scale bar: 500 μm. Insert was high magnification of the representative micropatterns. Scale bar: 200 μm. (c) Representative AFM scanning height image and section view image of micropatterns. (d) 3D image of micropatterns measured by AFM.

Photo-reactive PVA was coated on the bare TCPS surfaces and micropatterned through a designed photomask (Figure 2.4a). The photomask was composed of 200 μm-side-length dark micro-squares and

contained four-type square densities. The distance of center-to-center between the neighboring squares was designed to be 400, 600, 1000 and 1414 μm. The ratio of non-adhesive area to adhesive area was 4:1, 9:1, 25:1 and 50:1 for four-type square densities. The transparent photomask with dark micro-squares was exposed to UV light and the TCPS surfaces under the dark squares were not modified by the AzPhPVA. After ultrasonic washing, these concave micro-squares displayed bare TCPS surfaces to support cell attachment. Formation of micro-squares was confirmed according to a phase-contrast microscope (Figure 2.4b). The images indicated that the prepared micro-squares had the same structure and density as that of the designed photomask. In order to further investigate the good controllability of micropatterns, the micro-squares were scanned by AFM. Representative AFM scanning height image and section view image clearly disclosed the formation of the tiered structure on PVA-grafted TCPS surfaces in water contact mode (Figure 2.4c). The height of PVA-grafted layer was approximately 60 nm. 3D image of the border between PVA layer and TCPS surface was shown in Figure 2.4d. The micropatterning results suggested that square density and height of micropatterns could be well controlled on PVA-grafted TCPS surfaces.

2.4.3 Cell culture and density distribution

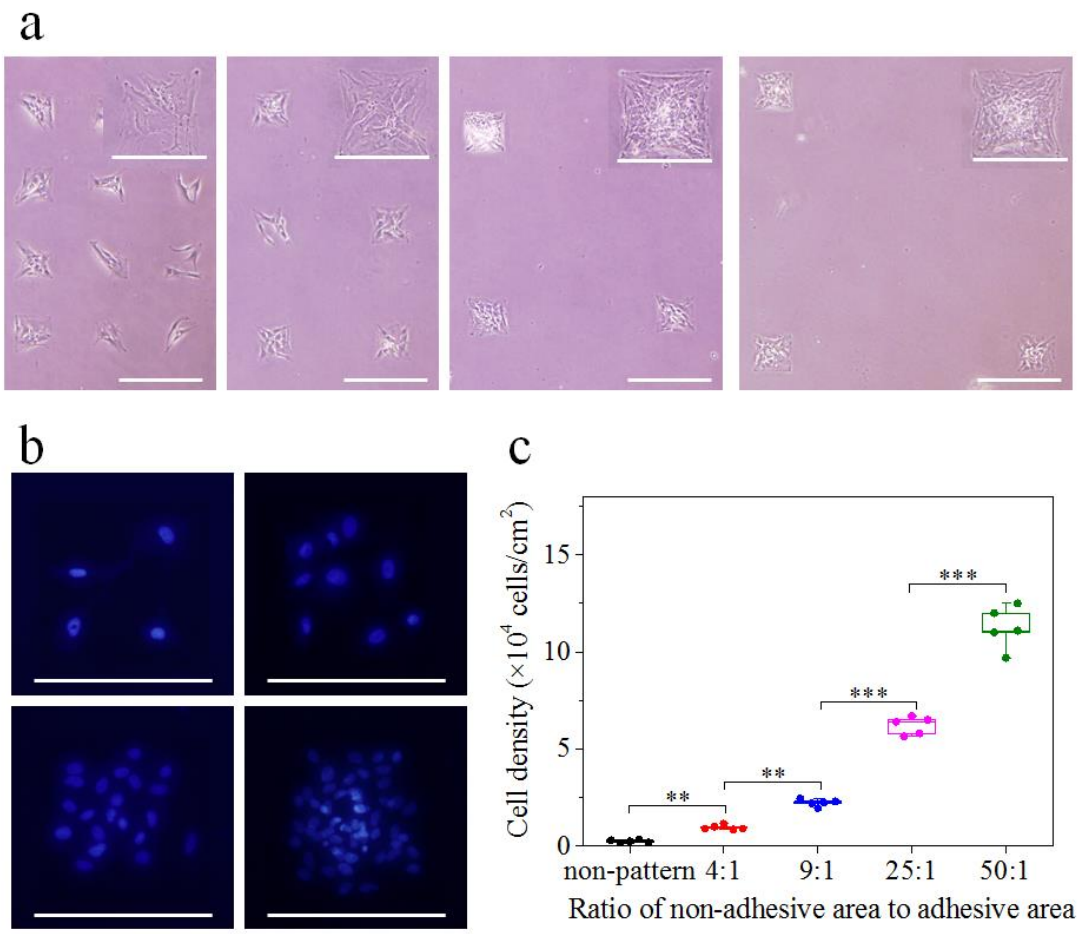

Figure 2.5 Characterization of cell adhesion and cell density on micropatterns. (a) Phase-contrast images of cell morphology on micropatterns with gradient square densities. Scale bar: 500 μm. Inserts were the magnified images. Scale bar: 200 μm. (b) Representative fluorescence images of nuclei (blue) of hMSCs cultured on micropatterns. Scale bar: 200 μm. (c) Cell density on micropatterned surfaces with gradient square density. Data represent the mean ± SD (n = 5), $^{**}p < 0.01$, $^{***}p < 0.001$.

The hMSCs at passage 4 were seeded on the micropatterned surfaces with gradient square density. Cell seeding density was selected as 2.5×10^3 cells/cm^2. Microscopic observation confirmed that hMSCs were distributed homogeneously on PVA-micropatterned surfaces. After cell culture for 24 h, the cells were only adhered on the micro-squares but not on the PVA-grafted regions (Figure 2.5a). Because of AzPhPVA efficient resistance against cell adhesion, the cells on the PVA-grafted regions migrated into the bare TCPS micro-squares during cell culture. Although each micro-square had the same cell adhesion area, the center-to-center distance of each micro-square was gradually increased. Four-type square densities of 4:1, 9:1, 25:1 and 50:1 were prepared to control cell density in each type of micro-squares. Considering that all of the seeded cells were assumed to move into the concave micro-squares, cell density in four-type micro-squares should be the same as the ratio of non-adhesive area to adhesive area. The meaning was to say that cell densities in four-type regions were theoretically 4, 9, 25 and 50 times as much as initial cell seeding density. To verify this hypothesis, nuclei were stained blue with Hoechst 33258 to count cell number in each type of micro-squares (Figure 2.5b). The density of hMSCs on non-patterned surfaces and four-type regions was calculated to be 2.5±0.7, 9.6±1.1, 22.3±1.6, 62.1±4.1, 112.6±9.6 × 10^3 cells/cm^2 (Figure 2.5c). The ratio of calculated cell density to initial cell seeding density was 1.0 ± 0.3, 3.8 ± 0.4, 8.9 ± 0.7, 24.8 ± 1.6 and 45.0 ± 3.8. The results indicated that cell density could be well controlled by changing the center-to-center distance of the neighboring micro-squares.

2.4.4 Influence of cell density on gene transfection

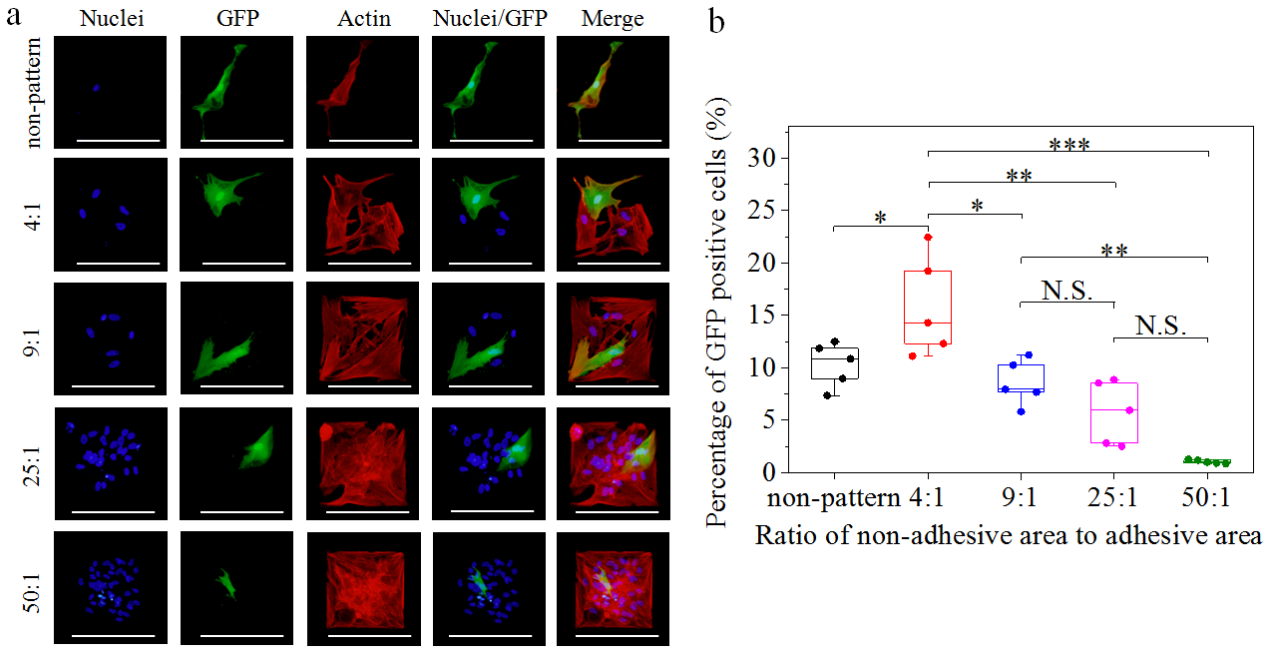

Figure 2.6 Influence of cell density on gene transfection efficiency. (a) Representative fluorescence images of transfected cells expressing GFP proteins (green). Actin filaments and nuclei were stained red and blue, respectively. Scale bar: 200 μm. (b) Percentage of successfully transfected cells in all checked cells. Data represent the mean ± SD (n = 5), N.S. represents no significant difference, *$p < 0.05$, **$p < 0.01$.

After incubation on the micro-squares for 24 h, the cells were transfected with the cationic liposome/GFP-plasmid complexes to investigate the influence of cell density on transfection efficiency through PVA-micropatterned TCPS surfaces. Representative fluorescence images of the transfected cells

expressing green fluorescence protein (GFP) were observed by a fluorescence microscope (Figure 2.6a). Nuclei and actin filaments were respectively stained blue and red. Cell number in each type of micropatterns gradually increased with increasing the center-to-center distance of the neighboring micro-squares. Gene transfection efficiency was calculated by comparing the percentage of GFP-positive cells in all examined cells (Figure 2.6b). Transfection efficiency firstly increased to the maximum of over 20% on 4:1 micropatterns and then dramatically decreased to less than 2% with increasing cell density. When the ratio of non-adhesive area to adhesive area was 50:1, gene transfection of hMSCs was almost suppressed. The results suggested that moderate cell density on 4:1 micropatterns was beneficial for gene transfection, while high cell density interfered with gene transfection.

2.4.5 Influence of cell density on cell uptake capacity

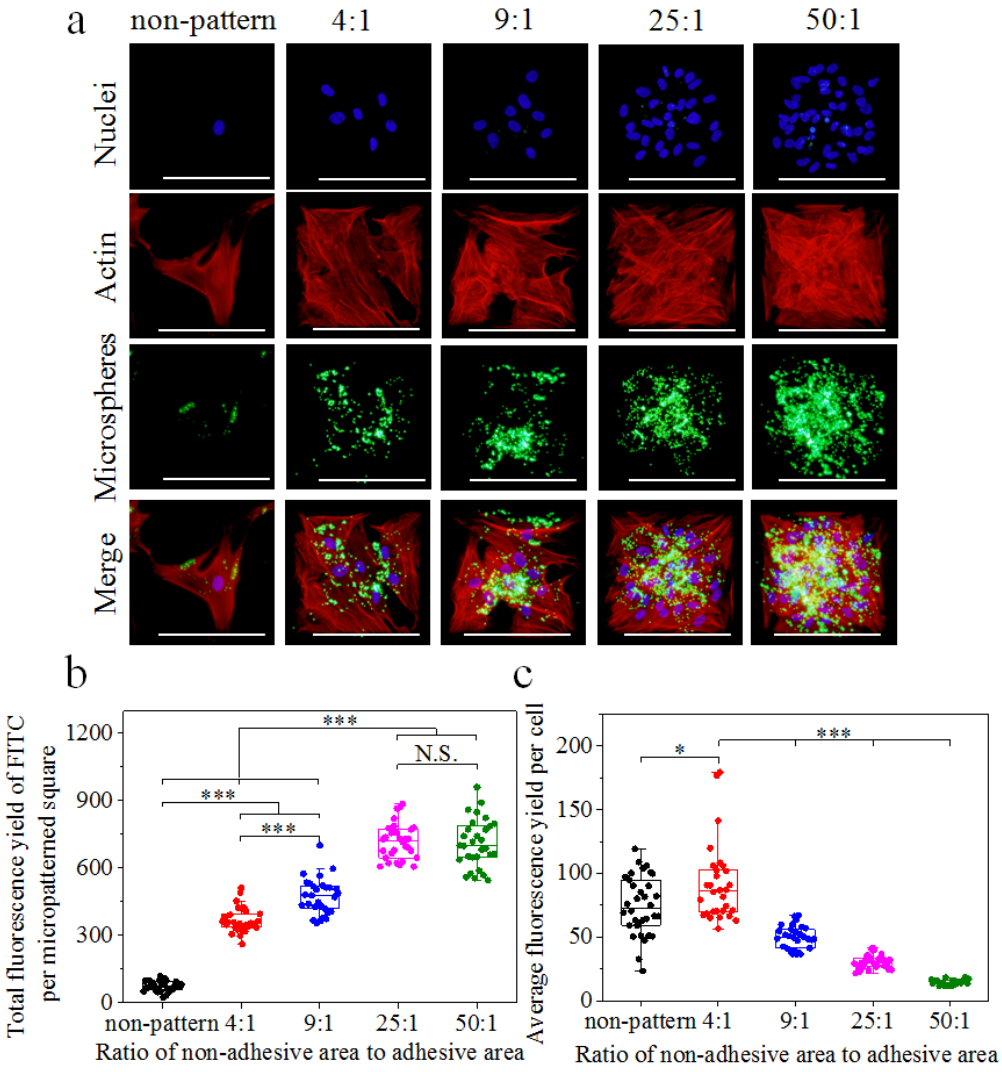

Figure 2.7 influence of cell density on cell uptake capacity. (a) Representative fluorescence images of hMSCs cultured on bare and micropatterned surfaces showing cellular uptake of FITC-labeled microspheres (green). Actin filaments and nuclei were stained red and blue, respectively. Scale bar: 200 μm. (b) Total fluorescence yield of FITC in each type square. (c) Average fluorescence yield of FITC per cell on each type micro-square. Data represent the mean ± SD (n = 30), N.S. represents no significant difference, *$p < 0.05$, ***$p < 0.001$.

Cell uptake capacity of hMSCs having different cell densities was an important aspect for efficient gene transfection. Therefore, Fluoresbrite carboxylate microspheres were applied to evaluate cell uptake capacity of nanoparticles into hMSCs. Green FITC-labeled microspheres were integrated into Lipofectamine™ 2000 transfection reagent to form the cationic complexes for the uptake experiment. Nuclei and actin filaments were stained blue and green with Hoechst 33258 and Alexa Fluor-594 phalloidin, respectively. The staining results showed that cell number increased with increasing the ratio of non-adhesive area and adhesive area (Figure 2.7a). Cytoskeleton structures were able to spread well in low density micro-squares, while the stretch of actin filaments was inhibited on the micropatterns with high cell density. Fluorescent images showed that all of the cells on the non-patterned surface and four type micropatterns presented the uptake of green microspheres and the uptake of cationic nanoparticles gradually increased in much denser cells. Further, the fluorescence yield of FITC was calculated by an ImageJ software. The quantitative results showed that the total yield of each type of squares was enhanced with increasing cell density, similar with the observation of fluorescent images (Figure 2.7b). However, the average fluorescence yield of FITC per cell showed first-increasing and then-decreasing tendency with increasing cell density (Figure 2.7c). The cells on 4:1 micropatterns showed the highest average fluorescence yield of FITC per cell. The results were similar with that of gene transfection.

2.4.6 Influence of cell density on DNA synthesis

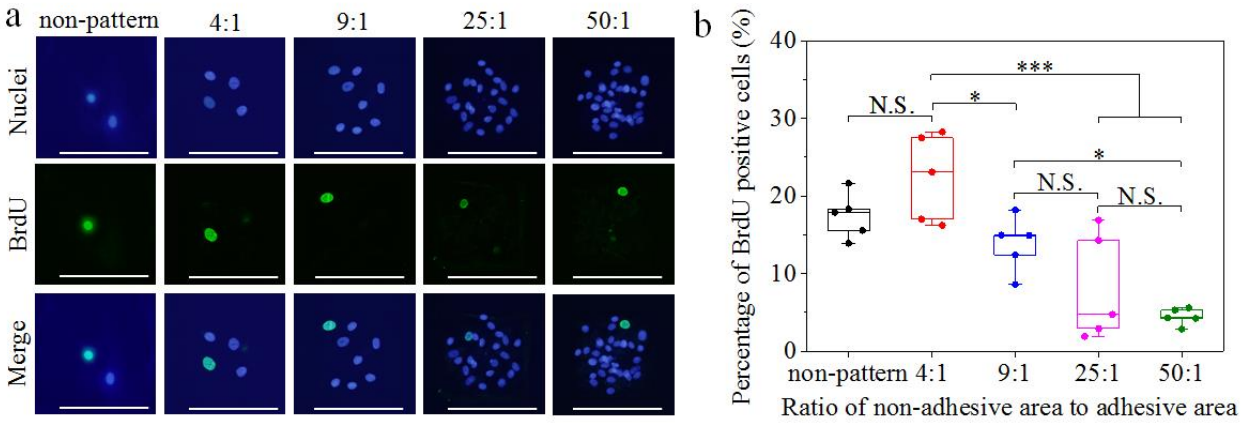

Figure 2.8 DNA synthesis of hMSCs cultured on bare and micropatterned surfaces with gradient square density. (a) Immunological fluorescence images of BrdU positive cells (green). Nuclei were stained blue. Scale bar: 200 μm. (b) Percentage of BrdU positive cells in all checked cells. Data represent the mean ± SD (n = 5), N.S. represents no significant difference, *$p < 0.05$, ***$p < 0.001$.

DNA synthesis activity played a crucial role in regulating the transfection efficiency of hMSCs on micropatterned surfaces. Therefore, the cells were stained with BrdU labeling reagent to investigate the influence of cell density on DNA synthesis activity (Figure 2.8a). Nuclei were stained blue with Hoechst 33258 to count cell number. DNA synthesis of hMSCs cultured on micropatterned surfaces with gradient density was explored by analyzing the proportion of BrdU positive cells in all checked cells. The percentage of BrdU positive cells was firstly enhanced and then diminished when cell density increased from low to high (Figure 2.8b). In specific, the percentage of BrdU positive cells on 4:1 micropatterns was as high as over 25%, while only less than 5% BrdU positive cells were observed in 50:1 micropatterned cells. BrdU staining results disclosed that DNA synthesis was enhanced in an appropriate cell density but significantly inhibited in super-high cell density.

2.5 Discussion

Cellular microenvironment plays an important role in regulating cell behaviors including cell migration, proliferation, differentiation and uptake [21-25, 29]. Micropatterning technique has been extensively cultivated to study distinct properties of cells because this method can accurately simulate cellular microenvironment [20, 34, 35]. Some studies have reported that cell density affects cellular fates through the micropatterned surfaces [27-29]. However, the influence of micropattern-dependent cell density on stem cell gene transfection is ambiguous. In this study, a square micropattern (Figure 2.4) was prepared to control gradient cell density from 2.5±0.7 to 112.6±9.6 × 10^3 cells/cm^2 on micropatterned surfaces and their influence on gene transfection of hMSCs was analyzed (Figure 5).

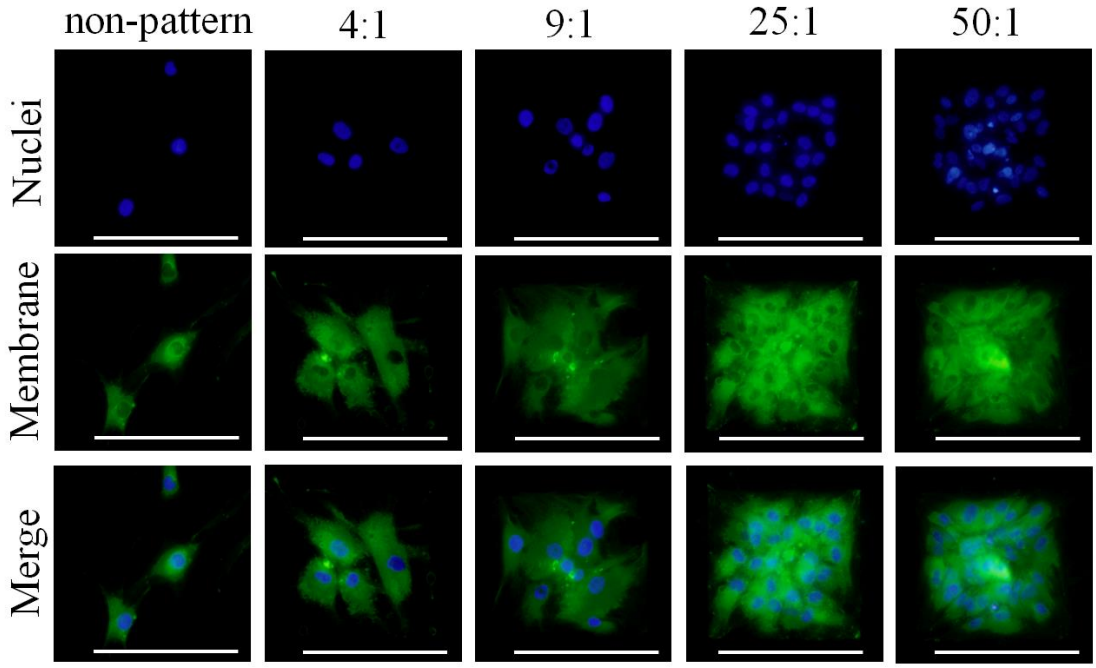

Figure 2.9 Fluorescent images of cell membrane staining of hMSCs with different density. Nuclei were stained blue. Scale bar: 200 μm.

Plasmid DNA expressing GFP proteins was incorporated into commercial Lipofectamine™ 2000 transfection reagent to carry out gene transfection experiment. The fluorescent images of transfected cells were confirmed by a fluorescence microscope (Figure 2.6a). The transfection results showed that low cell density had higher gene transfection efficiency than did high cell density. Further, transfection efficiency presented the first-increasing and then-decreasing tendency with increasing cell density (Figure 2.6b). Previous researches have reported that super-high cell density may lead to smaller cell size and induce cellular contact inhibition, while low cell density stimulates higher cell activity to promote proliferation [29, 36]. However, super-low cell density cannot stimulate cellular behaviors due to low-level cell interaction. It has been reported that appropriate cell density beneficially contributes to chondrocyte differentiation on TCPS surfaces [37]. Cell membrane was stained to evaluate cell size and cell-cell interaction (Figure 2.9). The staining results showed that cell size decreased with increasing cell density and the cells on 4:1 micropatterns presented proper cell-cell interaction. In order to verify this hypothesis, micropatterns having different diameters (30 and 60 μm) and different numbers of connecting lines (0, 1, 2, 4, and 6 short lines) were prepared to control cellular size and cell-cell interaction (Figure 2.10a, b). Transfection efficiency was enhanced with increasing cellular size and number of cell-cell contacts (Figure 2.10c), indicating that both

cell size and cell-cell interaction were able to mediate gene transfection of hMSCs. Additionally, to exclude the influence of cell protrusion on gene transfection, micropatterns with individual short lines were prepared to perform the transfection experiment (Figure 2.11a). Transfection efficiency was not affected by cell protrusion when the cell size was small, while gene transfection was slightly enhanced with increasing cell protrusion for the cells with 60-μm diameter due to increasing cell spreading area (Figure 2.11b). The results showed that gene transfection was closely associated with cell size and cell-cell interaction, rather than cell protrusion. Taken all factors together, the difference of gene transfection could be prominently affected by cell-density-dependent cell size and cell-cell interaction.

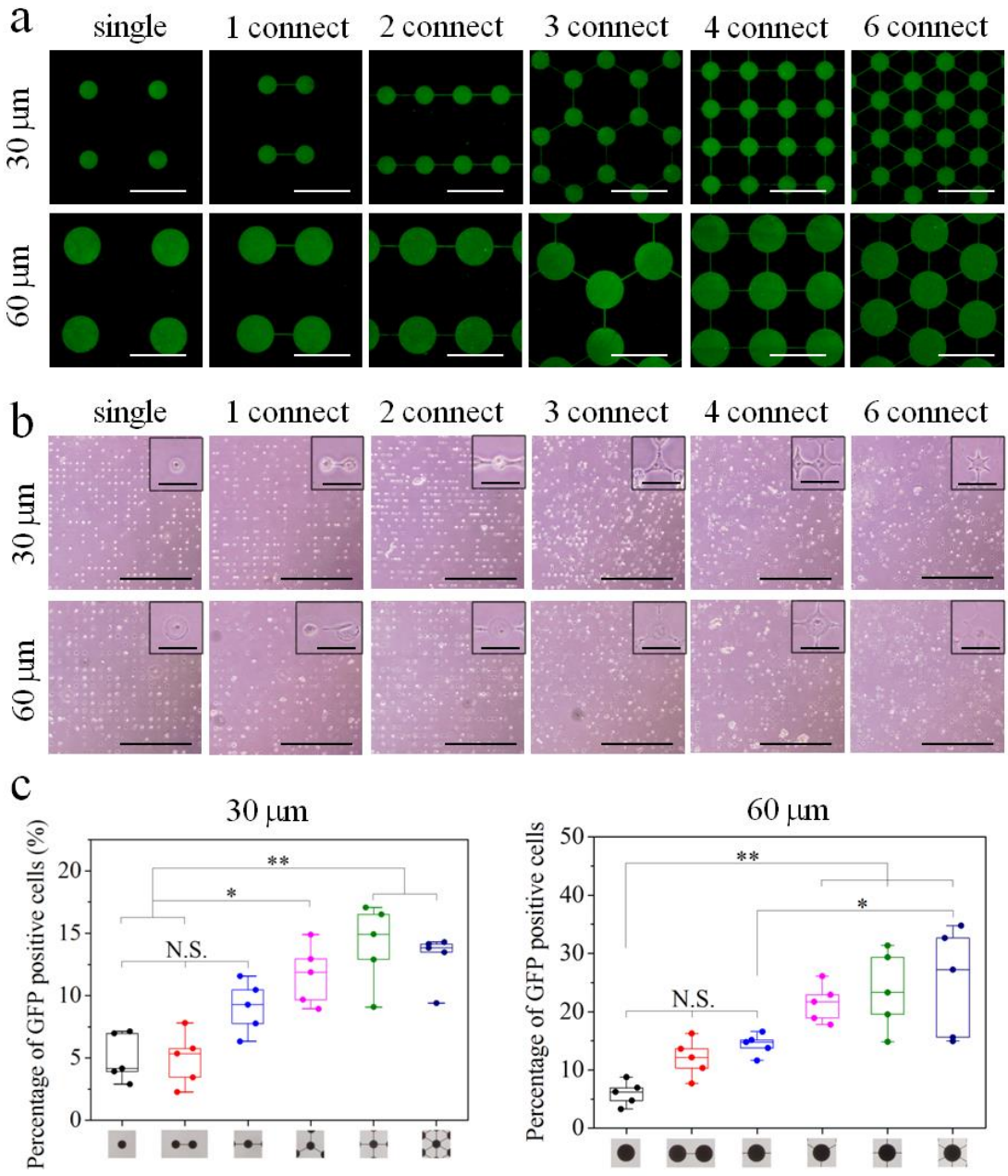

Figure 2.10 Influence of cell size and cell-cell interaction on gene transfection. (a) Immunofluorescent images of fibronectin-coated micropatterns (green) captured by a fluorescent microscope. Scale bar: 100 μm. (b) Phase-contrast images of cell morphology of hMSCs cultured on the micropatterns. Scale bar: 1000 μm. The inserts were the magnification of micropatterned cells. Scale bar: 50 μm. (c) Percentage of GFP positive cells in all examined cells on each micropattern. Data represent the mean ± SD (n = 5), N.S. represents no significant difference, *$p < 0.05$, **$p < 0.01$.

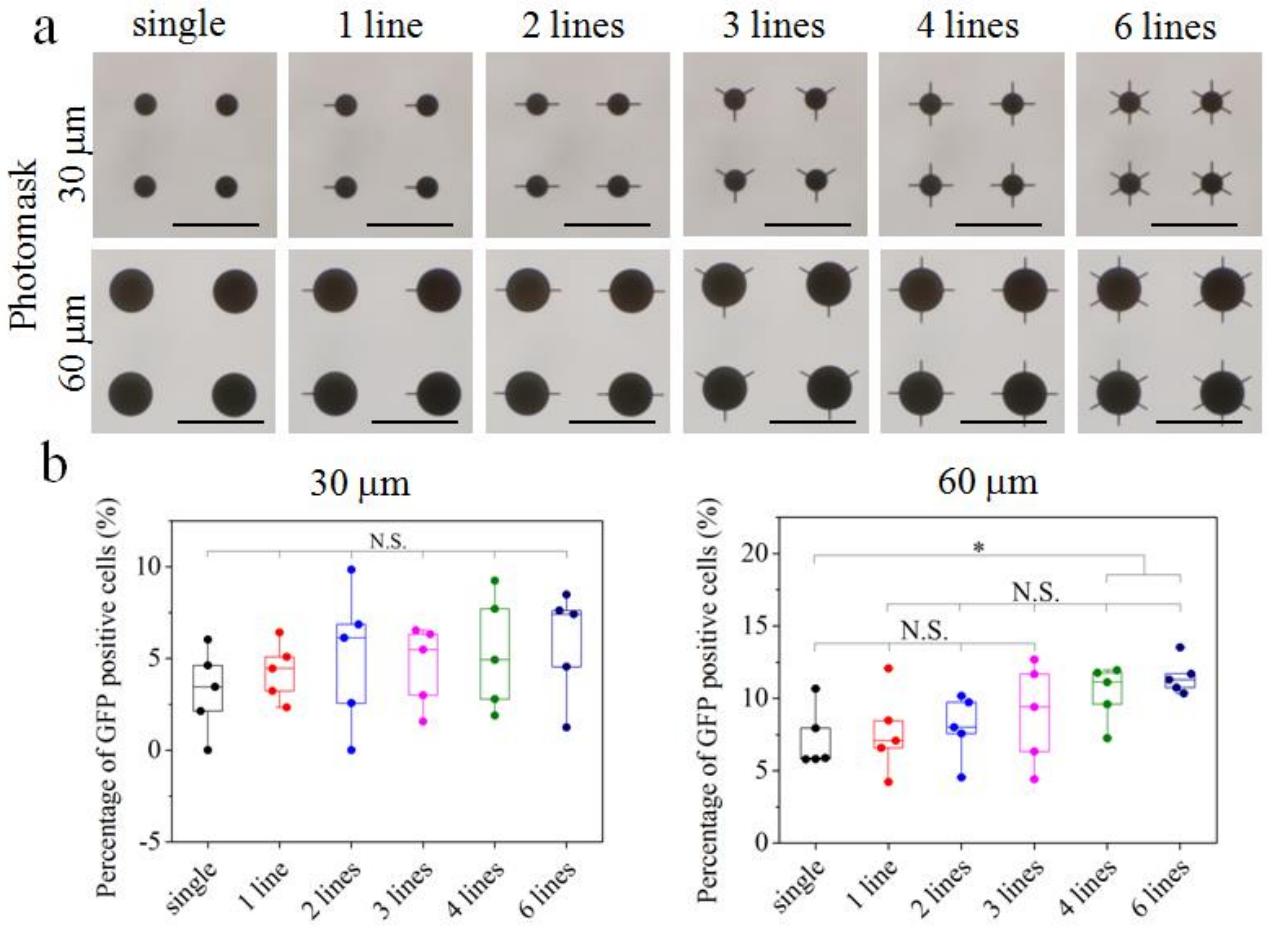

Figure 2.11 Influence of cell protrusion on gene transfection. (a) Phase-contrast images of micropatterns having different diameters (30 and 60 μm) and different numbers of short lines (0, 1, 2, 3, 4 and 6). Scale bar: 100 μm. (b) Percentage of GFP positive cells in all examined cells on each micropattern. Data represent the mean ± SD (n = 5), N.S. represents no significant difference, $*p < 0.05$.

Cell uptake capacity and DNA synthesis activity played the crucial role in regulating gene transfection of various cell densities. Here, cellular uptake of cationic nanoparticles and BrdU staining were performed to investigate their relationship with gene transfection. Both cell uptake capacity and DNA synthesis firstly increased and then decreased with increasing cell density, showing good compliance with gene transfection (Figure 2.7, Figure 2.8). In addition, it was also confirmed that larger cell sizes and more numbers of cell-cell contacts could promote cell uptake capacity (Figure 2.12a) and DNA synthesis (Figure 2.12b).

Recently, plenty of studies have concentrated on the correlation of cellular uptake and gene transfection to disclose the mechanism of internalization and trafficking in cells [16, 38-40]. It is reported that cellular uptake is partially due to cytoskeleton structures [41, 42]. The stained actin filaments showed that cells in low density formed thick stress fibers and spread well on micro-squares, while the cells with super-high density were tightly packed together and their growth was suppressed on micropatterns (Figure 2.7a). Similarly, larger cells assembled actin filaments along with both radius and concentric directions, while small cells formed the immature cortex actin at the periphery of cells (Figure 2.11c). Cell-cell line contacts could induce cells to develop actin filaments across whole short lines even nuclei. Some studies have shown that highly efficient internalization of nanoparticles strongly depends on clathrin-mediated endocytosis, which was correlated with actin filaments [43-46]. Therefore, cytoskeletal structures played the important role in regulating cell uptake capacity of exogenous particles in micropatterned cells.

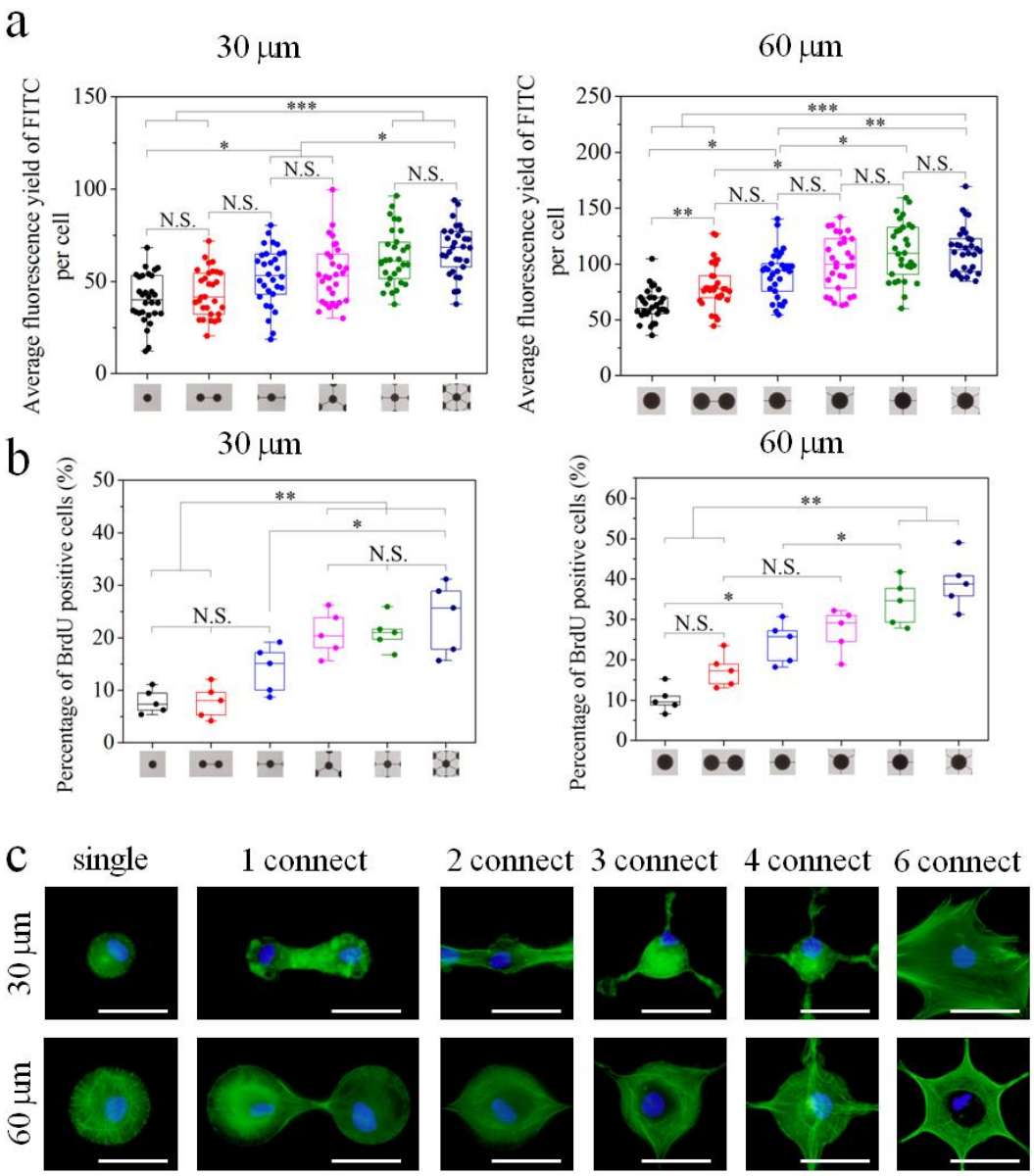

Figure 2.12 Influence of cell size and cell-cell interaction on cell uptake and DNA synthesis. (a) Cell uptake capacity of hMSCs adhered on micropatterns having different sizes and cell contact lines. Data represent the mean ± SD (n = 30), N.S. represents no significant difference, *$p < 0.05$, **$p < 0.01$, ***$p < 0.001$. (b) Percentage of BrdU positive cells on different micropatterns. Data represent the mean ± SD (n = 5), N.S. represents no significant difference, *$p < 0.05$, **$p < 0.01$. (c) Cytoskeleton structures regulated by micropatterns. Actin filaments and nuclei were stained green and blue, respectively. Scale bar: 50 μm.

Actin filaments can also weave their contractive stress fibers into the nucleus to stimulate cellular activity [47-50]. DNA synthesis is another crucial factor to affect gene transfection efficiency [32, 51]. BrdU staining demonstrated that proper cell density promoted DNA synthesis while super-high cell density inhibited DNA synthesis (Figure 2.8). It has been reported that cell-cell interaction can adjust cytoskeleton structures by cadherins and modulate intracellular tension via adherens junction [19, 52-54]. However, excessively dense colonies of stem cells lead to poor cell proliferation due to density-dependent inhibition [55, 56]. Limited nutrition and availability of signaling molecules would further decrease DNA synthesis in super-high cell density. Gene expression level was modulated by changing DNA synthesis in various cell densities. Therefore, cell density could affect transfection efficiency of exogenous genes by monitoring cell uptake and DNA synthesis.

2.6 Conclusions

A square pattern with gradient density was prepared by UV-grafting AzPhPVA onto TCPS surfaces. The micropatterns were used to control cell density arranging from 2.5±0.7 to 112.6±9.6 × 10^3 cells/cm^2. Transfection efficiency firstly increased and then significantly decreased with increasing cell density of hMSCs. The difference of transfection efficiency was strongly dependent on cell uptake capacity and DNA synthesis. Low-level cell-cell interaction leaded to low gene transfection efficiency in super-low cell density, while density-dependent inhibition caused low transfection efficiency due to limited nutrition and availability of signaling molecules in super-high cell density. Therefore, proper cell density was beneficial for gene transfection. Micropatterning technique provides a useful tool to investigate the potential application of stem cell transfection in gene therapy.

2.7 References

[1] C. E. Dunbar, K. A. High, J. K. Joung, D. B. Kohn, K. Ozawa, M. Sadelain, Gene therapy comes of age, Science 359(6372) (2018) eaan4672.
[2] J. Slone, T. Huang, The special considerations of gene therapy for mitochondrial diseases, NPJ Genomic Medicine 7 (2020) 7.
[3] C. M. Blakely, T. B. K. Watkins, W. Wu, B. Gini, J. J. Chabon, C. E. McCoach, N. McGranahan, G. A. Wilson, N. J. Birkbak, V. R. Olivas, J. Rotow, A. Maynard, V. Wang, M. A. Gubens, K. C. Banks, R. B. Lanman, A. F. Caulin, J. S. John, A. R. Cordero, P. Giannikopoulos, A. D. Simmons, P. C. Mack, D. R. Gandara, H. Husain, R. C. Doebele, J. W. Riess, M. Diehn, C. Swanton, T. G. Bivona, Evolution and clinical impact of co-occurring genetic alterations in advanced-stage EGFR-mutant lung cancers, Nature Genetics 49 (2017) 1693-1704.
[4] S. Y. Alhaji, S. C. Ngai, S. Abdullah, Silencing of transgene expression in mammalian cells by DNA methylation and histone modifications in gene therapy perspective, Biotechnology and Genetic Engineering Reviews 35(1) (2018) 1-25.
[5] S. L. Ginn, I. E. Alexander, M. L. Edelstein, M. R. Abedi, J. Wixon, Gene therapy clinical trials worldwide to 2012-an update, Journal of Gene Medicine 15(2) (2013) 65-77.
[6] G. Shim, D. Kim, Q. V. Le, G. T. Park, T. Kwon, Y. K. Oh, Nonviral delivery systems for cancer gene therapy: strategies and challenges, Current Gene Therapy 18(1) (2018) 3-20.
[7] Y. Wang, Y. Nie, Z. Ding, M. Yao, R. Du, L. Zhang, S. Wang, D. Li, Y. Wang, M. Cao, An amphiphilic peptide with cell penetrating sequence for highly efficient gene transfection, Colloids and Surfaces A: Physicochemical and Engineering Aspects 590 (2020) 124529.
[8] M. S. Al-Dosari, X. Gao, Nonviral gene delivery: principle, limitations, and recent progress, The AAPS Journal 11 (2009) 671.
[9] N. P. Gabrielson, D. W. Pack, Acetylation of polyethylenimine enhances gene delivery via weakened polymer/DNA interactions, Biomacromolecules 7(8) (2006) 2427-2435.
[10] J. Yang, Q. Zhang, H. Chang, Y. Cheng, Surface-engineered dendrimers in gene delivery, Chemical Reviews 115(11) (2015) 5274-5300.
[11] J. P. Gratton, J. Yu, J. W. Griffith, R. W. Babbitt, R. S. Scotland, R. Hickey, F. J. Giordano, W. C. Sessa, Cell-permeable peptides improve cellular uptake and therapeutic gene delivery of replication-deficient viruses in cells and in vivo, Nature Medicine 9 (2003) 357-362.
[12] B. Ma, S. Zhang, H. Jiang, B. Zhao, H. Lv, Lipoplex morphologies and their influences on transfection

efficiency in gene delivery, Journal of Controlled Release 123(3) (2007) 184-194.
[13] C. Liu, Q. Feng, J. Sun, Lipid nanovesicles by microfluidics: manipulation, synthesis, and drug delivery, Advanced Materials 31(45) (2019) 1804788.
[14] M. A. Mintzer, E. E. Simanek, Nonviral vectors for gene delivery, Chemical Reviews 109(2) (2009) 259-302.
[15] T. Niidome, L. Huang, Gene therapy progress and prospects: nonviral vectors, Gene Therapy 9 (2002) 1647-1652.
[16] I. A. Khalil, K. Kogure, H. Akita, H. Harashima, Uptake pathways and subsequent intracellular trafficking in nonviral gene delivery, Pharmacological Reviews 58(1) (2006) 32-45.
[17] E. L. Berg, Y. C. Hsu, J. A. Lee, Consideration of the cellular microenvironment: physiologically relevant co-culture systems in drug discovery, Advanced Drug Delivery Reviews 69-70 (2014) 190-204.
[18] E. Adachi, I. Hopkinson, T. Hayashi, Basement-membrane stromal relationships: interactions between collagen fibrils and the lamina densa, International Review of Cytology 173 (1997) 73-156.
[19] K. A. Purpura, J. E. Aubin, P. W. Zandstra, Sustained in vitro expansion of bone progenitors is cell density dependent, Stem Cells 22(1) (2004) 39-50.
[20] X. Wang, W. Song, N. Kawazoe, G. Chen, The osteogenic differentiation of mesenchymal stem cells by controlled cell-cell interaction on micropatterned surfaces, Journal of Biomedical Materials Research Part A 101(12) (2013) 3388-95.
[21] T. Hoshiba, N. Kawazoe, T. Tateishi, G. Chen, Development of extracellular matrices mimicking stepwise adipogenesis of mesenchymal stem cells, Advanced Materials 22(28) (2010) 3042-3047.
[22] K. Lee, Y. Chen, X. Li, Y. Wang, N. Kawazoe, Y. Yang, G. Chen, Solution viscosity regulates chondrocyte proliferation and phenotype during 3D culture, Journal of Materials Chemistry B 7(48) (2019) 7713-7722.
[23] Y. Yang, X. Wang, Y. Wang, X. Hu, N. Kawazoe, Y. Yang, G. Chen, Influence of cell spreading area on the osteogenic commitment and phenotype maintenance of mesenchymal stem cells, Scientific Reports 9 (2019) 6891.
[24] Y. Tsuda, T. Shimizu, M. Yamato, A. Kikuchi, T. Sasagawa, S. Sekiya, J. Kobayashi, G. Chen, T. Okano, Cellular control of tissue architectures using a three-dimensional tissue fabrication technique, Biomaterials 28(33) (2007) 4939-4946.
[25] W. Zauner, N. A. Farrow, A. M. R. Haines, In vitro uptake of polystyrene microspheres: effect of particle size, cell line and cell density, Journal of Controlled Release 71(1) (2001) 39-51.
[26] X. Wang, X. Hu, N. Kawazoe, Y. Yang, G. Chen, Manipulating cell nanomechanics using micropatterns, Advanced Functional Materials 26(42) (2016) 7634-7643.
[27] A. S. Mao, J. W. Shin, D. J. Mooney, Effects of substrate stiffness and cell-cell contact on mesenchymal stem cell differentiation, Biomaterials 98 (2016) 184-191.
[28] K. Kim, D. A. Dean, A. G. Mikos, J. P. Fisher, Effect of initial cell seeding density on early osteogenic signal expression of rat bone marrow stromal cells cultured on cross-linked poly(propylene fumarate) disks, Biomacromolecules 10 (2009) 1810-1817.
[29] W. Song, H. Lu, N. Kawazoe, G. Chen, Gradient patterning and differentiation of mesenchymal stem cells on micropatterned polymer surface, Journal of Bioactive and Compatible Polymers 26(3) (2011) 242-256.
[30] X. Wang, W. Song, N. Kawazoe, G. Chen, Influence of cell protrusion and spreading on adipogenic differentiation of mesenchymal stem cells on micropatterned surfaces, Soft Matter 9(16) (2013) 4160-4166.
[31] X. Wang, T. Nakamoto, I. Dulińska-Molak, N. Kawazoe, G. Chen, Regulating the stemness of mesenchymal stem cells by tuning micropattern features, Journal of Materials Chemistry B 4(1) (2016)

37-45.
[32] Y. Yang, X. Wang, X. Hu, N. Kawazoe, Y. Yang, G. Chen, Influence of cell morphology on mesenchymal stem cell transfection, ACS Applied Materials & Interfaces 11(2) (2019) 1932-1941.
[33] X. Wang, X. Hu, J. Li, A. C. M. Russe, N. Kawazoe, Y. Yang, G. Chen, Influence of cell size on cellular uptake of gold nanoparticles, Biomaterials Science 4(6) (2016) 970-978.
[34] J. Fan, P. Ray, Y. W. Lu, G. Kaur, J. J. Schwarz, L. Q. Wan, Cell chirality regulates intercellular junctions and endothelial permeability, Science Advances 4(10) (2018) eaat2111.
[35] Y. H. Tee, T. Shemesh, V. Thiagarajan, R. F. Hariadi, K. L. Anderson, C. Page, N. Volkmann, D. Hanein, S. Sivaramakrishnan, M. M. Kozlov, A. D. Bershadsky, Cellular chirality arising from the self-organization of the actin cytoskeleton, Nature Cell Biology 17 (2015) 445-457.
[36] Y. K. Luu, E. Capilla, C. J. Rosen, V. Gilsanz, J. E. Pessin, S. Judex, C. T. Rubin, Mechanical stimulation of mesenchymal stem cell proliferation and differentiation promotes osteogenesis while preventing dietary-induced obesity, Biomaterials 24(1) (2009) 50-61.
[37] M. Takagi, Y. Umetsu, M. Fujiwara, S. Wakitani, High inoculation cell density could accelerate the differentiation of human bone marrow mesenchymal stem cells to chondrocyte cells, Journal of Bioscience and Bioengineering 103(1) (2007) 98-100.
[38] S. F. Peng, M. T. Tseng, Y. C. Ho, M. C. Wei, Z. X. Liao, H. W. Sung, Mechanisms of cellular uptake and intracellular trafficking with chitosan/DNA/poly(γ-glutamic acid) complexes as a gene delivery vector, Biomaterials 32(1) (2011) 239-248.
[39] M. R. Rekha, C. P. Sharma, Hemocompatible pullulan-polyethyleneimine conjugates for liver cell gene delivery: in vitro evaluation of cellular uptake, intracellular trafficking and transfection efficiency, Acta Biomaterialia 7(1) (2011) 370-379.
[40] J. Shi, J. L. Choi, B. Chou, R. N. Johnson, J. G. Schellinger, S. H. Pun, Effect of polyplex morphology on cellular uptake, intracellular trafficking, and transgene expression, ACS Nano 7(12) (2013) 10612-10620.
[41] Y. Wang, Y. Yang, X. Wang, T. Yoshitomi, N. Kawazoe, Y. Yang, G. Chen, Micropattern-controlled chirality of focal adhesions regulates the cytoskeletal arrangement and gene transfection of mesenchymal stem cells, Biomaterials 271 (2021) 120751.
[42] O. L. Mooren, B. J. Galletta, J. A. Cooper, Roles for actin assembly in endocytosis, Annual Review of Biochemistry 81 (2012) 661-686.
[43] M. Kaksonen, C. P. Toret, D. G. Drubin, A modular design for the clathrin- and actin-mediated endocytosis machinery, Cell 123(2) (2005) 305-320.
[44] M. Kaksonen, C. P. Toret, D. G. Drubin, Harnessing actin dynamics for clathrin-mediated endocytosis, Nature Reviews Molecular Cell Biology 7 (2006) 404-414.
[45] Y. Wang, Y. Yang, X. Wang, N. Kawazoe, Y. Yang, G. Chen, The varied influences of cell adhesion and spreading on gene transfection of mesenchymal stem cells on a micropatterned substrate, Acta Biomaterialia 125 (2021) 100-111.
[46] D. Yarar, C. M. Waterman-Storer, S. L. Schmid, A dynamic actin cytoskeleton functions at multiple stages of clathrin-mediated endocytosis, Molecular Biology of the Cell 16(2) (2005) 964-975.
[47] G. Nardone, J. O. Cruz, J. Vrbsky, C. Martini, J. Pribyl, P. Skládal, M. Pešl, G. Caluori, S. Pagliari, F. Martino, Z. Maceckova, M. Hajduch, A. Sanz-Garcia, N. M. Pugno, G. B. Stokin, G. Forte, YAP regulates cell mechanics by controlling focal adhesion assembly, Nature Communications 8 (2017) 15321.
[48] J. Stricker, T. Falzone, M. L. Gardel, Mechanics of the F-actin cytoskeleton, Journal of Biomechanics 43(1) (2010) 9-14.
[49] X. Wang, X. Hu, I. Dulińska-Molak, N. Kawazoe, Y. Yang, G. Chen, Discriminating the independent influence of cell adhesion and spreading area on stem cell fate determination using micropatterned surfaces,

Scientific Reports 6 (2016) 28708.
[50] C. M. Lewis, A. K. Smith, B. A. Kamen, Receptor-mediated folate uptake is positively regulated by disruption of the actin cytoskeleton, Cancer Research 58(14) (1998) 2952-2956.
[51] Y. Wang, Y. Yang, T. Yoshitomi, N. Kawazoe, Y. Yang, G. Chen, Regulation of gene transfection by cell size, shape and elongation on micropatterned surfaces, Journal of Materials Chemistry B 9 (2021) 4329-4339.
[52] Z. Liu, J. L. Tan, D. M. Cohen, M. T. Yang, N. J. Sniadecki, S. A. Ruiz, C. M. Nelson, C. S. Chen, Mechanical tugging force regulates the size of cell-cell junctions, PNAS 107(22) (2010) 9944-9949.
[53] G. Charras, A. S. Yap, Tensile forces and mechanotransduction at cell-cell junctions, Current Biology 28(8) (2018) R445-R457.
[54] C. M. Nelson, C. S. Chen, VE-cadherin simultaneously stimulates and inhibits cell proliferation by altering cytoskeletal structure and tension, Journal of Cell Science 116 (2003) 3571-3581.
[55] M. G. P. Stoker, H. Rubin, Density dependent inhibition of cell growth in culture, Nature 215 (1967) 171-172.
[56] T. Ooki, N. Murata-Kamiya, A. Takahashi-Kanemitsu, W. Wu, M. Hatakeyama, High-molecular-weight hyaluronan is a hippo pathway ligand directing cell density-dependent growth inhibition via PAR1b, Developmental Cell 49(4) (2019) 590-604.

Chapter 3

Regulation of gene transfection by cell size, shape and elongation on micropatterned surfaces

3.1 Abstract

Gene transfection has been widely studied due to its potential applications in tissue repair and gene therapy. Many studies have focused on designing gene carriers and developing novel transfection techniques. However, the influence of cell size, shape and elongation on gene transfection has rarely been investigated. In this study, poly(vinyl alcohol)-micropatterned surfaces were prepared to precisely manipulate the size, shape and elongation of mesenchymal stem cells, and the influences of these factors on gene transfection were investigated. Cell size showed a significant influence on gene transfection. Elongation could affect the gene transfection of large cells but not small cells. Cells with a large spreading area and high aspect ratio showed high transfection with exogenous plasmid DNA. In particular, the transfection efficiency was the highest in micropatterned cells with a spreading area of 5024 μm^2 and an aspect ratio of 8:1. In contrast, cell shape had no significant influence on gene transfection. The different influences of cell size, shape and elongation were correlated with their respective impacts on cytoskeletal structures, cellular nanoparticle uptake and DNA synthesis. Cells with a large size and elongated morphology showed well-organized actin filaments with a high cellular modulus, therefore promoting cellular nanoparticle uptake and DNA synthesis. Cells with different shapes showed similarities in actin filament organization, cellular modulus, uptake capacity and DNA synthesis. The results suggest the importance of cell size and elongation in exogenous gene transfection and should provide useful information for gene transfection and gene therapy.

3.2 Introduction

Interaction between cells and the microenvironment is critical for the maintenance of cell activity and tissue metabolism [1-5]. Biological and physicochemical cues from the microenvironment provide various necessary signals to induce cellular responses [6]. In particular, physical cues, such as matrix viscoelasticity and cell morphology, have recently been found to play a crucial role in controlling cell functions [7-12]. Cells in tissues present various morphologies to adapt to the microenvironment [13-15]. Cell size, geometry and aspect ratio have been shown to regulate cell functions, including cell adhesion, migration, division, matrix secretion and differentiation [16-19]. Physical cellular cues can be controlled through a variety of

micropattern structures [20, 21]. Cells with different morphologies respond to microenvironmental signals by reorganizing their cytoskeletal structures and transducing the signals to the nucleus [9, 22-24]. The morphological features of cells not only directly affect cell functions but also have some influence on the uptake of extracellular vesicles and nanoparticles [25, 26].

The transportation of extracellular nanoparticles, such as liposomes, into cells is an initial and critical step for gene transfection, which has broad applications in gene therapy and stem cell research [27-31]. The highly efficient transmembrane delivery of exogenous DNA into target cells is considered critical for successful gene transfection [32, 33]. Research has been focused on the design of efficient gene carriers and the development of novel transfection techniques [34, 35]. In contrast, the influence of cellular morphology on exogenous gene transfection has barely been recognized. In our previous research, we found that cell size and elongation could influence exogenous plasmid DNA transfection into human bone marrow-derived mesenchymal stem cells [36]. However, only round cells and aspect ratio of cell size having a spreading area of 5027 μm^2 were investigated. It remains unclear whether different cell shapes, such as triangles, squares, pentagons and hexagons, and cell elongation of different cell sizes have any influence on exogenous plasmid DNA transfection. Therefore, in this study, a series of micropatterns with different shapes, sizes and aspect ratios were produced through photolithography. The micropatterned surfaces were used to precisely control the shape, size and elongation of human mesenchymal stem cells to systematically investigate their influences on gene transfection. The correlations between cytoskeletal structures and gene transfection of cells on micropatterned surfaces were clarified.

3.3 Materials and methods

3.3.1 Production and analysis of micropatterns

The designed micropatterns with different sizes, shapes and aspect ratios were successfully produced on TCPS discs using photoreactive PVA through photolithography, as mentioned in 2.3.2. The photomasks contained micropatterns of different sizes (spreading areas of 314, 706, 1256, 2826 and 5024 μm^2), shapes (geometries of circles, triangles, squares, pentagons and hexagons) and elongations (aspect ratios of 1:1, 2:1, 4:1 and 8:1). The micropatterns were generated after ultrasonic washing. A phase-contrast microscope was used to capture images of the prepared micropatterns. An MFP-3D-BIO atomic force microscope (Oxford Instruments, CA, USA) was used to further characterize the micropatterns. A cantilever with a nitride tip was fixed on the holder to scan the micropatterns. Examination was performed in contact mode in water, and the scanned area was 90×90 μm^2. The mean and standard deviation (SD) were calculated from three independent measurements of different micropatterns.

Fibronectin was coated on the micropatterned surfaces to enhance cell attachment. To visualize the coated fibronectin on the micropatterns, mouse anti-fibronectin primary antibody (1:200 in BSA) was incubated with the fibronectin-coated micropatterns at 4°C overnight, followed by washing and incubation with the secondary antibody (Alexa Fluor-488-labelled goat anti-mouse IgG antibody, 1:1000 in PBS) in the dark. A fluorescence microscope was applied to observe fluorescence images of the stained micropatterns.

3.3.2 Cell culture and fluorescence staining of actin filaments and nuclei

The hMSCs at passage 2 were subcultured to passage 4 in BulletKit™ mesenchymal stem cell growth medium (MSCGM, Lonza) at 37°C in a 5% CO_2 incubator. The hMSCs suspension at passage 4 in a 25-cm^2

cell culture flask (Falcon, Corning Life Sciences, MA, USA) were dropped into each glass ring. After hMSCs were cultured at 37°C in a 5% CO_2 incubator for 6 h, the glass rings were removed, and the DMEM was refreshed to wash away nonadherent hMSCs. After incubation for 18 h, an Olympus BX51 microscope was used to observe the micropatterned cells. Then, the cells were fixed with 4% paraformaldehyde for 10 min and washed with PBS. Then, 1% Triton™ X-100 (Sigma-Aldrich, USA) and 2% BSA were used to permeabilize and block the micropatterned cells. After 3 PBS washes, Alexa Fluor-488 phalloidin (1:40 in PBS, Invitrogen, CA, USA) was used to stain actin filaments in the dark for 20 min. Hoechst 33258 (1:1000 in PBS, FUJIFILM Wako Pure Chemical, Osaka, Japan) was used to stain nuclei in the dark for 10 min. A fluorescence microscope with a DP-70 CCD camera (Olympus) was used to observe the fluorescence images.

3.3.3 Analysis of cellular stiffness

Young's modulus of the micropatterned hMSCs was analyzed using a point-contact nanoindentation system installed in an MFP-3D-BIO AFM instrument. Nanoindentation was performed using a silicon nitride cantilever with a nominal spring constant of 0.06 N/m (Novascan Technologies, IA, USA). A silica sphere 600 nm in diameter was attached to the cantilever. Before measurement of the living cells, the thermal noise method was used to correct the real spring constant of the cantilever. The trigger force was set to 2 nN, and the indentation rate was 4 μm/s. After hMSCs were cultured on the micropatterns for 24 h as described above, the cells were measured in DMEM. A phase-contrast microscope was used to observe the silica sphere as it approached the highest region of micropatterned cells. Each sample was measured within 2 h to avoid the influence of cell viability. Young's modulus of the cells was analyzed from force-distance curves. A Hertz model was used to correct baseline tilt with a Poisson ratio of 0.5. Twenty force-distance curves were analyzed from each cell, and a total of ten cells were measured from each sample to calculate the mean and SD.

3.3.4 Gene transfection of micropatterned hMSCs

Lipofectamine™ 2000 transfection reagent was used to increase the transfection efficiency of the pAcGFP1-N1 gene in micropatterned cells, as mentioned in 2.3.5. The size of cationic liposome/plasmid complexes was measured by dynamic light scattering (DLS, Beckman Coulter, Fullerton, USA). After washing with PBS, a fluorescence microscope was used to capture fluorescence images of the transfected cells. The fluorescent yield of GFP was characterized using ImageJ software (National Institutes of Health, Bethesda, MD, USA). Only single cells were counted. Finally, the transfection efficiency of exogenous plasmid DNAs was determined by the percentage of GFP-positive cells among the total number of single cells. The mean and SD were calculated from five independent experiments ($\geq$ 200 cells).

3.3.5 Cellular uptake of Fluoresbrite carboxylate microspheres

Fluoresbrite carboxylate microspheres with a radius of 250 nm were used to investigate the cellular uptake of nanoparticles. The uptake experiment was performed by the same procedures described in 2.3.6. A fluorescence microscope was applied to observe the fluorescence images of the micropatterned cells. The fluorescence images were analyzed by ImageJ software. Only single cells were counted. The fluorescence yield of FITC per cell was evaluated by the same method described above. The mean and SD were calculated

from five independent experiments.

3.3.6 Analysis of DNA synthesis by BrdU staining

BrdU staining was applied to evaluate the DNA synthesis of the micropatterned hMSCs, as mentioned in 2.3.7. A fluorescence microscope was used to observe the stained cells and count BrdU-positive cells among all checked hMSCs. Only single cells were counted. The percentage of BrdU-positive cells relative to the total number of cells was calculated as an indicator of DNA synthesis activity. The mean and SD were calculated from five independent experiments (≥ 200 cells).

3.3.7 YOYO-1 and LysoTracker deep red staining

Subcellular accumulation of the lipoplexes was evaluated with YOYO-1 (Abcam, USA) and LysoTracker deep red (Life Technologies, USA) staining. Plasmid was labeled with YOYO-1 (0.1 μM in Opti-MEM medium) for 1 h. YOYO-1-labeled plasmid was incorporated into Lipofectamine 2000 solution and incubated for 30 min to prepare the lipoplexes. After hMSCs were cultured on the micropatterns and non-patterned surfaces for 24 h, the cells were transfected with YOYO-1-labeled plasmid/Lipofectamine lipoplexes. At different time points (5 min, 15 min, 30 min, 1 h, 2 h, 4 h and 6 h), Opti-MEM medium with the lipoplexes was removed and washed with PBS. The endosomes were stained with LysoTracker deep red (0.75 nM in Opti-MEM medium) for 1 h. After that, the cells were fixed with 4% paraformaldehyde for 10 min and muclei were stained with Hoechst 33258 in the dark for 10 min. The stained cells were observed with a fluorescence microscope.

3.3.8 Statistical analysis

Statistical analysis was carried out in KyPlot 5.0 software (KyensLab, Tokyo, Japan), and the quantitative and fluorescence results are presented as the mean ± SD. Significant differences were determined by one-way analysis of variance (ANOVA) with Tukey's post-test for multiple variables. When the *p* value was less than 0.05, the results were considered significantly different.

3.4 Results

3.4.1 Micropatterned surfaces and cellular morphology

As a protein-resistant polymer, photoreactive PVA was coated onto TCPS discs and subsequently micropatterned using the designed photomasks through photolithography (Figure 3.1a). The photomasks were composed of transparent micropatterns containing different spreading areas, shapes and aspect ratios (Figure 3.1b, c). The dark regions were designed against UV light and prevented crosslinking of the photoreactive AzPhPVA. During UV irradiation, the UV-irradiated AzPhPVA molecules were inter- and intramolecularly crosslinked and grafted to the TCPS discs, while the AzPhPVA molecules under the dark regions remained uncrosslinked. After the samples were ultrasonically washed in a water bath, the uncrosslinked AzPhPVA was removed to expose the bare TCPS micropatterns. The formation of micropatterns was confirmed by phase-contrast microscopic observation (Figure 3.2). These results show

that the prepared micropatterns had the same size, shape and elongation as those of the designed photomasks.

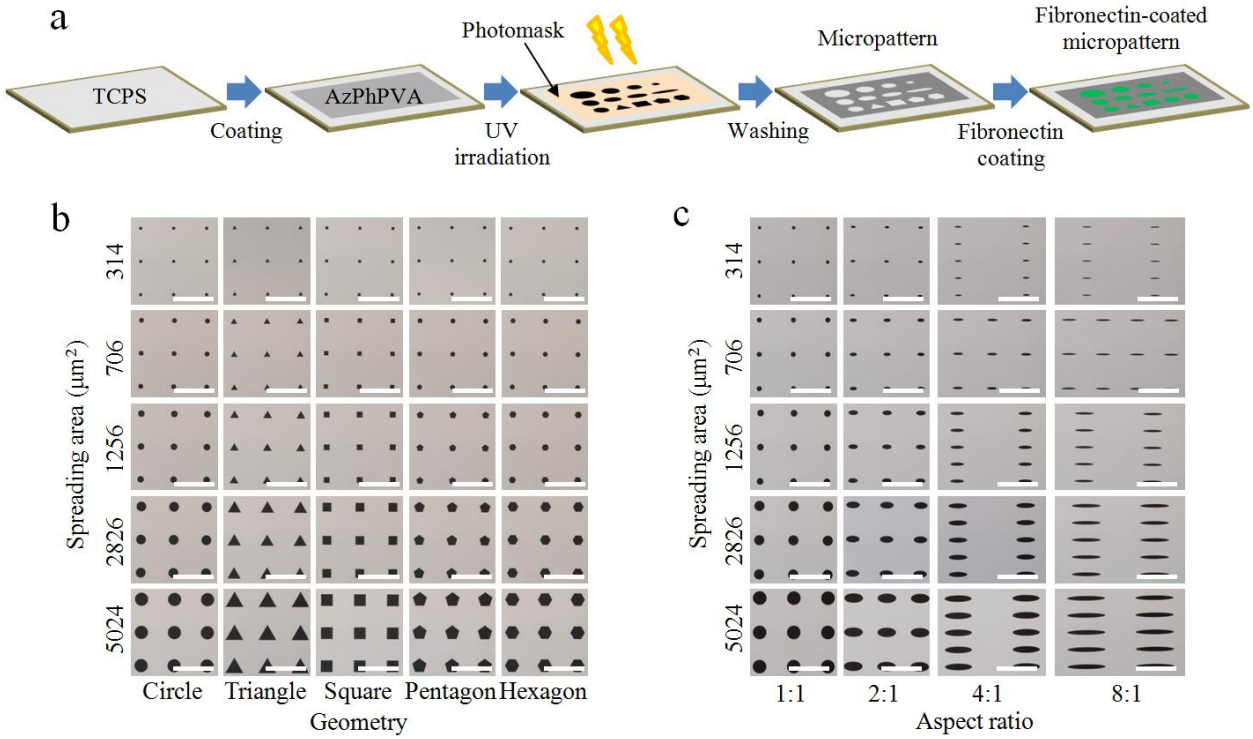

Figure 3.1 (a) Preparation scheme of micropatterns using photoreactive AzPhPVA. (b, c) Representative phase-contrast photomicrographs of photomasks containing micropatterns with different shapes (b) and aspect ratios (c). Spreading area was 314, 706, 1256, 2826 and 5024 μm^2. Scale bar: 200 μm.

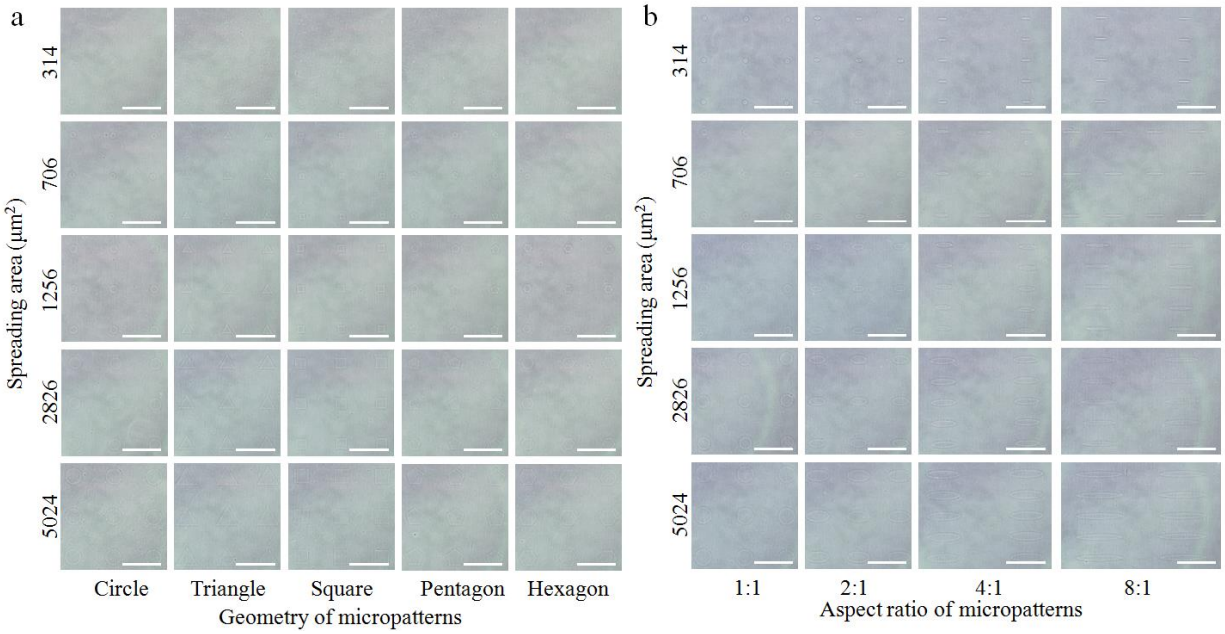

Figure 3.2 (a, b) Representative phase-contrast photomicrographs of photomasks containing micropatterns with different shapes (a) and aspect ratios (b). Spreading area was 314, 706, 1256, 2826 and 5024 μm^2. Scale bar: 200 μm.

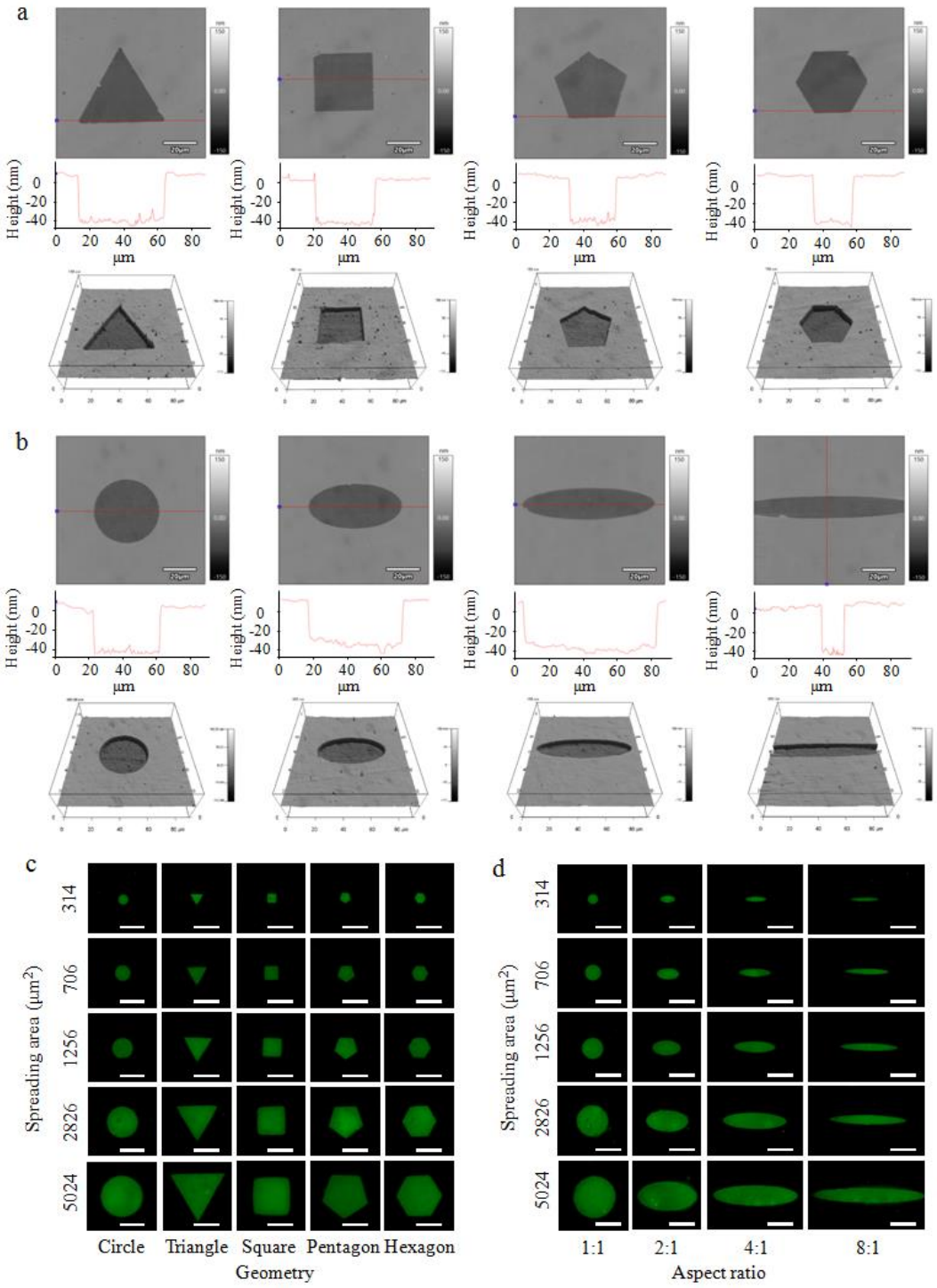

Figure 3.3 Characterization of micropatterns with different sizes, shapes and aspect ratios. (a, b) Height (top), cross-sectional view (middle) and 3D (bottom) images of the micropatterns obtained by AFM. The micropatterns shown here had an area of 1256 μm^2 and different shapes (triangles, squares, pentagons and hexagons) and aspect ratios (1:1, 2:1, 4:1 and 8:1). (c, d) Representative fluorescence photomicrographs of fibronectin-coated micropatterns. Scale bar: 50 μm.

The characteristics of the micropatterned surfaces were further analyzed by AFM. Representative AFM images of the micropatterns with a spreading area of 1256 μm^2 were obtained in contact mode in water (Figure 3.3a, b). For the polygonal micropatterns, the side length was measured to be 53.8±0.8, 35.6±0.3, 27.3±0.5 and 21.9±0.4 μm for triangles, squares, pentagons and hexagons, respectively. The corresponding area was calculated to be 1252.9±37.3, 1266.5±14.2, 1285.1±47.0 and 1243.8±45.5 μm^2, respectively. For

the elongated micropatterns, the long axis was measured to be 41.1±0.2, 58.0±0.8 and 81.4±0.5 μm for the 1:1, 2:1 and 4:1 micropatterns, respectively. The short axis was 40.0±0.2, 28.1±0.7, 20.7±0.4 and 14.3±1.0 μm for the 1:1, 2:1, 4:1 and 8:1 micropatterns, respectively. The elongation (1.0±0.2:1, 2.1±0.3:1, 3.9±0.5:1) and micropattern area (1271.4±23.5, 1264.6±27.6, 1249.4±18.9 μm^2) for the 1:1, 2:1 and 4:1 micropatterns were calculated to be almost the same as those of the designed parameters. The long-axis length for the 8:1 micropattern was not measured because it exceeded the AFM scanning range. Furthermore, the thickness of the PVA-grafted layer was 49.8±0.4, 50.7±2.0, 49.6±0.7, and 49.8±1.2 nm for the polygonal micropatterns and 50.2±0.9, 50.1±0.5, 49.7±0.8, and 49.0±0.7 nm for the elongated micropatterns, indicating that the thickness of the PVA-grafted layer was well controlled by adjusting the concentration and amount of AzPhPVA aqueous solution used for micropatterning.

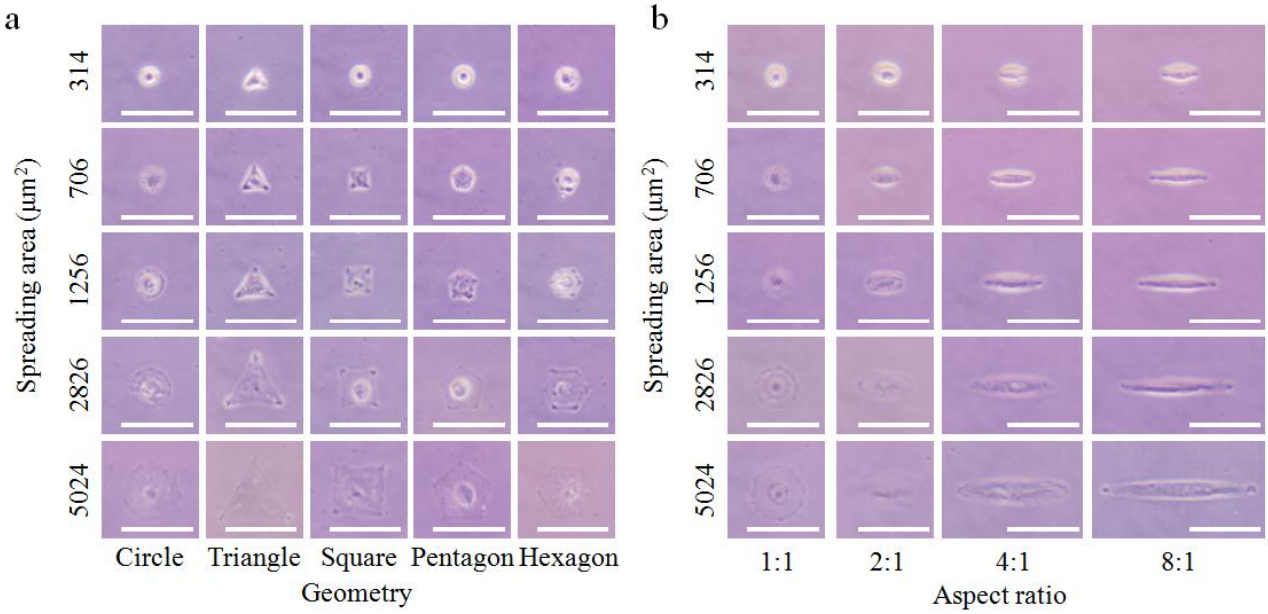

Figure 3.4 Influence of cell size, shape and aspect ratio on gene transfection efficiency. (a, b) Representative phase-contrast photomicrographs of hMSCs cultured on micropatterns of different sizes (spreading areas of 314, 706, 1256, 2826 and 5024 μm^2), shapes (circles, triangles, squares, pentagons and hexagons) and aspect ratios (1:1, 2:1, 4:1 and 8:1) in DMEM. Scale bar: 100 μm.

To facilitate cell adhesion on the micropatterned surfaces, fibronectin was coated on the micropatterned surfaces. Immunological staining demonstrated that fibronectin adsorbed only on the TCPS regions, not on the PVA-grafted regions, following the micropattern characteristics (Figure 3.3c, d). The nonfouling PVA resisted fibronectin adsorption. When hMSCs were cultured on the micropatterned surfaces, they were able to attach to the micropatterned surfaces and spread along the micropatterns (Figure 3.4). These results indicate that the micropatterned surfaces could be used to precisely control cell size, shape and elongation.

3.4.2 Influence of cell size, shape and elongation on exogenous plasmid DNA transfection

After hMSCs were cultured on the micropatterned surfaces for 1 day, the cationic liposome/plasmid complexes were applied to transfect the micropatterned cells. The size of the cationic liposome/plasmid complexes was 145.0±46.0 nm. A fluorescence microscope was used to observe the GFP-positive cells (Figure 3.5a, b). The influence of cell size, shape and elongation on gene transfection was investigated by comparing the percentage of GFP-positive cells among all checked hMSCs. Cells with the same spreading

area but different shapes, including circles, triangles, squares, pentagons and hexagons, showed the same percentage of transfected cells (Figure 3.5c). These results indicate that cell shape had no significant influence on gene transfection efficiency. However, gene transfection efficiency was enhanced with increasing cell spreading area for all types of cell shapes (Figure 3.5d). The largest cells on the micropattern with an area of 5024 μm^2 showed the highest gene transfection efficiency.

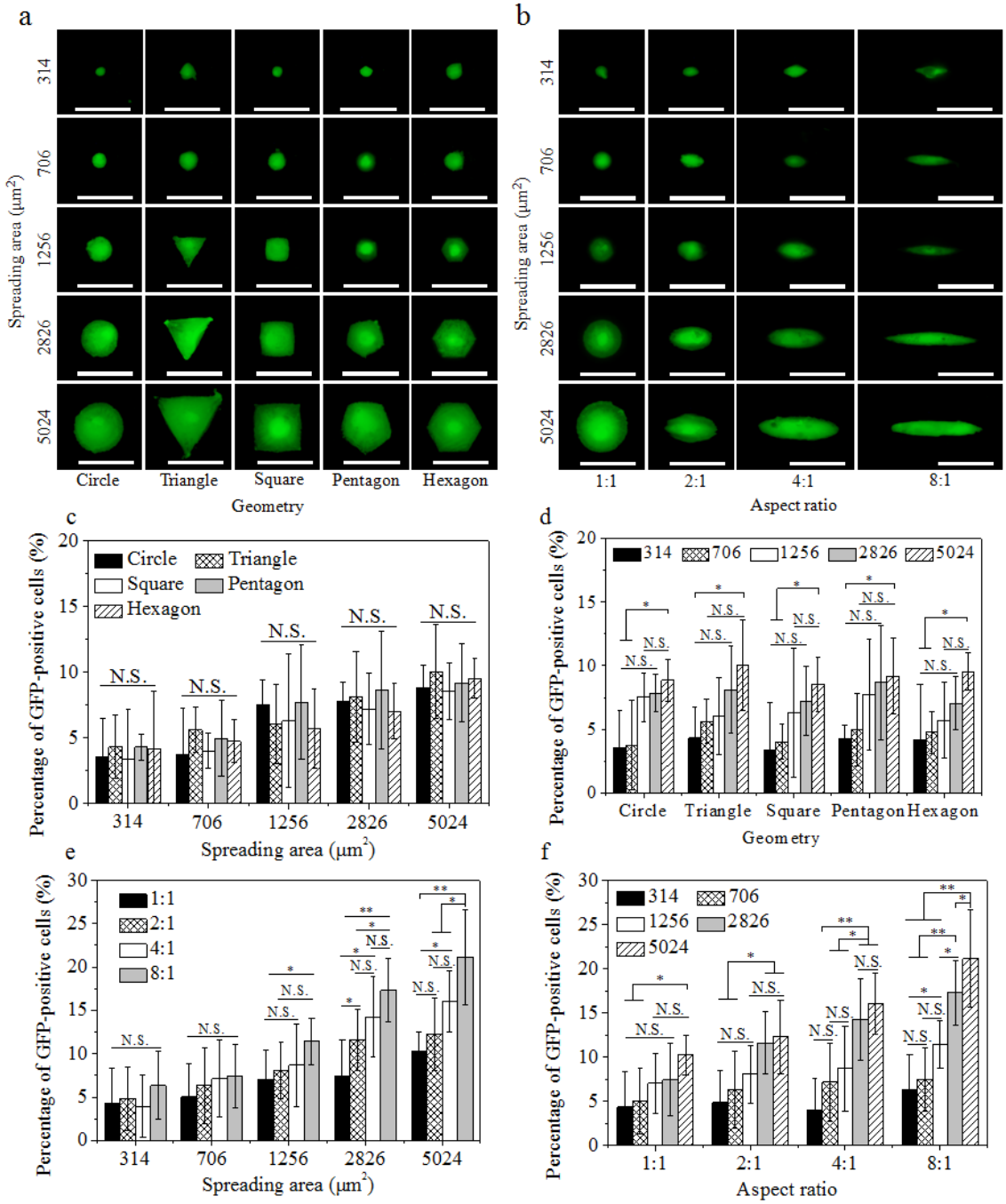

Figure 3.5 Representative fluorescence photomicrographs of GFP-positive cells on micropatterns with different shapes (a) and aspect ratios (b). Spreading area was 314, 706, 1256, 2826 and 5024 μm^2. Scale bar: 100 μm. (c) Relationship of transfection efficiency and cell shape of hMSCs with different spreading areas. (d) Relationship of transfection efficiency and spreading area of hMSCs with different shapes. (e) Relationship of transfection efficiency and aspect ratio of hMSCs with different spreading areas. (f) Relationship of transfection efficiency and spreading area of hMSCs with different aspect ratios. Data represent the mean ± SD (n = 5), N.S. represents no significant difference, *p < 0.05, **p < 0.01.

For the elongated hMSCs, both cell size and elongation showed a significant influence on gene transfection (Figure 3.5e, f). When the cell spreading area was small (314 and 706 μm^2), the influence of the aspect ratio was not evident, and all cells with different aspect ratios showed the same level of transfection efficiency. As the cell spreading area increased to 1256, 2826 or 5024 μm^2, the gene transfection efficiency increased significantly with increases in the aspect ratio, particularly for cells on micropatterns with an area of 5024 μm^2 (Figure 3.5e). When the aspect ratio was kept constant, the gene transfection efficiency increased with increasing cell size (Figure 3.5f). The increase was more evident for high aspect ratios (4:1 and 8:1). In particular, the gene transfection efficiency was significantly increased to 21% for cells with a spreading area of 5024 μm^2 and an aspect ratio of 8:1. These results suggest that cell spreading and elongation were beneficial for gene transfection.

3.4.3 Influence of cell size, shape and aspect ratio on cellular uptake

The cationic complexes of Lipofectamine™ 2000 and Fluoresbrite carboxylate microspheres were used to investigate the influence of cell size, shape and aspect ratio on cellular uptake. After the cells were cultured with the cationic microsphere solution on the micropatterns, actin filaments and nuclei were stained red and blue, respectively, to confirm cell location and morphology (Figure 3.6a, b). The green fluorescence clearly showed the uptake of microspheres by the micropatterned hMSCs. The yield of FITC-labelled green fluorescence was calculated to evaluate the cellular uptake of the micropatterned cells. The fluorescence yield of FITC per cell was not significantly different between cells with the same spreading area but different shapes (Figure 3.6c). In contrast, the fluorescence yield was enhanced with increasing cell spreading area for all micropatterned hMSCs of different shapes (Figure 3.6d). For the elongated cells, the fluorescence yield showed a gradually increasing tendency with increases in the aspect ratio when the cells had a spreading area of 1256, 2826 or 5024 μm^2 (Figure 3.6e). However, the fluorescence yield was not affected when the cell spreading area was controlled below 706 μm^2. Additionally, the fluorescence yield of FITC per cell increased with increases in the cell spreading area when the aspect ratio was controlled at the same level (Figure 3.6f). These results reveal that a large cell spreading area and high aspect ratio beneficially contributed to the cellular uptake of exogenous nanoparticles.

3.4.4 Influence of cell size, shape and aspect ratio on DNA synthesis

DNA synthesis plays a critical role in regulating efficient gene transfection. BrdU staining was applied to evaluate the DNA synthesis of the micropatterned hMSCs. The percentage of BrdU-positive cells among all checked hMSCs was counted according to the fluorescence images (Figure 3.7). Cell shape did not affect DNA synthesis when the cells had the same spreading area (Figure 3.8a). In contrast, when the cells had the same shape but different spreading areas, DNA synthesis gradually increased with increasing cell spreading area (Figure 3.8b). In particular, micropatterned hMSCs with a spreading area of 5024 μm^2 presented the highest DNA synthesis. For the elongated cells, DNA synthesis increased with increases in the aspect ratio when the cells had large spreading areas (1256, 2826 and 5024 μm^2) (Figure 3.8c). However, DNA synthesis activity was not affected when the cell spreading area was below 706 μm^2. When cells with the same elongation were compared, DNA synthesis showed a tendency to increase with increasing cell spreading area (Figure 3.8d). These results indicate that DNA synthesis could be enhanced by cell size and elongation.

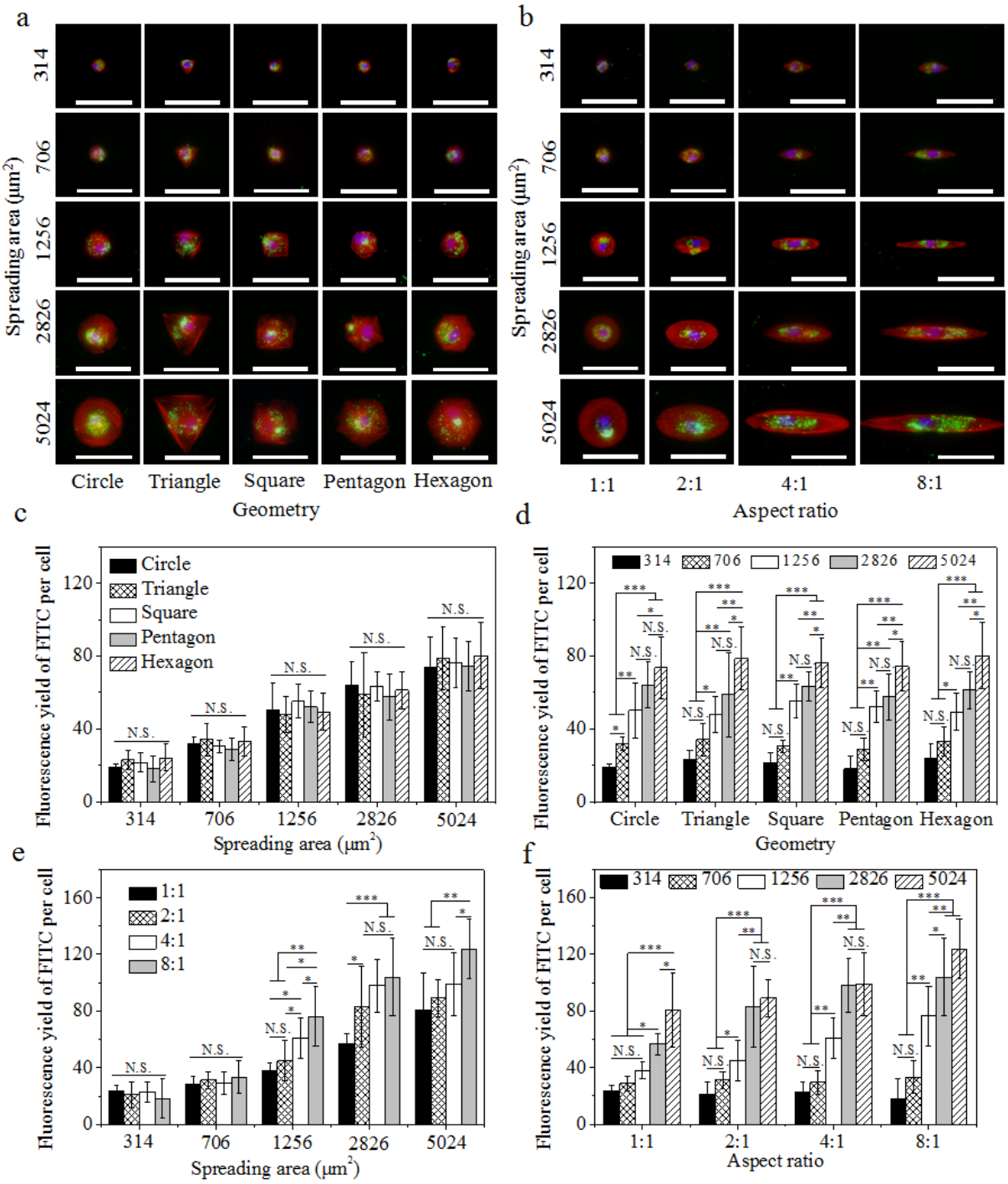

Figure 3.6 Influence of cell size, shape and aspect ratio on cellular uptake. (a, b) Representative fluorescence photomicrographs of hMSCs cultured on micropatterns of different sizes, shapes and aspect ratios after uptake of cationically modified Fluoresbrite carboxylate microspheres (green). Actin filaments and nuclei are stained red and blue, respectively. Scale bar: 100 μm. (c) Relationship of fluorescence yield of FITC-labelled microspheres per cell and cell shape of hMSCs with different spreading areas. (d) Relationship of fluorescence yield of FITC-labelled microspheres per cell and spreading area of hMSCs with different shapes. (e) Relationship of fluorescence yield of FITC-labelled microspheres per cell and aspect ratio of hMSCs with different spreading areas. (f) Relationship of fluorescence yield of FITC-labelled microspheres per cell and spreading area of hMSCs with different aspect ratios. Data represent the mean ± SD (n = 5), N.S. represents no significant difference, *$p < 0.05$, **$p < 0.01$, ***$p < 0.001$.

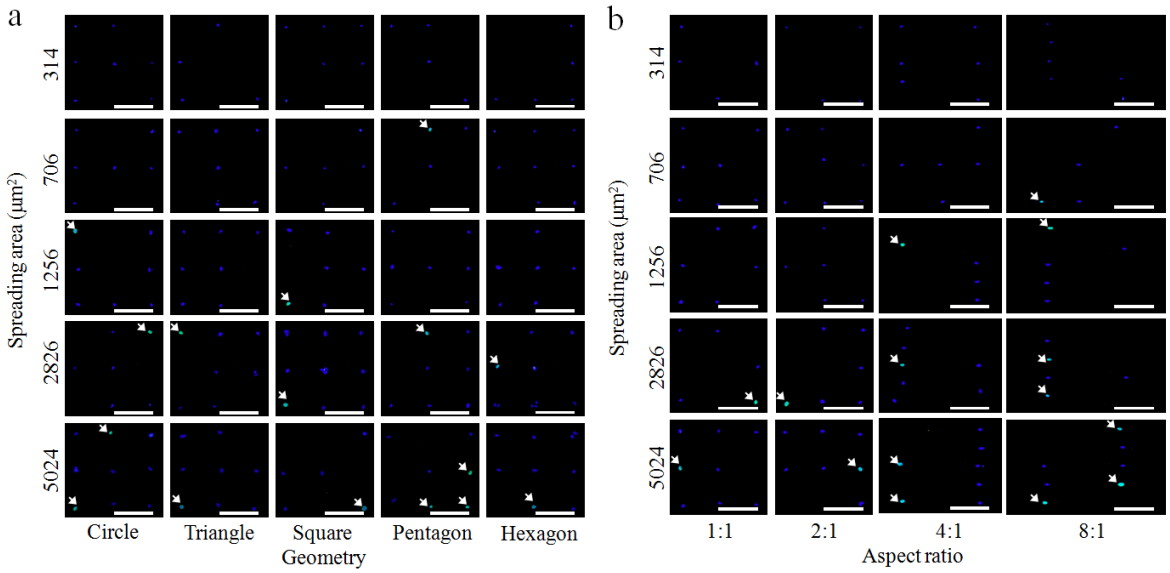

Figure 3.7 Representative fluorescence photomicrographs of hMSCs on micropatterns after nuclear (blue) and BrdU (green, white arrow) staining. Scale bar: 200 μm.

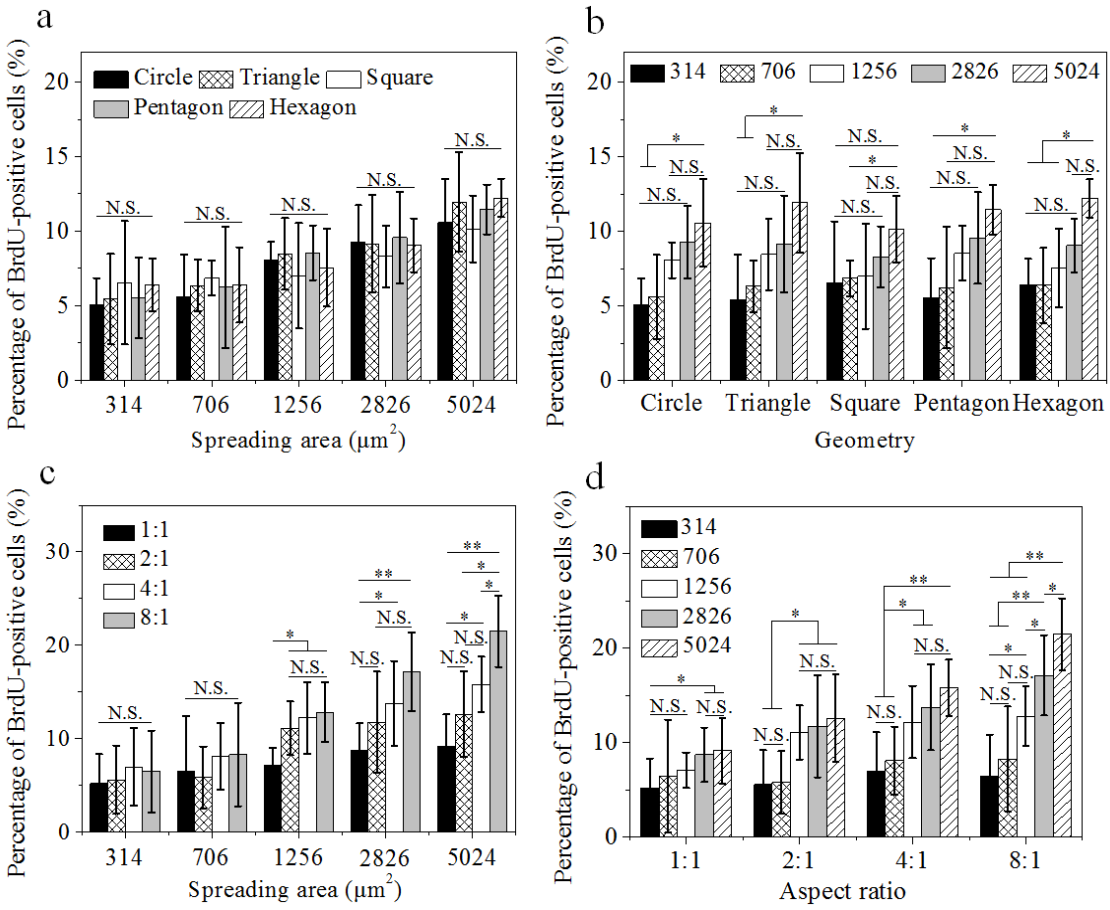

Figure 3.8 Influence of cell size, shape and elongation on DNA synthesis. (a) Relationship of percentage of BrdU-positive hMSCs and cell shape of hMSCs with different spreading areas. (b) Relationship of percentage of BrdU-positive hMSCs and spreading area of hMSCs with different shapes. (c) Relationship of percentage of BrdU-positive hMSCs and aspect ratio of hMSCs with different spreading areas. (d) Relationship of percentage of BrdU-positive hMSCs and spreading area of hMSCs with different aspect ratios. Data represent the mean ± SD (n = 5), N.S. represents no significant difference, *$p < 0.05$, **$p < 0.01$.

3.4.5 Cytoskeletal structures and cellular stiffness

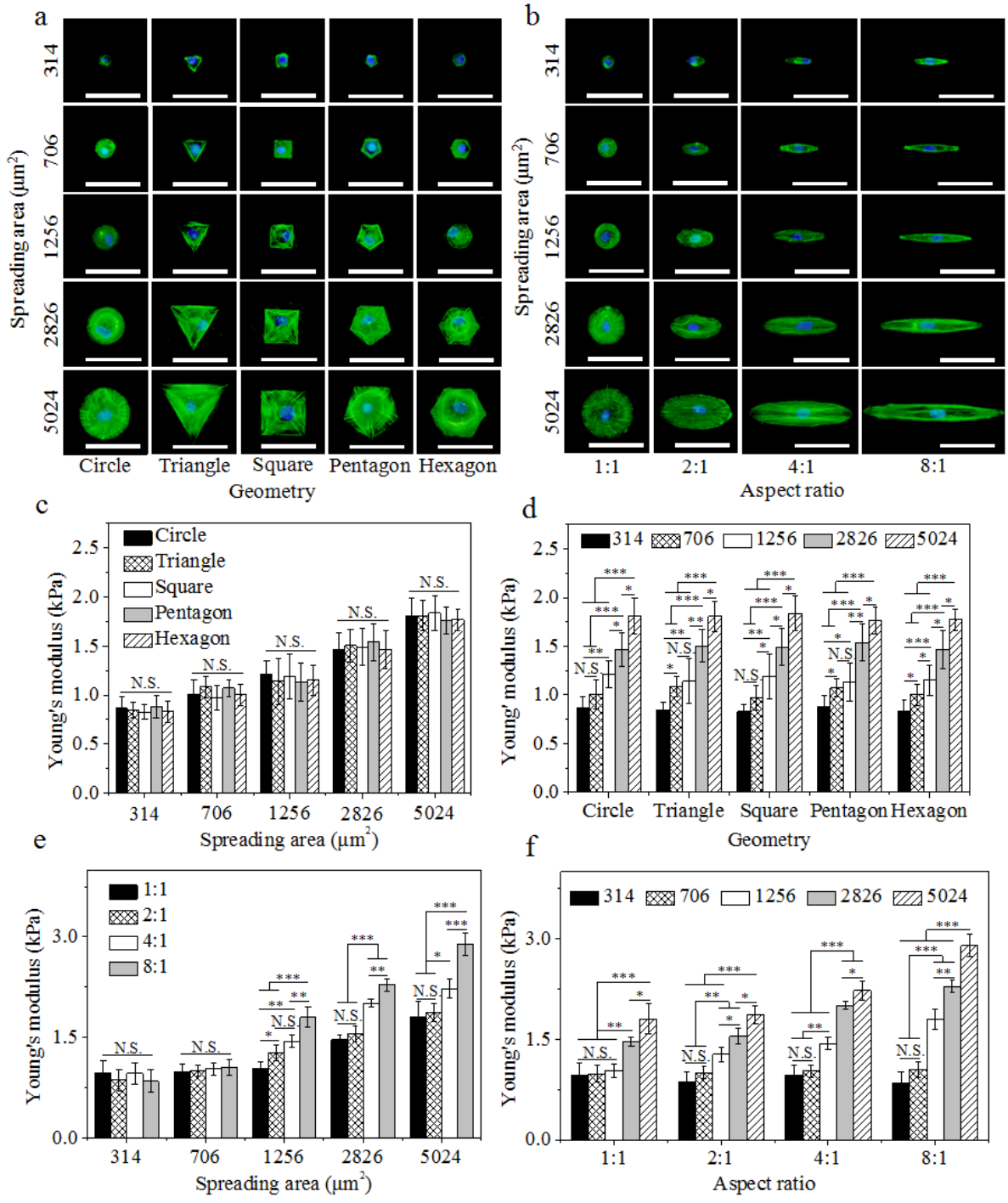

Figure 3.9 Influence of cell size, shape and elongation on cytoskeletal structures and cell stiffness. (a, b) Representative fluorescence photomicrographs of cytoskeletal structures in hMSCs cultured on micropatterns. Nuclei and actin filaments are stained blue and green, respectively. Scale bar: 100 μm. (c) Relationship of Young's modulus and cell shape of hMSCs with different spreading areas. (d) Relationship of Young's modulus and spreading area of hMSCs with different cell shapes. (e) Relationship of Young's modulus and aspect ratio of hMSCs with different spreading areas. (f) Relationship of Young's modulus and spreading area of hMSCs with different aspect ratios. Data represent the mean ± SD (n = 10), N.S. represents no significant difference, *$p < 0.05$, **$p < 0.01$, ***$p < 0.001$.

Cytoskeletal structures are anchored to the adhesive proteins of the cell membrane and create traction in cells to affect cell functions, such as cellular uptake [26]. Therefore, the influence of cell size, shape and elongation on cytoskeletal structures was analyzed. The cytoskeletal staining results showed that when the spreading area of the micropatterned cells was controlled at 1256, 2826 or 5024 μm^2, the circular cells developed actin filaments in both the radial and concentric directions of the microcircles. Actin bundles of the polygonal cells were prominently gathered at the vertexes of polygons and along the concentric direction (Figure 3.9a). However, when the cell spreading area was less than 706 μm^2, the micropatterned cells predominately assembled cortical actin at the edge of the micropatterns. Interestingly, the actin filaments of the elongated cells were assembled and organized along the long axis of cells and spanned over the nuclei, especially for the cells having a spreading area of 5024 μm^2 and an aspect ratio of 8:1 (Figure 3.9b).

Actin structures of the micropatterned cells could stimulate cytoskeletal tension. Therefore, the cellular Young's modulus was analyzed by AFM nanoindentation. Cell shape did not affect Young's modulus when the cells had the same spreading area (Figure 3.9c). However, Young's modulus was gradually enhanced with increasing cell spreading area for the same cell shape (Figure 3.9d). In the elongated cells, Young's modulus increased with increasing elongation when the cell spreading area was controlled at 1256, 2826 or 5024 μm^2, while there was no difference when the cell spreading area was below 706 μm^2 (Figure 3.9e). When the elongation of the micropatterned cells was controlled at the same level, Young's modulus increased with cell enlargement (Figure 3.9f). These results could be explained by the assembly and organization of actin filaments in the respective cells.

3.4.6 Distribution of plasmid/lipid complexes in cells

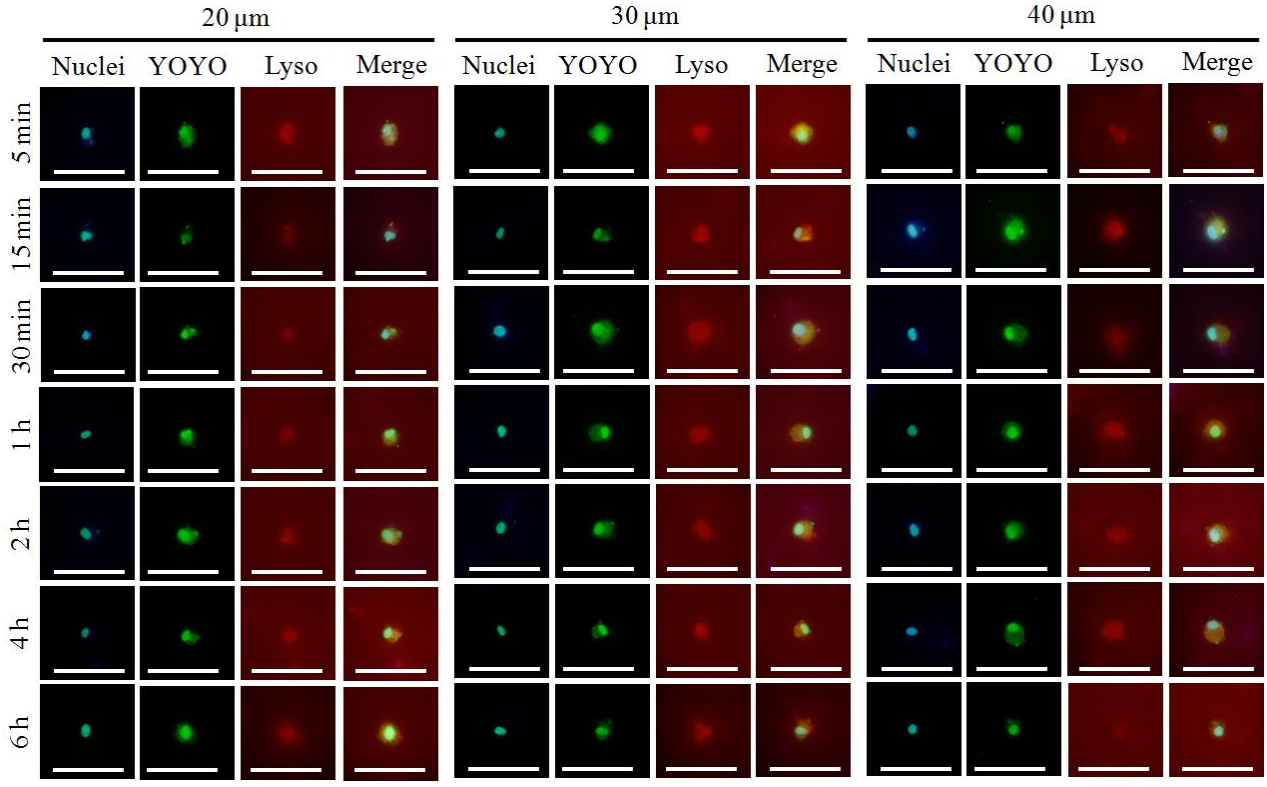

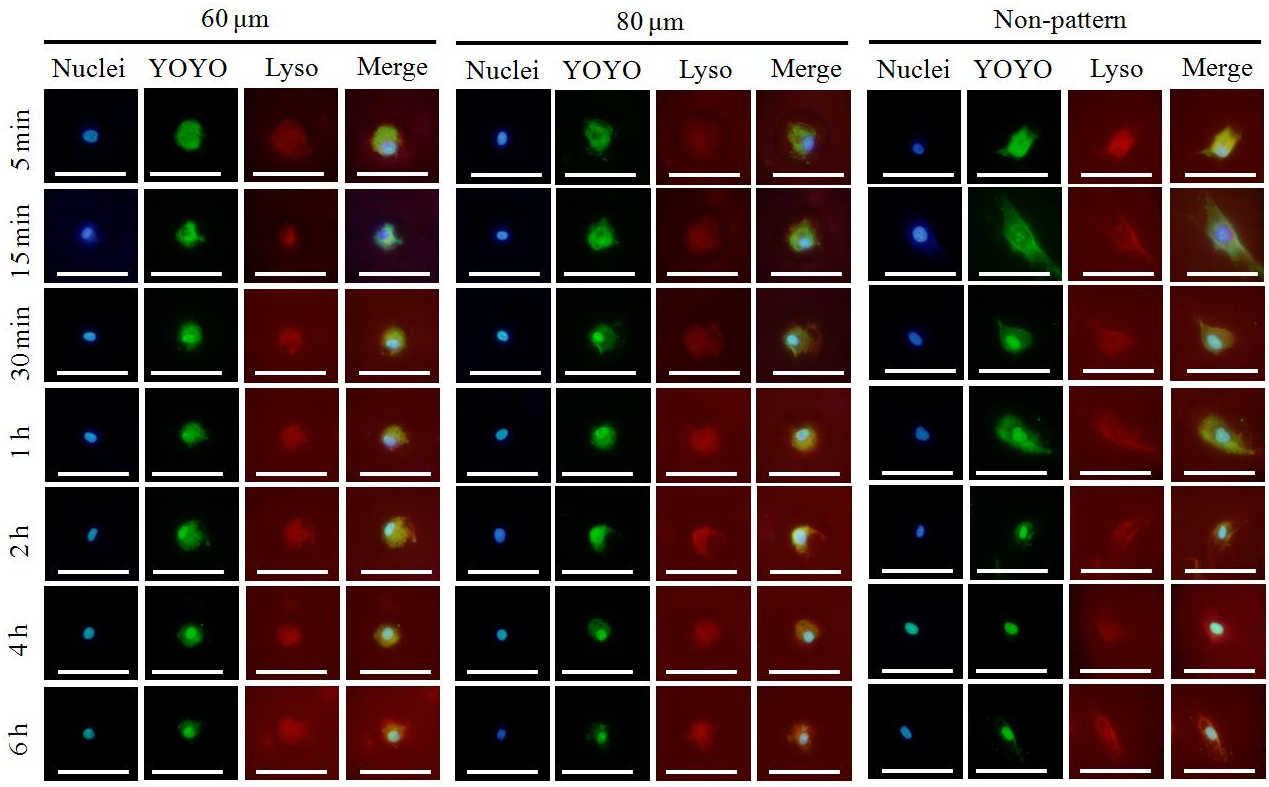

Figure 3.10 Representative fluorescence photomicrographs of hMSCs after incubated with YOYO-1-labeled plasmid/Lipofectamine 2000 complexes for 5 min, 15 min, 30 min, 1 h, 2 h, 4 h and 6 h. The cells were cultured on circular micropatterns with the spreading area of 314, 706, 1256, 2826 and 5024 μm^2 and non-patterned surfaces. Plasmid (green) and endosomes (red) were stained with YOYO-1 (YOYO) and LysoTracker deep red (Lyso), respectively. Nuclei were stained blue. Scale bar: 100 μm.

Distribution of plasmid/lipid complexes in cells was investigated with plasmid and endosome staining (Figure 3.10). Plasmid and endosomes were stained green and red with YOYO-1 and LysoTracker deep red, respectively. Nuclei were stained blue. After 5 and 15 min transfection, plasmid and endosomes were localized in cytosol, but not accumulated in nuclei. At 30 min, plasmid started to accumulate in nuclei. After 1 and 2 h, DNA was further localized in nuclei. When the cells were transfected for 4 and 6 h, plasmid was almost localized in nuclei. The results showed that the distribution of plasmid presented the similar behavior on the micropatterns and non-micropatterned surfaces. The cells on the micropatterns and non-micropatterned surfaces showed the same uptake pathway.

3.5 Discussion

Biophysical cues, including mechanics and topography, can affect cell morphology to regulate cell functions [15-19, 38-40]. In this study, the size, shape and elongation of hMSCs were controlled by micropatterned surfaces, and their influences on the exogenous gene transfection were systematically investigated. Micropatterned surfaces were produced by micropatterning photoreactive PVA on TCPS discs. The micropatterned surfaces were further coated with fibronectin to facilitate cell adhesion because fibronectin can be specifically recognized by integrins on cell membranes. The coated fibronectin showed the same micropatterns as the micropatterned surfaces (Figure 3.3). The cell adhesion area should be the same as the spreading area due to the specific interaction between cells and coated fibronectin. The cell

adhesion area and cell spreading area have been reported to have different influences on cell functions [18, 24]. Therefore, the coated fibronectin could prevent discrimination of the cell adhesion area and cell spreading area. The hMSCs cultured on the micropatterned surfaces showed well-controlled morphologies of different spreading areas (sizes), shapes and degrees of elongation (aspect ratios), as shown in Figure 3.4.

The gene transfection efficiency of the cells on the micropatterned surfaces was dependent on the cell spreading area and on cell elongation but not on cell shape. For all of the investigated shapes (circles, triangles, squares, pentagons and hexagons), the cells showed the same level of gene transfection efficiency if the size of the cells was the same (Figure 3.5c). In other words, cell shape did not affect gene transfection efficiency. Cell elongation could affect gene transfection efficiency, but its influence was dependent on cell size (Figure 3.5e). Small cells (spreading areas of 314 and 706 μm^2) did not show a significant difference in gene transfection efficiency even when the aspect ratio changed from 1:1 to 8:1. Large cells (spreading areas of 1256, 2826 and 5024 μm^2) showed increased gene transfection efficiency with increasing cell size. In contrast, the cell size could significantly increase the gene transfection efficiency regardless of whether the cells had different shapes or degrees of elongation (Figure 3.5d, f). Cells with a spreading area of 5024 μm^2 and an aspect ratio of 8:1 showed the highest transfection efficiency.

The influence of cell morphology on gene transfection could be explained by the dependence of cellular uptake capacity and gene expression on cell morphology. Cellular uptake and gene expression are the first and last steps of gene transfection process, respectively [41]. In this study, cellular uptake of fluorescent microspheres was used to investigate the transmembrane delivery capacity. DNA synthesis activity was used to investigate the gene expression capacity. High cellular uptake of exogenous genes and high DNA synthesis are required for high gene transfection efficiency. Uptake experiments and BrdU staining indicated that the cellular nanoparticle uptake (Figure 3.6) and DNA synthesis (Figure 3.7 and Figure 3.8) showed dependence on cell morphology similar to that of gene transfection efficiency. Cell shape did not affect cellular uptake or DNA synthesis. Cell elongation could increase the cellular uptake and DNA synthesis of large cells (spreading areas of 1256, 2826 and 5024 μm^2) but not small cells (spreading areas of 314 and 706 μm^2). An increase in cell size resulted in enhanced cellular uptake and DNA synthesis when either cell shape or elongation was changed. These results indicate strong correlations among gene transfection efficiency, cellular uptake and DNA synthesis, suggesting that cell morphology affected gene transfection through the regulation of cellular uptake and DNA synthesis.

Cytoskeletal structures play critical roles in regulating cellular uptake and the intracellular trafficking of exogenous genes [42]. Focal adhesions (FAs) on the cytoplasmic membrane serve as binding bridges between integrins and actin filaments in cells [43]. More FAs can induce the formation of actin bundles in well-spread and elongated cells [18, 44]. The uptake of cationic exogenous complexes has been reported to be dependent on clathrin-mediated endocytosis, and the pathway is correlated with cytoskeletal structures [45]. The larger fibronectin-coated micropatterns could promote more FA formation and cytoskeletal assembly. The results of actin staining verified that the assembly and organization of the cytoskeleton were dependent on the size, shape and aspect ratio of the micropattern (Figure 3.9). Cells cultured on micropatterns with a large spreading area formed actin bundles not only in the radial direction (circular micropatterns) or at the vertexes of polygons (polygonal micropatterns) but also in the concentric direction. The cells with high elongation formed a well-organized actin filament network along the long axis of the micropatterns. Some studies have reported that ventral and dorsal stress fibers (VSFs and DSFs) develop along the radial direction, while transverse arcs (TAs) develop along the concentric direction of circular micropatterns [18, 46, 47]. Thick VSFs are connected with FAs on both sides and provide high contractility for cells, while DSFs are thin fibers with non-contractive activity that bond to FAs [48]. DSFs are weaved towards nuclei and transfer extracellular signals into nuclei [49]. The contractive TAs bond to DSFs and play

an important role in affecting cell elasticity [18]. Cellular stiffness testing showed that Young's modulus was significantly enhanced in well-spread and elongated cells (Figure 3.9). Accordingly, cytoskeletal structures and cell mechanics could regulate the cellular uptake capacity and DNA synthesis, thus inducing effective gene transfection. YOYO-1 and LysoTracker deep red staining results showed that the cells on micropatterns and non-patterned surfaces presented the same uptake pathway of the lipoplexes. Therefore, gene transfection was correlated with actin filaments and cellular activity.

3.6 Conclusions

PVA-micropatterned surfaces were produced to precisely control cell size, shape and elongation for systematic investigation of their influences on exogenous gene transfection. hMSCs were cultured on micropatterned surfaces and transfected with lipid/plasmid complexes. The transfection efficiency was significantly enhanced in well-spread and elongated cells. Cell size had a dominant influence on gene transfection, independent of cell shape. Elongation could increase the transfection efficiency in large cells but not small cells. Cell shape had no influence on gene transfection efficiency. High transfection efficiency was strongly correlated with high cellular uptake and DNA synthesis through the regulation of cytoskeletal structures and cell mechanics. These results provide useful information for gene transfection and gene therapy applications.

3.7 References

[1] A. Higuchi, Q. D. Ling, Y. Chang, S. T. Hsu, A. Umezawa, Physical cues of biomaterials guide stem cell differentiation fate, Chemical Reviews 113 (2013) 3297-3328.
[2] J. Barthes, H. Özçelik, M. Hindié, A. Ndreu-Halili, A. Hasan, N. E. Vrana, Cell microenvironment engineering and monitoring for tissue engineering and regenerative medicine: the recent advances, BioMed Research International 2014 (2014) 921905.
[3] A. Higuchi, Q. D. Ling, S. S. Kumar, Y. Chang, A. A. Alarfaj, M. A. Munusamy, K. Murugan, S. T. Hsu, A. Umezawa, Physical cues of cell culture materials lead the direction of differentiation lineages of pluripotent stem cells, Journal of Materials Chemistry B 3 (2015) 8032-8058.
[4] Y. Zhou, C. Wu, J. Chang, Bioceramics to regulate stem cells and their microenvironment for tissue regeneration, Materials Today 24 (2019) 41-56.
[5] B. Yang, H. Wolfenson, V. Y. Chung, N. Nakazawa, S. Liu, J. Hu, R. Y. Huang, M. P. Sheetz, Stopping transformed cancer cell growth by rigidity sensing, Nature Materials 19 (2020) 239-250.
[6] M. Rahmati, E. A. Silva, J. E. Reseland, C. A. Heyward, H. J. Haugen, Biological responses to physicochemical properties of biomaterial surface, Chemical Society Reviews 49 (2020) 5178-5224.
[7] K. Lee, Y. Chen, X. Li, Y. Wang, N. Kawazoe, Y. Yang, G. Chen, Solution viscosity regulates chondrocyte proliferation and phenotype during 3D culture, Journal of Materials Chemistry B 7 (2019) 7713-7722.
[8] K. Lee, Y. Chen, T. Yoshitomi, N. Kawazoe, Y. Yang, G. Chen, Osteogenic and adipogenic differentiation of mesenchymal stem cells in gelatin solutions of different viscosities, Advanced Healthcare Materials 9 (2020) 2000617.
[9] G. Nardone, J. O. D. L. Cruz, J. Vrbsky, C. Martini, J. Pribyl, P. Skládal, M. Pešl, G. Caluori, S. Pagliari, F. Martino, Z. Maceckova, M. Hajduch, A. Sanz-Garcia, N. M. Pugno, G. B. Stokin, G. Forte, YAP regulates cell mechanics by controlling focal adhesion assembly, Nature Communications 8 (2017) 15321.

[10] C. Zhao, X. Wang, L. Gao, L. Jing, Q. Zhou, J. Chang, The role of the micro-pattern and nano-topography of hydroxyapatite bioceramics on stimulating osteogenic differentiation of mesenchymal stem cells, Acta Biomaterialia 73 (2018) 509-521.
[11] C. Yang, C. Zhao, X. Wang, M. Shi, Y. Zhu, L. Jing, C. Wu, J. Chang, Stimulation of osteogenesis and angiogenesis by micro/nano hierarchical hydroxyapatite via macrophage immunomodulation, Nanoscale 11 (2019) 17699-17708.
[12] Y. Chen, K. Lee, N. Kawazoe, Y. Yang, G. Chen, PLGA-collagen-ECM hybrid scaffolds functionalized with biomimetic extracellular matrices secreted by mesenchymal stem cells during stepwise osteogenesis-co-adipogenesis, Journal of Materials Chemistry B 7 (2019) 7195-7206.
[13] T. Vignaud, C. Copos, C. Leterrier, M. Toro-Nahuelpan, Q. Tseng, J. Mahamid, L. Blanchoin, A. Mogilner, M. Théry, L. Kurzawa, Stress fibres are embedded in a contractile cortical network, Nature Materials 20 (2021) 410-420.
[14] R. Changede, H. Cai, S. J. Wind, M. P. Sheetz, Integrin nanoclusters can bridge thin matrix fibres to form cell-matrix adhesions, Nature Materials 18 (2019) 1366-1375.
[15] J. Y. Li, Y. C. Ho, Y. C. Chung, F. C. Lin, W. L. Liao, W. B. Tsai, Preparation of micron/submicron hybrid patterns via a two-stage UV-imprint technique and their dimensional effects on cell adhesion and alignment, Biofabrication 5 (2013) 035003.
[16] Y. Yang, X. Wang, Y. Wang, X. Hu, N. Kawazoe, Y. Yang, G. Chen, Influence of cell spreading area on the osteogenic commitment and phenotype maintenance of mesenchymal stem cells, Scientific Reports 9 (2019) 6891.
[17] Y. Zhang, R. D. Mets, C. Monzel, V. Acharya, P. Toh, J. F. L. Chin, N. V. Hul, I. C. Ng, H. Yu, S. S. Ng, S. T. Rashid, V. Viasnoff, Biomimetic niches reveal the minimal cues to trigger apical lumen formation in single hepatocytes, Nature Materials 19 (2020) 1026-1035.
[18] X. Wang, X. Hu, I. Dulińska-Molak, N. Kawazoe, Y. Yang, G. Chen, Discriminating the independent influence of cell adhesion and spreading area on stem cell fate determination using micropatterned surfaces, Scientific Reports 6 (2016) 28708.
[19] H. W. Chien, T. Y. Chang, W. B. Tsai, Spatial control of cellular adhesion using photo-crosslinked micropatterned polyelectrolyte multilayer films, Biomaterials 30 (2009) 2209-2218.
[20] K. Zhang, X. Xiao, X. Wang, Y. Fan, X. Li, Topographical patterning: characteristics of current processing techniques, controllable effects on material properties and co-cultured cell fate, updated applications in tissue engineering, and improvement strategies, Journal of Materials Chemistry B 7 (2019) 7090-7109.
[21] M. Ermis, E. Antmen, V. Hasirci, Micro and nanofabrication methods to control cell-substrate interactions and cell behavior: a review from the tissue engineering perspective, Bioactive Materials 3 (2018) 355-369.
[22] J. Lee, A. A. Abdeen, K. L. Wycislo, T. M. Fan, K. A. Kilian, Interfacial geometry dictates cancer cell tumorigenicity, Nature Materials 15 (2016) 856-862.
[23] Y. Wang, Y. Yang, X. Wang, T. Yoshitomi, N. Kawazoe, Y. Yang, G. Chen, Micropattern-controlled chirality of focal adhesions regulates the cytoskeletal arrangement and gene transfection of mesenchymal stem cells, Biomaterials 271 (2021) 120751.
[24] Y. Wang, Y. Yang, X. Wang, N. Kawazoe, Y. Yang, G. Chen, The varied influences of cell adhesion and spreading on gene transfection of mesenchymal stem cells on a micropatterned substrate, Acta Biomaterialia 125 (2021) 100-111.
[25] F. Xie, X. Zhou, M. Fang, H. Li, P. Su, Y. Tu, L. Zhang, F. Zhou, Extracellular vesicles in cancer immune microenvironment and cancer immunotherapy, Advanced Science 6 (2019) 1901779.

[26] X. Wang, X. Hu, J. Li, A. C. M. Russe, N. Kawazoe, Y. Yang, G. Chen, Influence of cell size on cellular uptake of gold nanoparticles, Biomaterials Science 4 (2016) 970-978.
[27] C. E. Dunbar, K. A. High, J. K. Joung, D. B. Kohn, K. Ozawa, M. Sadelain, Gene therapy comes of age, Science 359 (2018) eaan4672.
[28] T. K. Kim, J. H. Eberwine, Mammalian cell transfection: the present and the future, Analytical and Bioanalytical Chemistry 397 (2010) 3173-3178.
[29] S. Cui, B. Wang, Y. Zhao, H. Chen, H. Ding, D. Zhi, S. Zhang, Transmembrane routes of cationic liposome-mediated gene delivery using human throat epidermis cancer cells, Biotechnology Letters 36 (2014) 1-7.
[30] Y. Inoh, D. Kitamoto, N. Hirashima, M. Nakanishi, Biosurfactant MEL-A dramatically increases gene transfection via membrane fusion, Journal of Controlled Release 94 (2004) 423-431.
[31] V. V. Sokolova, I. Radtke, R. Heumann, M. Epple, Effective transfection of cells with multi-shell calcium phosphate-DNA nanoparticles, Biomaterials 27 (2006) 3147-3153.
[32] T. Niidome, L. Huang, Gene therapy progress and prospects: nonviral vectors, Gene therapy 9 (2002) 1647-1652.
[33] K. Kamimura, T. Suda, G. Zhang, D. Liu, Advances in gene delivery systems, Pharmaceutical Medicine 25 (2011) 293-306.
[34] D. Su, M. Coste, A. Diaconu, M. Barboiu, S. Ulrich, Cationic dynamic covalent polymers for gene transfection, Journal of Materials Chemistry B 8 (2020) 9385-9403.
[35] F. Liu, L. Huang, Development of non-viral vectors for systemic gene delivery, Journal of Controlled Release 78 (2002) 259-266.
[36] Y. Yang, X. Wang, X. Hu, N. Kawazoe, Y. Yang, G. Chen, Influence of cell morphology on mesenchymal stem cell transfection, ACS Applied Materials & Interfaces 11 (2019) 1932-1941.
[37] W. Song, H. Lu, N. Kawazoe, G. Chen, Gradient patterning and differentiation of mesenchymal stem cells on micropatterned polymer surface, Journal of Bioactive and Compatible Polymers 26 (2011) 242-256.
[38] P. G. Childs, C. A. Boyle, G. D. Pemberton, H. Nikukarc, A. S. G. Curtisb, F. L. Henriquez, M. J. Dalby, S. Reid, Use of nanoscale mechanical stimulation for control and manipulation of cell behavior, Acta Biomaterialia 34 (2016) 159-168.
[39] M. Bao, J. Xie, W. T. S. Huck, Recent advances in engineering the stem cell microniche in 3D, Advanced Science 5 (2018) 1800448.
[40] L. Wang, S. Wu, G. Cao, Y. Fan, N. Dunne, X. Li, Biomechanical studies on biomaterial degradation and co-cultured cells: mechanisms, potential applications, challenges and prospects, Journal of Materials Chemistry B 7 (2019) 7439-7459.
[41] I. A. Khalil, K. Kogure, H. Akita, H. Harashima, Uptake pathways and subsequent intracellular trafficking in nonviral gene delivery, Pharmacological Reviews 58 (2006) 32-45.
[42] T. Gonzalez-Fernandez, B. N. Sathy, C. Hobbs, G. M. Cunniffe, H. O. McCarthy, N. J. Dunne, V. Nicolosi, F. J. O'Brien, D. J. Kelly, Mesenchymal stem cell fate following non-viral gene transfection strongly depends on the choice of delivery vector, Acta Biomaterialia 55 (2017) 226-238.
[43] F. G. Giancotti, E. Ruoslahti, Integrin signaling, Science 285 (1999) 1028-1033.
[44] M. J. P. Biggs, R. G. Richards, S. McFarlane, C. D. W. Wilkinson, R. O. C. Oreffo, M. J. Dalby, Adhesion formation of primary human osteoblasts and the functional response of mesenchymal stem cells to 330 nm deep microgrooves, Journal of the Royal Society Interface 5 (2018) 1231-1242.
[45] S. Loebrich, The role of F-actin in modulating clathrin-mediated endocytosis: lessons from neurons in health and neuropsychiatric disorder, Communicative & Integrative Biology 7 (2014) e28740.
[46] T. Vallenius, Actin stress fibre subtypes in mesenchymal-migrating cells, Open Biology 3 (2013)

130001.
[47] Y. H. Tee, T. Shemesh, V. Thiagarajan, R. F. Hariadi, K. L. Anderson, C. Page, N. Volkmann, D. Hanein, S. Sivaramakrishnan, M. M. Kozlov, A. D. Bershadsky, Cellular chirality arising from the self-organization of the actin cytoskeleton, Nature Cell Biology 17 (2015) 445-457.
[48] J. Stricker, T. Falzone, M. L.Gardel, Mechanics of the F-actin cytoskeleton, Journal of Biomechanics 43 (2010) 9-14.
[49] B. Kovac, J. L. Teo, T. P. Mäkelä, T. Vallenius, Assembly of non-contractile dorsal stress fibers requires α-actinin-1 and rac1 in migrating and spreading cells, Journal of Cell Science 126 (2013) 263-273.

Chapter 4

Influences of cell adhesion and spreading on gene transfection of micropatterned mesenchymal stem cells

4.1 Abstract

Transmembrane transport of exogenous genes is broadly explored due to the flourishing gene therapy. Both gene carriers and cellular conditions can affect gene transfection efficiency. Although cell morphology has been reported to affect cell functions, the influence of cell adhesion area and spreading area on transfection of exogenous genes remains unclear because it has been difficult to separate the individual influence from cell adhesion area and spreading area during normal cell culture. In this study, micropatterns were prepared to separately control adhesion area and spreading area of human bone marrow-derived mesenchymal stem cells (hMSCs). Transfection efficiency of green fluorescent protein gene to hMSCs cultured on the micropatterns was compared. The cells with larger adhesion area showed higher transfection efficiency, while cell spreading area hardly affected gene transfection efficiency. Cell adhesion area had a dominant influence on gene transfection. Uptake of microparticles and BrdU staining showed that cellular uptake capacity and DNA synthesis activity increased with cell adhesion area, but were not affected by cell spreading area. The different influence of cell adhesion area and spreading area on gene transfection was correlated with their influence on cellular uptake capacity, DNA synthesis activity, focal adhesion formation, cytoskeletal mechanics and mechano-signal activation. The results suggested that cell adhesion area and spreading area had different influences on gene transfection, which should provide useful information for manipulation of cell functions in gene therapy, protein modification and cell reprogramming.

4.2 Introduction

Gene transfection in mammalian cells has become a hot topic to disclose the internalization mechanism and intracellular trafficking of gene delivery due to the increasing potential of gene therapy, gene silencing and reprogramming [1-5]. Cell plasma membrane as a natural boundary plays an important role in managing the import or export of molecules in cells [6, 7]. Exogenous particles are internalized into cells by different pathways including passive diffusion and active transport [8-11]. Small nonpolar molecules can cross over lipid bilayer of cell membrane by direct diffusion and ions can be transported through cell membrane by ion

channels and ion pumps [12]. However, internalization or uptake of large particles such as lipids, DNAs and polypeptides is related with active transport such as energy-mediated endocytosis [13-16]. Except viral-mediated endocytosis, cationic polyplexes and lipoplexes have been frequently used as effective transfection carriers [17-20]. For example, cationic fluorinated-core nano-micelles and poly(amidoamine) dendrimers have shown strong DNA-binding affinity and high gene transfection efficacy [21, 22]. Cationic lipids can regulate cellular internalization through altering nitrogen/phosphate ratio, lipid concentration and transient surface potential [23-27].

Not only gene carriers, but also cellular morphology can affect the transfection of exogenous genes [28]. Cells show various morphologies that are dependent on the adhesion matrix and substrate. Cell morphology has been reported to regulate cytoskeleton and mechanotransduction signals, therefore affecting cell functions such as migration, proliferation, differentiation, uptake and apoptosis [29-34]. Cell morphology such as adhesion area, spreading area, geometry and aspect ratio can be easily controlled by micropatterns [35-37]. However, cell adhesion is always accompanied with cell spreading during culture on normal cell culture plates. It is difficult to make difference between cell adhesion area and spreading area. Due to the difficult discrimination of the two factors, it remains unclear how cell adhesion area and spreading area independently affect the transfection of exogenous genes. In order to elucidate how cell adhesion area and spreading area affect transmembrane delivery of exogenous genes, micropatterns were prepared to discriminate cell adhesion and spreading areas. Human bone marrow-derived mesenchymal stem cells (hMSCs) were cultured on the micropatterns and their adhesion and spreading areas were precisely controlled. Transfection of green fluorescent protein gene to the micropatterned cells demonstrated different influences of cell adhesion and spreading areas on gene transfection efficiency. Furthermore, focal adhesion, cytoskeleton structure, uptake of exogenous nanoparticles, mechanotransduction signals and DNA synthesis activity of the micropatterned cells were investigated to disclose the reasons for the different morphological influences on gene transfection.

4.3 Materials and methods

4.3.1 Preparation and characterization of micropatterns

Micropatterns with various spreading area and adhesion area were prepared on one tissue culture polystyrene (TCPS) disc by photolithography as mentioned in 2.3.2. AzPhPVA-coated polystyrene discs were covered with a pre-designed photomask containing micropatterns of different circle size and transparent area and exposed to UV light with a wavelength of 254 nm. The photomask micropatterns consisted of 2 μm diameter microdots that formed large circles. After ultrasonic washing in Milli-Q water bath, the micropatterns were generated. The micropatterns were observed by a phase-contrast microscope with a DP-70 CCD camera.

The micropattern topography was analyzed by a MFP-3D-BIO atomic force microscope. A cantilever with a spring constant of 0.06 N/m and an oscillation frequency of 12-24 kHz was used for the analysis. The scanning scope was set at a square of 90×90 μm^2 with a contact mode in Milli-Q water. The diameter and height of micropatterns were acquired from 3 random images to calculate mean and standard deviation. Before the micropatterned TCPS discs were used for cell culture, they were coated with 20 μg/mL fibronectin. The fibronectin-coated micropattern TCPS discs were stained with anti-fibronectin primary antibody and Alexa Fluor-488 labeled secondary antibody to visualize the coated fibronectin. The stained discs were observed with a fluorescence microscope.

4.3.2 Cell culture

Human bone marrow-derived mesenchymal stem cells (hMSCs; passage 2; lot number: 2F3478, 18TL312488 and 18TL113327) were bought from American Lonza Walkersville Inc and subcultured twice (passage 4) in BulletKit medium (MCSGM, catalog number: PT-3238, Lonza Group Ltd., Switzerland) at 37°C in a 5% CO_2 incubator for the following experiments. Cell suspension solution was added onto the micropatterns. Cell seeding density was 2.8×10^3 cells/cm^2. After incubation for 24 hours, cell morphology was observed by a phase-contrast microscope. Five micropattern TCPS discs were used for nucleus staining with Hoechst 33258 (1:1000 in PBS) to visualize single or multiple cells on the micropatterns. Fluorescent images were obtained by an Olympus fluorescence microscope. The micropatterned circles occupied by single cell or multiple cells were counted from the fluorescence micrographs of the five micropattern TCPS discs to calculate the percentage of micropatterned circles occupied by cells and the percentage of single cell occupation.

4.3.3 Immunofluorescent staining of vinculin

After 24 hours culture on micropatterns, hMSCs were washed with PBS for 3 times and fixed with 4% paraformaldehyde solution for 10 minutes. The fixed cells were treated with 1% Triton™ X-100 for 10 minutes and 0.02% Tween-20 for 30 minutes. After washing, the cells were blocked with 2% BSA for 30 minutes. After PBS washing, the cells were used for staining of vinculin by incubation with mouse anti-vinculin antibody (1:100 in BSA, catalog number: MAB3574, Merck KGaA, Germany) at 4°C overnight. After being rinsed with 0.02% Tween-20 and PBS solution for 3 times, the cells were incubated with the second antibody, Alexa Fluor 488 labeled donkey anti-mouse IgG antibody (1:1000 in PBS) at 37°C in the dark for 1 hour. Nucleus was stained with Hoechst 33258 (1:1000 in PBS) at room temperature for 10 minutes. A confocal laser scanning fluorescence microscope (Zeiss, Germany) was used to capture the fluorescent images of vinculin. The total area and average size of focal adhesion were analyzed from the stained vinculin images through step-by-step quantitative analysis using an ImageJ software, as previously reported [39]. 25 cells from each micropattern and five independent micropatterns were used for the analysis to calculate means and standard deviations.

4.3.4 Gene transfection and live/dead staining

After hMSCs were cultured on the micropatterns for 24 hours, the cells were transfected with GFP gene as mentioned in 2.3.5. To evaluate gene transfection efficiency, fluorescent images of the cells were captured through a fluorescent microscope. The images were analyzed by ImageJ software. The percentage of positive GFP cells in total number of examined cells was defined as gene transfection efficiency. Five independent experiments (≥200 cells) at each condition were executed to calculate mean and standard deviation.

Cell viability was checked by live/dead staining before and after gene transfection. The micropatterned cells before and after transfection were incubated with a live/dead double staining kit containing calcein-AM and propidium iodide (PI) (catalog number: 341-07381, Dojindo, Japan) for 15 minutes and followed by PBS washing. The fluorescent images were captured by a fluorescence microscope.

To investigate the influence of cytoskeleton disturbance on gene transfection, the micropatterned hMSCs were treated with actin and myosin inhibitors before gene transfection. After incubation of the micropatterned hMSCs for 6 hours, the cells were respectively cultured with 0.2 μg/mL cytochalasin D (Cyto

D, catalog number: C8273, Sigma-Aldrich Co. LLC., USA) or 50 μM blebbistatin (Bleb, catalog number: SLBM6960V, Sigma-Aldrich Co. LLC., USA) in DMEM medium for 18 hours. And then, gene transfection experiment was executed in the same way as above described.

Cell viability was assessed by live/dead staining by using a Cell stain Double Staining Kit (Dojindo Laboratories, Japan) immediately after preparation of the samples and after 21 days of culture. All hydrogel discs were washed with PBS twice and incubated in serum-free medium containing calcein-AM (2 μM) and propidium iodide (4 μM) at 37ºC for 15 min. The stained samples were cut in a vertical direction and observed with a confocal laser microscope (Zeiss LSM 510 Meta, Germany).

4.3.5 Cellular uptake of microspheres

Cellular uptake experiment was carried out, as mentioned in 2.3.6. Firstly, 1 μL Lipofectamine™ 2000 solution and 0.1 μL Fluoresbrite carboxylate microspheres were diluted in 100 μL Opti-MEM medium, respectively. After incubation for 5 minutes, microspheres solution was poured into Lipofectamine™ 2000 solution to form cationic liposome/FITC-labeled microsphere complexes. The complexes were further incubated for 30 minutes and used for the following experiments. 25 cells from each sample and five independent samples were used for measurement to calculate mean and standard deviation.

4.3.6 DNA synthesis activity by BrdU staining

BrdU staining was used to indicate DNA synthesis activity, as mentioned in 2.3.7. The cells were incubated with monoclonal mouse anti-BrdU primary antibody at room temperature for 1.5 hours and followed by incubation with Alexa Fluor-488 donkey anti-mouse IgG antibody (1:1000 in PBS) in the dark for 1 hour. Nucleus was stained by Hoechst 33258 for 10 minutes at room temperature. The stained cells were observed with a fluorescence microscope and BrdU positive cells were counted. The percentage of BrdU positive cells to the total cells was calculated. More than 200 cells from each sample and five independent samples were used for the experiments to calculate mean and standard deviation.

4.3.7 Fluorescent staining of actin filaments and immunofluorescent staining of actinin and myosin

After 24 hours culture on micropatterns, hMSCs were washed and fixed in the same way as that described in immunofluorescent staining of vinculin. After PBS washing, the cells were used for staining of actinin and myosin by incubation with their respective antibodies at 4°C overnight. Mouse anti-actinin antibody (1:100 in BSA, catalog number: ab9465, Abcam, USA) and rabbit anti-myosin IIA antibody (1:100 in BSA, catalog number: M8064, Sigma-Aldrich Co. LLC., USA) were used as the respective first antibodies. After being rinsed with 0.02% Tween-20 and PBS solution for 3 times, the cells were incubated with the second antibody, Alexa Fluor 488 labeled donkey anti-mouse IgG antibody (1:1000 in PBS) for actinin and Alexa Fluor-488 labeled donkey anti-rabbit IgG antibody (1:1000 in PBS) for myosin, at 37°C in the dark for 1 hour. In addition, nucleus and actin filaments were stained with Hoechst 33258 (1:1000 in PBS) at room temperature for 10 minutes and Alexa Fluor-594 phalloidin (1:40 in PBS) in the dark for 20 minutes. The fluorescent images were obtained by an Olympus fluorescence microscope.

4.3.8 Measurement of cell stiffness

AFM was used to measure cell stiffness, as mentioned in 3.3.3. 10 cells were selected for each micropattern and 20 force-distance curves for each cell were analyzed. The average Young's modulus of 10 cells was calculated as mean and standard deviation. The micropatterned cells after treatment with cytochalasin D or blebbistatin were also used for the same measurements to investigate the influence of cytoskeleton on cell stiffness.

4.3.9 Statistical analysis

The data were presented as mean ± standard deviation (SD) in Microsoft Excel. Significant difference of the results was performed by one-way ANOVAs with a Tukey's post-test for multiple variables and the confidence level was defined as 0.05 for all statistical results by using a KyPlot 5.0 software. The significant difference was considered when $p < 0.05$.

4.4 Results

4.4.1 Characteristics of micropatterns

The micropatterns were prepared by photo-grafting the azidophenyl-derived photo-reactive PVA (AzPhPVA) onto TCPS surfaces through a photomask. The dark regions in the photomask were not transparent for UV light (Figure 4.1a) and the TCPS surfaces under the dark regions remained un-modified. These regions were bare TCPS surfaces allowing cell adhesion (Figure 4.1b). The transparent regions in the photomask allowed photo-grafting of AzPhPVA under UV irradiation, which regions did not support cell adhesion. The photomask micropatterns had large and black circles with a diameter of 40, 60 and 80 μm, or the same large circles composed of 2 μm-diameter dark microdots. The area of large circles in the same row was the same, while the total surface area of the dark microdots in the same column was the same. The prepared micropatterns showed the same micropatterning structure as that of the designed photomask (Figure 4.1b). Cells cultured on the micropatterns were allowed to adhere only on TCPS surface regions, not on PVA surface regions. Therefore, the micropatterns in the same row could allow cells to have the same spreading area, but different adhesion area. In contrast, the micropatterns in the same column could allow cells to have the same adhesion area, but different spreading area. By using the micropatterns, cell spreading and adhesion areas could be independently controlled. S1256, S2826, and S5024 in Figure 4.1 indicated that cells on the micropatterns could spread to have an area of 1256, 2826 and 5024 μm^2, while A1256, A2826, and A5024 indicated cells could have an adhesion area of 1256, 2826 and 5024 μm^2.

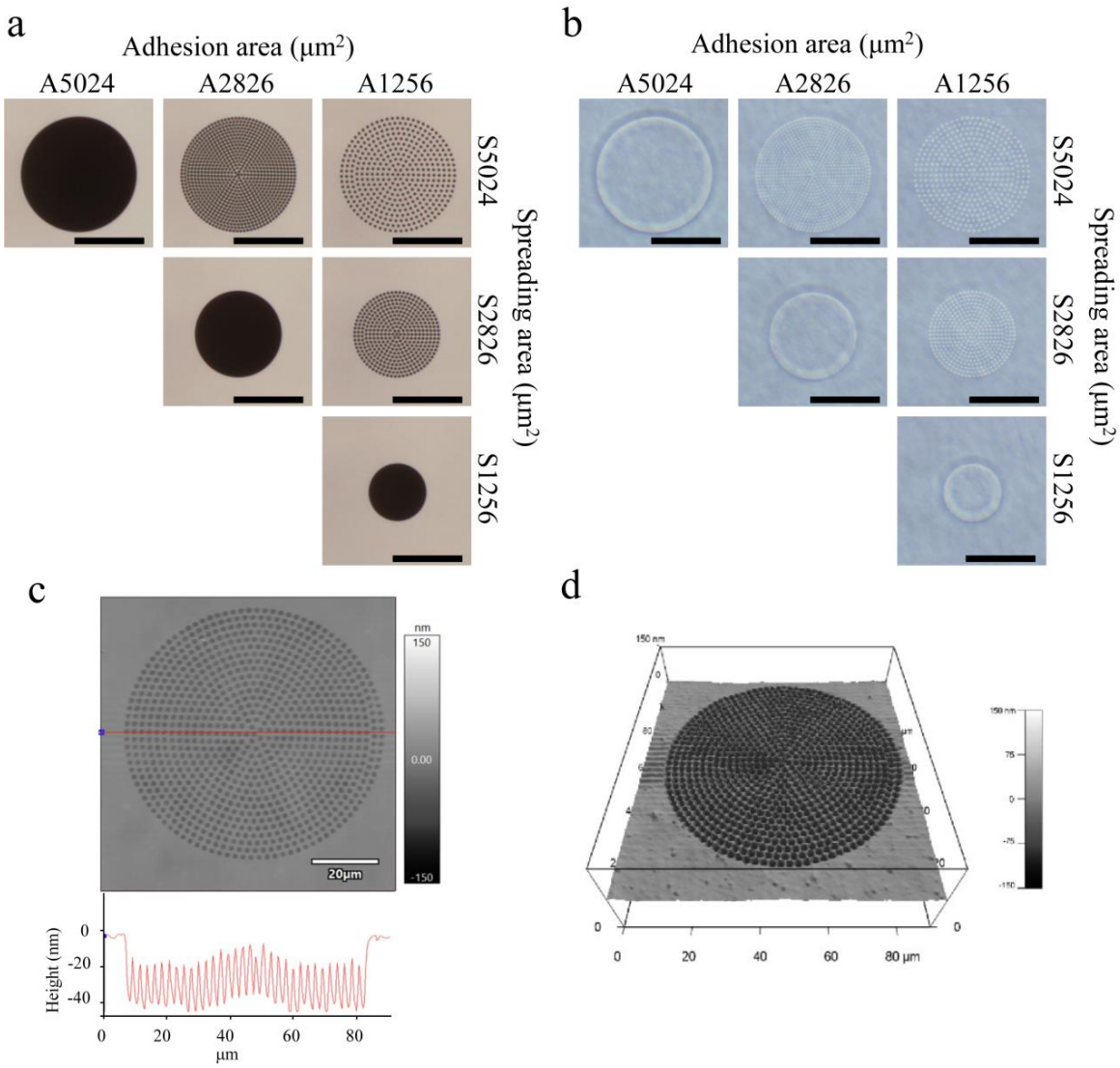

Figure 4.1 Characterization of micropatterns. (a) Phase-contrast micrographs of photomask. Scale bar: 50 μm. (b) Phase-contrast micrographs of the micropatterns. Scale bar: 50 μm. (c) AFM scanning height image (top) and section view (down) of a representative micropattern with an adhesion area of 2826 μm^2 and a spreading area of 5024 μm^2. (d) AFM 3D view of the micropattern shown in (c).

Table 4.1 Measured parameters of the micropatterns. Data represent the mean ± SD (n = 3).

Pattern types	S1256 A1256	S2826 A1256	S2826 A2826	S5024 A1256	S5024 A2826	S5024 A5024
Spreading area (μm^2)	1268.6±25.4	2863.8±47.6	2835.4±66.5	5112.3±50.8	5061.8±63.2	5074.3±191.2
Adhesion area (μm^2)	1268.6±25.4	1384.7±276.4	2835.4±66.5	1281.2±135.1	2969.1±296.7	5074.3±191.2
Size of microdots (μm)		2.1±0.3		2.0±0.2	2.1±0.1	
Distance between microdots (μm)		1.6±0.1		2.4±0.7	1.0±0.3	
PVA thickness (nm)	40.4±2.0	40.2±1.0	41.1±0.9	40.1±1.3	40.0±1.0	40.5±1.4

Each type of micropatterns was further characterized by AFM (Figure 4.1c, d). The AFM scanning images clearly showed the formation of microdots and micropattern structures. The microdot size, large circle size, distance between the microdots and PVA thickness were measured from the images (Table 4.1). Microdot size and large circle size were used to calculate the adhesion area and spreading area of each micropattern (Table 4.1). The spreading area, adhesion area, diameter of microdots and distance between microdots were almost the same as those of designed photomask. The thickness of photo-grafted PVA layers in each micropattern was also measured and shown in Table 4.1. The thickness of PVA graft layers was ~40 nm.

4.4.2 Cell morphology on micropatterns

To enhance cell attachment on micropatterns, fibronectin was coated on the micropatterns. Immunological staining showed that fibronectin was absorbed on the TCPS regions of the micropatterns (Figure 4.2). hMSCs were seeded and cultured on the micropatterns. After 24 hours culture, the cells adhered on the micropatterns and showed the same morphology as that of the large circles (Figure 4.3a). The results indicated that the area of large circles in the micropatterns could allow cells to fully spread to cover all the surface area and could restrain the cells in the large circles. The spreading area of the cells could be well controlled by the area of the large circles. Further, the percentage of micropattern circles occupied by cells and the percentage of single cell occupation were calculated by nuclei staining. More than 40% of the micropattern circles were occupied by hMSCs and the percentage of single cell occupation was over 60%.

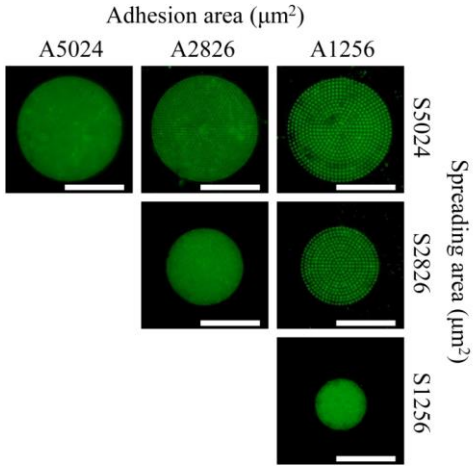

Figure 4.2 Representative fluorescence images of fibronectin-coated micropatterns observed by a fluorescent microscope. Scale bar: 50 μm.

4.4.3 FAs assembly on micropatterns

Cells can assemble focal adhesions (FAs) at the interface of cells and substrates [40]. Vinculin is associated with FAs and adhesion junctions. Vinculin was stained to investigate adhesion function of hMSCs on the micropatterns. Immunological staining results showed that FAs formation of hMSCs was confirmed for the cells cultured on all the micropatterns (Figure 4.3b). The cells having large adhesion area assembled fiber-like FAs, while those having small adhesion area had little influence on FAs organization even though the cells had large spreading area. The results indicated that FAs development was dominantly regulated by

cell adhesion area rather than spreading area. The total area and average size of FAs were measured by using a step-by-step quantitative analysis in an ImageJ software (Figure 4.3c, d). Both total area and average size of FAs increased significantly with increasing adhesion area, while spreading area did not have evident influence. The cells on A5024/S5024 micropatterns formed the most FAs (over 600 μm^2), twice larger than that of the cells on micropatterns having the smallest adhesion area (A1256/S1256, A1256/S2826 and A1256/S5024). The average size of FAs in the cells on A5024/S5024 micropattern was about 5 μm^2 while that on micropatterns having the smallest adhesion area (A1256/S1256, A1256/S2826 and A1256/S5024) was below 2 μm^2. Therefore, FAs formation was closely correlated with cell adhesion area, rather than cell spreading area.

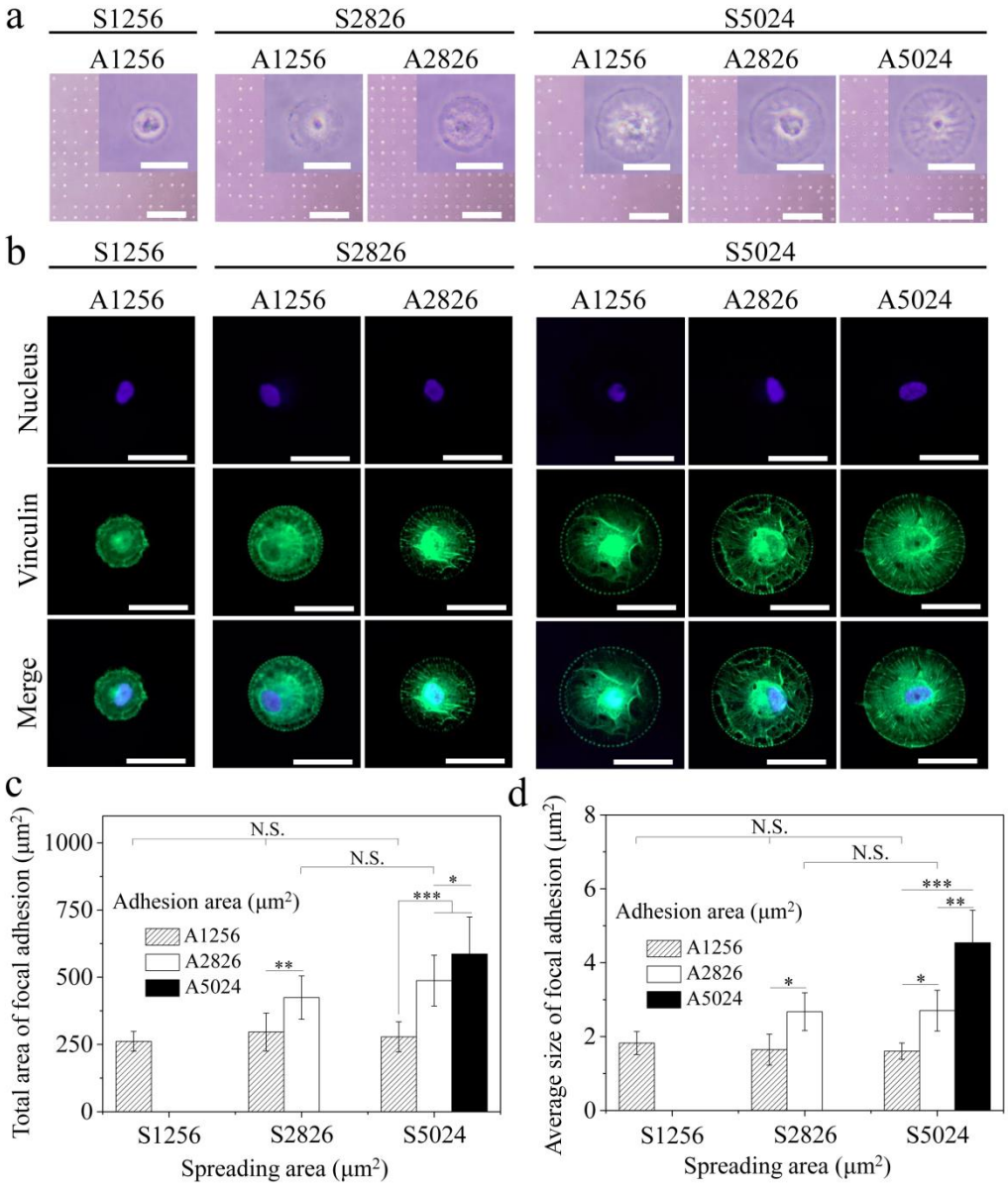

Figure 4.3 (a) Phase-contrast micrographs of hMSCs cultured on the micropatterns for 24 hours. The low magnification images show cell adhesion and distribution (bright dots) on the micropatterns. Scale bar: 500 μm. The inserts are the high magnification of representative images of micropatterned cells. Scale bar: 50 μm. (b) Representative images of stained FAs (green fluorescence) in the micropatterned hMSCs. Nucleus was stained blue. Scale bar: 50 μm. (c) Total area and (d) average size of FAs. Data represent the mean ± SD (n = 25), N.S. represents no significant difference, *p < 0.05, **p < 0.01, ***p < 0.001.

4.4.4 Influence of cell adhesion and spreading areas on gene transfection

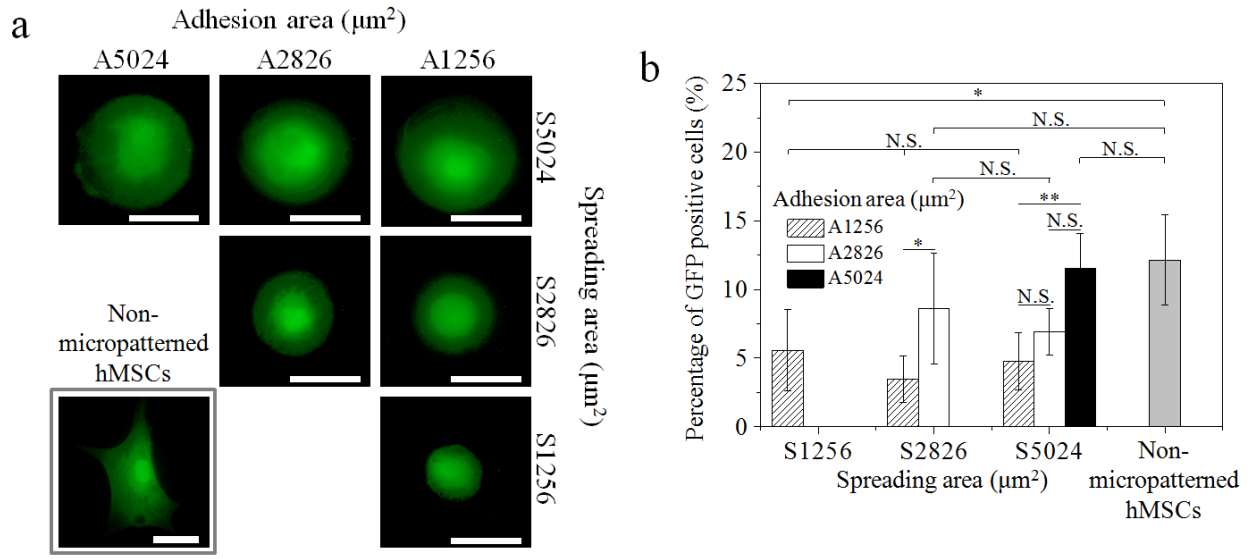

Figure 4.4 Influence of cell spreading and adhesion areas on gene transfection of hMSC cultured on the micropatterns and non-micropatterned TCPS. (a) Representative images of green GFP positive cells. The green GFP positive cell at the lower left is the representative image of hMSCs on the TCPS surface without micropatterns. Scale bar: 50 μm. (b) Gene transfection efficiency. Data represent the mean ± SD (n = 5), N.S. represents no significant difference, $*p < 0.05$, $**p < 0.01$.

After hMSCs were cultured with cationic lipoplexes for 24 hours, the cells expressing GFP proteins were observed with a fluorescent microscope. The transfected cells expressed green fluorescence as shown in Figure 4.4a. The percentage of transfected cells was calculated by dividing the number of transfected cells with total cell number (Figure 4.4b). The percentage of transfected cells increased significantly with cell adhesion area, while remained at the same level for cells having different spreading areas but the same adhesion area. The cells with an adhesion area of 5024 μm^2 had the highest gene transfection efficiency (over 10%), which was almost twice higher than that of cells with an adhesion area of 1256 μm^2. In addition, hMSCs were seeded on the fibronectin-coated TCPS surfaces as control group. Gene transfection efficiency of the cells on fibronectin-coated TCPS surface was compared with that of cells on A1256/S1256, A2826/S2826 and A5024/S5024 micropatterns. Further, gene transfection was performed in hMSCs of another two batches (lot number: 18TL312488 and 18TL113327) to confirm that transfection efficiency was affected by cell adhesion area, rather than cell spreading area. The results indicated that cell adhesion area had a dominant effect on gene transfection, while cell spreading area had little effect.

It has been reported that lipofectamine/pDNA complexes may be cytotoxic with increasing lipofectamine concentration [41]. In order to investigate the influence of lipoplexes on cell viability, the cells on the micropatterns before and after gene transfection were stained with calcein-AM and propidium iodide to visualize living cells and dead cells. 92.6~97.6% of the cells on the micropatterns were alive. Cell viability on all the micropatterns was very high. Living cell percentage before and after gene transfection was not significantly different. The results suggested that plasmid/lipofectamine lipoplexes did not show an obvious influence on cell viability.

Furthermore, gene transfection was carried out after treatment with actin filaments or myosin inhibitor (Figure 4.5). Few cells after inhibitor treatment were detected positive for GFP fluorescence, suggesting few cells after inhibitor treatment were transfected with the GFP genes. The results indicated that cytoskeletal

structures played an important role in regulating gene transfection.

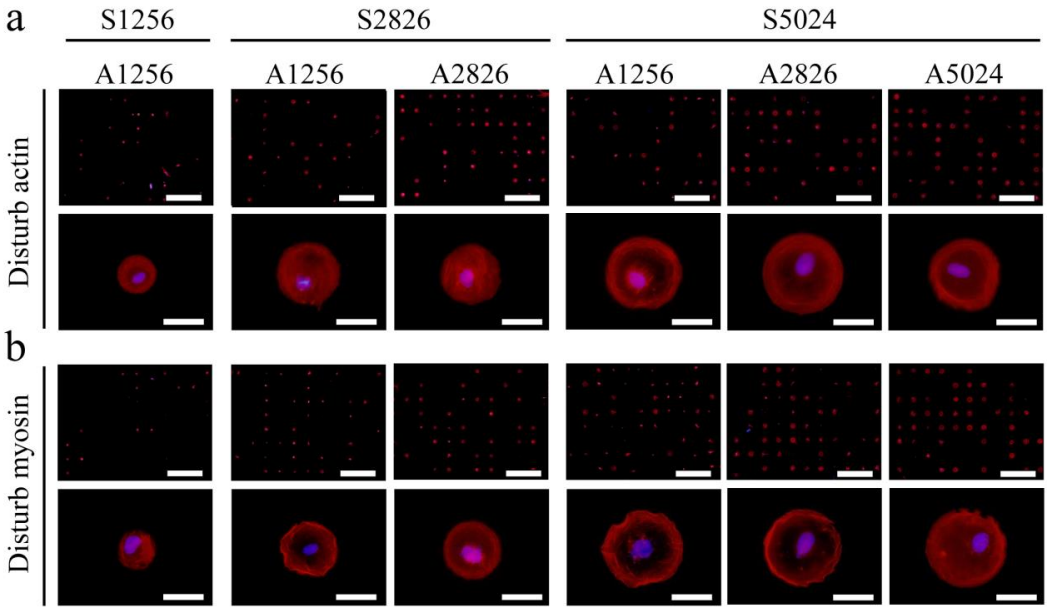

c

	Cyto D treatment	Bleb treatment
S1256/A1256	1/246	0/296
S2826/A1256	0/261	0/277
S2826/A2826	0/358	1/391
S5024/A1256	0/284	0/306
S5024/A2826	0/368	0/356
S5024/A5024	4/434	2/466

Figure 4.5 Influence of actin (Cyto D) or myosin (Bleb) inhibitor treatment on gene transfection. Representative fluorescence images of hMSCs cultured on the micropatterns after treatment with (a) cytochalasin D or (b) blebbistatin. Top row is the representative images at a low magnification (scale bar: 500 μm) and bottom row is those at a high magnification (scale bar: 50 μm). Transfected cells expressed GFP (green). Actin filaments and nucleus were stained red and blue, respectively. (c) Ratio of GFP positive cells to the total cells.

4.4.5 Cellular uptake of FITC-labeled microspheres

Cellular uptake of exogenous genes should be one of the aspects that affect gene transfection. Therefore, FITC-labeled microspheres were used to replace plasmids to investigate cellular uptake capacity. The FITC-labeled microspheres were incorporated into the lipoplexes for the transfection experiment. Fluorescence microscopy observation showed that the green FITC-labeled microspheres were observed in hMSCs on the micropatterns (Figure 4.6a). Quantification of total fluorescent yield of FITC in each cell showed that fluorescence yield significantly increased with increasing cell adhesion area, while did not change with cell spreading area (Figure 4.6b). The fluorescence yield of FITC on micropatterns having an adhesion area 5024 μm^2 was almost twice higher than that on micropatterns having an adhesion area 1256 μm^2. The results indicated that cell adhesion area had a correlative relationship with the uptake of exogenous microspheres, while cell spreading area did not affect the uptake. Therefore, high uptake capacity of large cell adhesion area should be one of the reasons for its promotive influence on gene transfection.

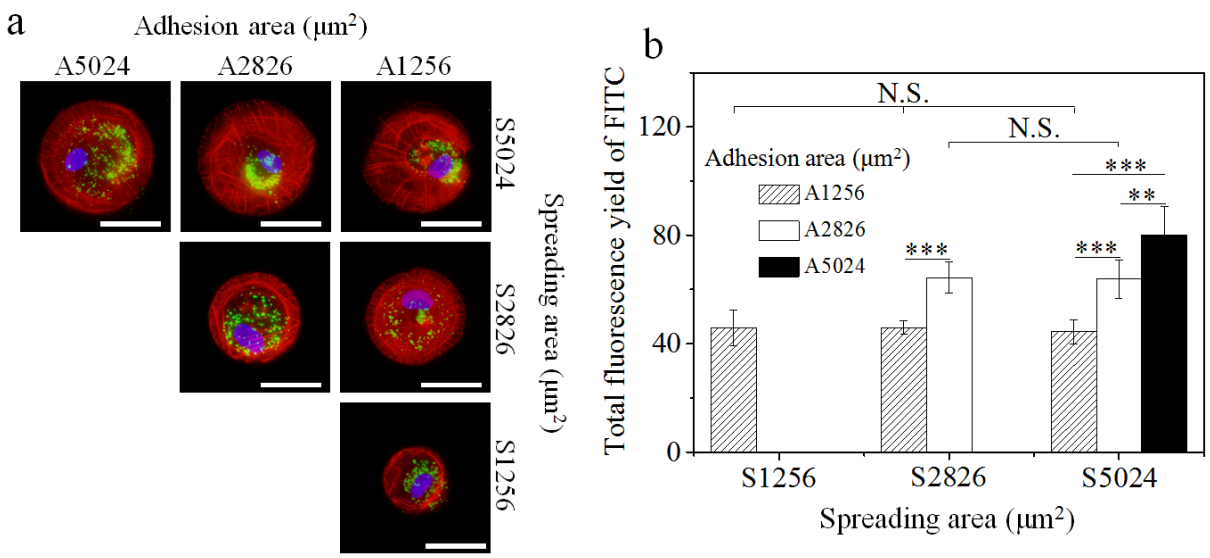

Figure 4.6 Cellular uptake capacity of FITC-labeled microspheres in hMSCs cultured on the micropatterns. (a) Representative fluorescence images of hMSCs showing cellular uptake of green FITC microspheres (green fluorescence). Nucleus and actin filaments were stained blue and red, respectively. Scale bar: 50 μm. (b) Total fluorescence yield of FITC in the micropatterned hMSCs. Data represent the mean ± SD (n = 25), N.S. represents no significant difference, $^{**}p < 0.01$, $^{***}p < 0.001$.

4.4.6 DNA synthesis activity of hMSCs on micropatterns

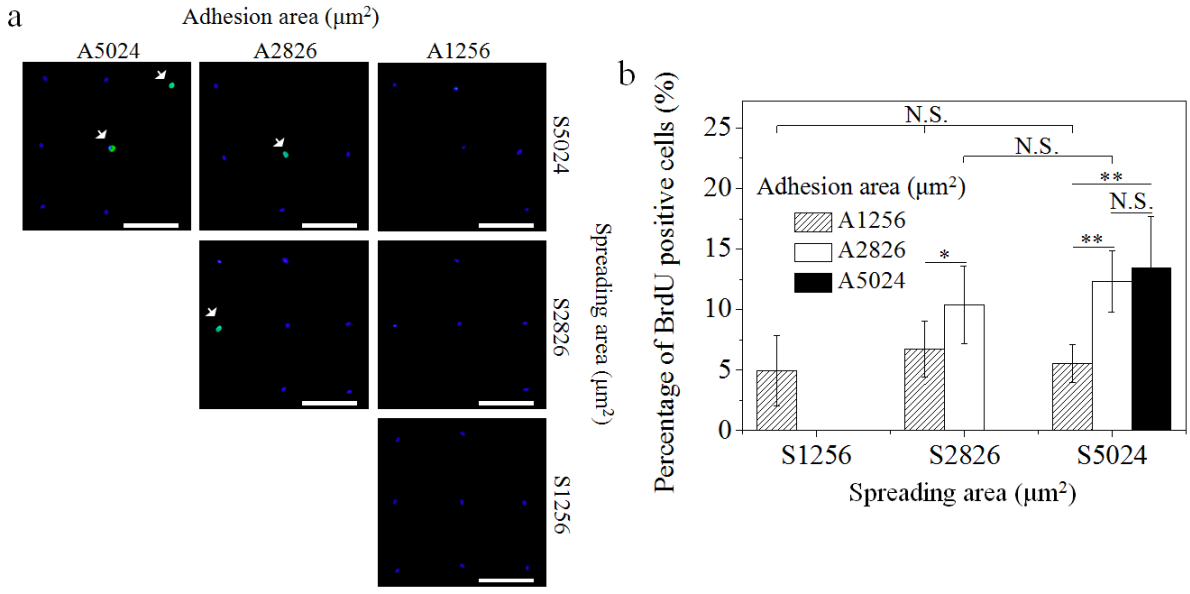

Figure 4.7 DNA synthesis activity of hMSCs cultured on the micropatterns. (a) Representative fluorescence images of nucleus (blue) and BrdU (green) staining. Scale bar: 200 μm. (b) Percentage of BrdU positively stained hMSCs. Data represent the mean ± SD (n = 5), N.S. represents no significant difference, $^{*}p < 0.05$, $^{**}p < 0.01$.

DNA synthesis activity is another important aspect for transfection and expression of exogenous genes. DNA synthesis activity of hMSCs cultured on the micropatterns was investigated by BrdU staining (Figure 4.7a). The single cell number with positive BrdU staining was counted and its percentage to the total cell

number was calculated (Figure 4.7b). The percentage of positively stained cells increased significantly with cell adhesion area. The positively stained cells with an adhesion area of 5024 μm^2 were two folds higher than those with an adhesion area of 1256 μm^2 even the cells presented the same spreading area of 5024 μm^2. The percentage of positively stained cells with the same adhesion areas remained almost unchanged even cell spreading area increased. The results suggested that DNA synthesis activity of the micropatterned cells was dominantly regulated by cell adhesion area, while hardly affected by cell spreading area. High DNA synthesis activity should facilitate the expression of transfected GFP gene.

4.4.7 Cytoskeletal structures of hMSCs on micropatterns

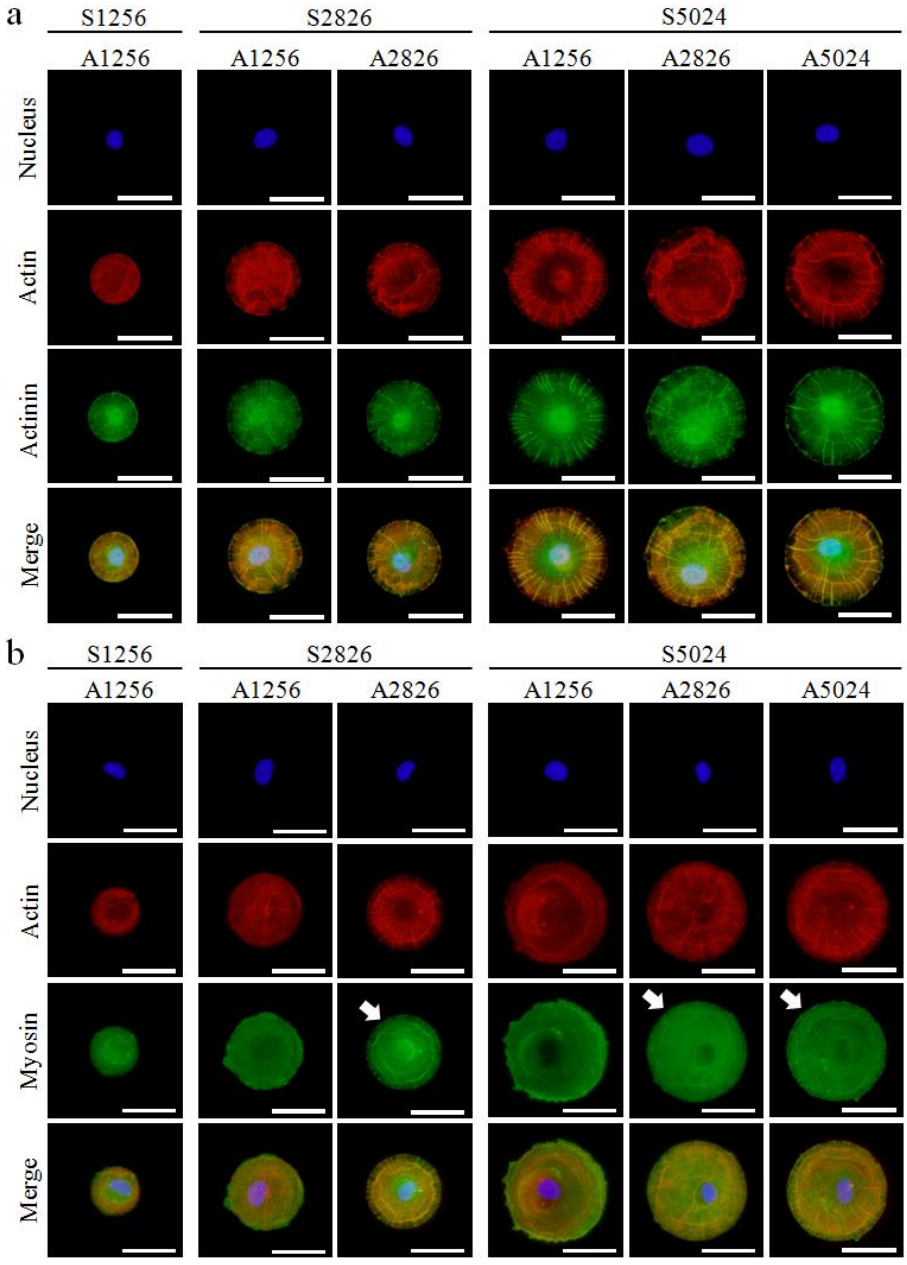

Figure 4.8 Assembly of cytoskeletal structures of hMSCs cultured on the micropatterns. (a) Staining of actin filaments (red), actinin (green) and nucleus (blue). Scale bar: 50 μm. (b) Staining of actin filaments (red), myosin (green) and nucleus (blue). The white arrows show the fiber-like myosin structures in the micropatterned cells. Scale bar: 50 μm.

Cytoskeleton not only serves as cellular framework, but also plays an important role in regulating cell functions [29, 42-45]. The micropatterns might affect gene transfection through the regulation of cytoskeleton structures. Therefore, actin filaments and their binding proteins, actinin and myosin, were stained to investigate the change of cytoskeleton when hMSCs were cultured on the micropatterns (Figure 4.8). Interestingly, hMSCs with a large adhesion area assembled actin filaments in both radius and concentric directions. It has been reported that actinin can bond with the end of actin fibers and gather the fibers together to weave actin filaments into intercalated disc of cell membrane [46, 47]. Actinin staining showed that fiber-like actinin structures were observed in cells with a large adhesion area. However, well-organized actin filaments were hardly observed and fiber-like actinins disappeared in cells with a small adhesion area even the cells had a large spreading area (Figure 4.8a).

Myosin staining showed that fiber-like myosin structures were formed in cells with a large adhesion area of 2826 and 5024 μm^2, marked by white arrows (Figure 4.8b). The cells arranged the fiber-like myosin structures in both radius and concentric directions similar to actin filaments and actinin distribution. The merged actin and myosin images disclosed the co-localization of fiber-like myosin structures and actin filaments in the cells with a large adhesion area, indicating that punctuated myosin was always bonded to actin filaments. However, small adhesion area did not show evident effect on formation of fiber-like myosin structures even the spreading area was large. The results together with vinculin staining results suggested that cell adhesion area affected cytoskeleton organization more strongly than did cell spreading area.

4.4.8 Young's modulus of hMSCs on micropatterns

After hMSCs were cultured on the micropatterns for 24 hours, the mechanical assay was conducted to obtain Young's modulus of the cells. The results showed that cell stiffness increased from 1.0 to 1.6 kPa with increasing cell adhesion area, while did not change with cell spreading area (Figure 4.9a). The high stiffness of cells with large adhesion area should be due to their well-developed actin and myosin structures as shown above. Young's modulus of the micropatterned cells after treatment with cytochalasin D and blebbistatin was measured to verify the influence of actin and myosin formation on cellular mechanics. After treatment by actin filaments or myosin inhibitor, the actin filament and myosin staining images showed that fiber-like structures disappeared in all the micropatterned cells. The Young's modulus of cells after treatment with the inhibitors decreased to 0.8-1.0 kPa (Figure 4.9b, c). All the treated cells showed lower Young's modulus than did their respective cells before treatment. Interestingly, Young's modulus of cells with a large adhesion area showed a bigger decrease (decreasing by 0.6 kPa) than did the cells with a small adhesion area. Disturbance of cytoskeleton decreased cell stiffness, demonstrating the strong relationship between cell stiffness and cytoskeleton structure.

4.4.9 Mechanotransduction of hMSCs on micropatterns

It has been reported that cells can transduce their cytoskeletal tension into nuclei to affect cell functions including differentiation and uptake through the mechanotransduction process [36]. Yes-associated protein (YAP) and transcriptional coactivator with PDZ-binding motif (TAZ) serve as the mechanical sensor and signal mediator in Hippo pathway [48]. Nuclear localized YAP/TAZ has been considered as a primary regulatory component managing gene expression of hMSCs in response to biophysical stimuli [49]. Therefore, staining of YAP/TAZ was conducted to show the mechanotransduction signals in the micropatterned hMSCs. Cell nucleus was co-stained with YAP/TAZ (Figure 4.9d). The cells on the A5024

and A2826 micropatterns showed obvious nuclear localization of YAP/TAZ, while the cells on the A1256 micropatterns showed more distribution of YAP/TAZ in cytoplasm. Further quantitative analysis of nuclear localization of YAP/TAZ is shown in Figure 4.9e. The percentage of cells with obvious nuclear YAP/TAZ location increased from 20% to 60% and 73% when the cell adhesion area increased from 1256 μm^2 (A1256) to 2826 (A2826) and 5024 (A5024) μm^2. However, the percentage remained at the same level when cell spreading area increased from 1256 to 5024 μm^2 if cell adhesion area did not change. The results suggested that cell adhesion area could affect cell functions through nuclear YAP/TAZ localization, while cell spreading area did not affect nuclear YAP/TAZ localization.

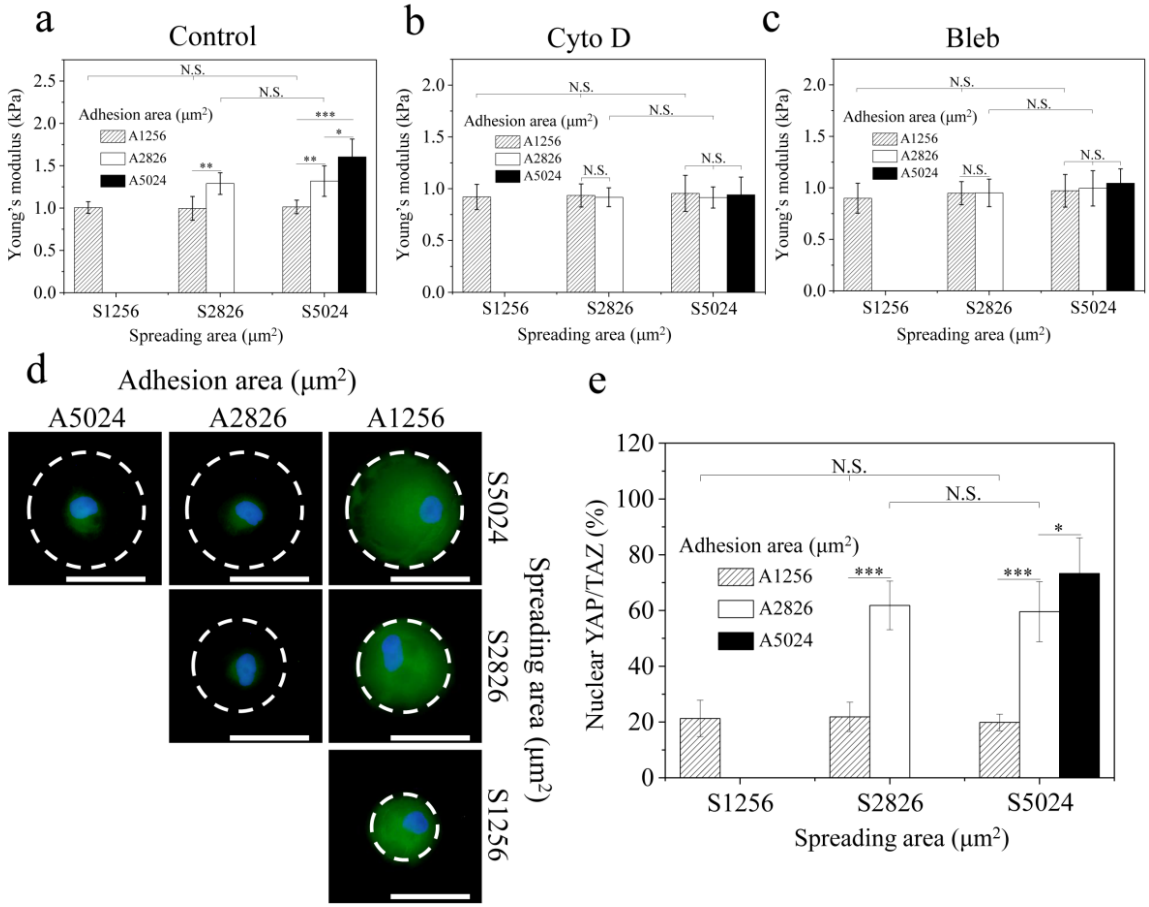

Figure 4.9 Young's modulus of hMSCs cultured on the micropatterns before (a) and after treatment with actin (b, Cyto D) or myosin (c, Bleb) inhibitor. Data represent the mean ± SD (n = 10), N.S. represents no significant difference, *p < 0.05, **p < 0.01, ***p < 0.001. (d) Representative fluorescence staining images of YAP/TAZ (green) and nucleus (blue). The dashed white lines show the contours of cells. Scale bar: 50 μm. (e) Percentage of micropatterned hMSCs with local accumulation of nuclear YAP/TAZ. Data represent the mean ± SD (n = 5), N.S. represents no significant difference, *p < 0.05, ***p < 0.001.

4.5 Discussion

Microfabrication techniques open an accessible door to control single cell morphology [28-36]. Many researches have shown that cell morphology can affect cell functions such as cell adhesion, spreading, proliferation, apoptosis and differentiation [50-52]. However, the influence of cell morphology on gene transfection remains exclusive. In particular, it is not clear how cell adhesion and spreading areas affect

exogenous gene transfection. Therefore, micropatterns were designed to separate cell adhesion and spreading areas (Figure 4.1) and their influence on the transfection of exogenous genes was compared.

GFP encoded exogenous plasmid was applied to investigate the effect of cell adhesion and spreading areas on gene transfection. The transfected hMSCs could express GFP and therefore be observed by a fluorescence microscope (Figure 4.4a). The difference in gene transfection efficiency was confirmed when cell adhesion area changed. The efficiency increased significantly with increasing of cell adhesion area, while it was not affected by cell spreading area (Figure 4.4b). The results could be explained by the high uptake capacity and DNA synthesis activity of hMSCs having a large adhesion area. Cellular uptake capacity of exogenous microparticles increased with cell adhesion area, while cell spreading area did not affect cellular uptake capacity (Figure 4.6). DNA synthesis activity also increased with cell adhesion area, while was not affected by cell spreading area (Figure 4.7). The gene transfection efficiency had a good correlation with cellular uptake capacity and DNA synthesis activity.

These results should be due to the different cytoskeleton organization and mechanotransduction of hMSCs when their spreading area and adhesion area were regulated by different micropatterns. The micropatterned hMSCs wove their actin cytoskeleton and the bonding protein actinin in radius or concentric directions. The fiber-like actinin and actin were well organized in the cells with large adhesion area but less organized in the cells with small adhesion area, which was independent on cell spreading area (Figure 4.8a). Actinin can enable to organize the thick actin bundles onto the intercalated disc in cell membrane to regulate cellular functions [29]. Myosin is an ATP-dependent motor protein in eukaryotes [53]. One side of myosin is connected to contractive vertical stress fibers and transverse arcs as the mechanical anchor to take charge of actin motility and the other side can combine with exogenous cargos to mediate cell uptake [45, 54]. Thus, myosin plays a fatal role in regulating cytoskeletal contractility and cellular internalization. The fiber-like myosin structures were formed in the large adhesion area cells but rarely found in the small adhesion area cells, while myosin structures had no significant difference when cell spreading area changed (Figure 4.8b).

The fiber-like myosin structures are capable to induce cytoskeletal tension [55]. Young's modulus of the micropatterned hMSCs increased significantly with increasing of cell adhesion area, while was not affected by cell spreading area (Figure 4.9a). After treatment with actin filament or myosin inhibitor, Young's modulus decreased and showed no significant difference among all the micropatterned cells (Figure 4.9b, c). Few of the treated cells could be transfected with exogenous genes. The results confirmed that well-organized actin filaments and fiber-like myosin structures were required for cellular mechanics and regulation of gene transfection.

FAs structure is also efficient in the regulation of cellular uptake capacity [53, 56]. FAs are an intimate bonding between actin filaments and integrins on plasma membrane and act as the anchors between cells and ECMs [35, 57]. They are also regarded as the mechanosensor for extracellular stimuli to regulate the expression of FA-related genes and RhoA GTPase activity [58]. The morphologic diversity induced by different spreading and adhesion area in this study might intertwine FAs, cytoskeleton and related proteins together to affect cellular uptake. Vinculin was stained to show FAs formation. Fiber-like mature and large FAs (5 μm^2) were formed in cells with large adhesion area, while small FAs complexes (< 2 μm^2) were formed in the cells with small adhesion area even if the spreading area was large (Figure 4.3).

Organization of cytoskeleton can generate mechanotransduction signals to affect cell activity [48, 59]. The mechanotransduction signal, YAP/TAZ, showed different activation in the micropatterned hMSCs (Figure 4.9d). YAP/TAZ was mainly localized in nuclear region of the cells with large adhesion area, while was almost diffused in cytoplasm in the cells with small adhesion area even the cells had large spreading area (Figure 4.9e). The results should be due to the different intracellular tension in the micropatterned cells. Some studies have shown that change of YAP/TAZ transcriptional activity can be induced by diversified cell

mechanics and therefore modulate cell functions [35, 48]. High intracellular tension facilitated the nuclear accumulation of YAP/TAZ in the cells with large adhesion area, while low tension induced YAP/TAZ in the whole cytoplasm in the cells with small adhesion area, which was independent on cell spreading area. Based on the results, a possible mechanism of influence of cell adhesion and spreading areas on gene transfection was proposed as shown in Figure 4.10. The cells with small adhesion area predominantly formed cortex actin at the periphery of cells, independent of cell spreading area. This could lead to weak cytoskeletal tension, YAP/TAZ dispersion in the cytoplasm and low DNA synthesis activity, therefore resulting in low transfection efficiency. On the other hand, cells with large adhesion area could develop well-organized cytoskeleton structures (actin, actinin and myosin). Strong cytoskeletal tension could induce YAP/TAZ nuclear localization and high cellular activity, thus resulting in high transfection efficiency. The promotive effect of cell adhesion area on gene transfection should provide some important information for therapeutic potential of non-viral gene therapies. Large adhesion area should be considered to achieve high transfection efficiency for such applications.

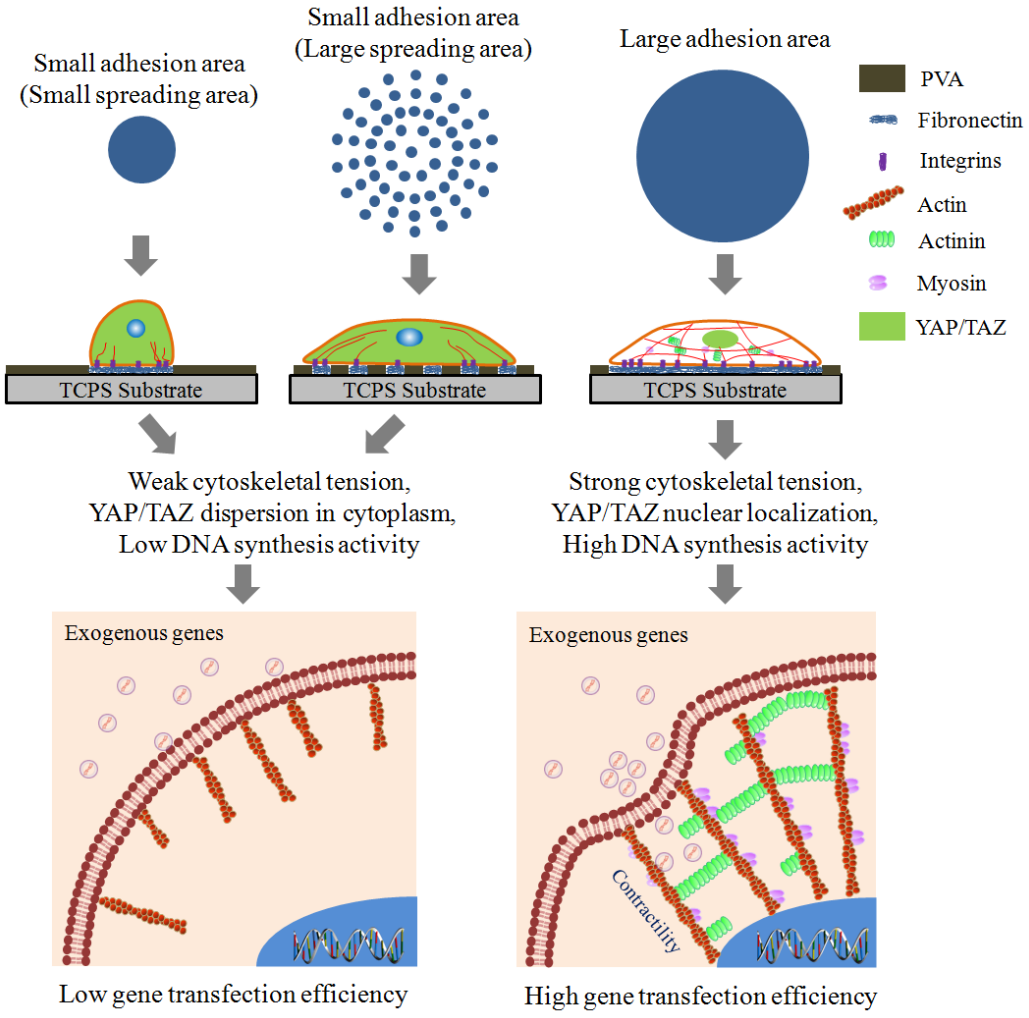

Figure 4.10 Illustrative mechanism of influence of cytoskeleton structures on gene transfection of micropatterned hMSCs. The cells with small adhesion area predominantly formed cortex actin at the periphery of cells, independent of cell spreading area. This could lead to weak cytoskeletal tension, YAP/TAZ dispersion in cytoplasm and low DNA synthesis activity, therefore resulting in low transfection efficiency. On the other hand, cells with large adhesion area could develop well-organized cytoskeleton structures (actin, actinin and myosin). Strong cytoskeletal tension could induce YAP/TAZ nuclear localization and high cellular activity, thus resulting in high transfection efficiency.

4.6 Conclusions

PVA micropatterns on TCPS surfaces were prepared and used for the culture of hMSCs to independently separate adhesion and spreading areas of hMSCs. Influence of cell adhesion and spreading areas on transfection of exogenous genes was compared on the micropatterns. Cell adhesion area showed dominant influence on gene transfection, while cell spreading area did not affect gene transfection. The high transfection efficiency of the cells having large adhesion area should be due to their high uptake capacity and DNA synthesis activity through FAs formation, cytoskeletal mechanics and YAP/TAZ nuclear localization. The results will provide some useful information for understanding of transfection mechanism and development of new transfection techniques.

4.7 References

[1] T. K. Kim, J. H. Eberwine, Mammalian cell transfection: the present and the future, Analytical and Bioanalytical Chemistry 397(8) (2010) 3173-3178.
[2] B. S. Joshi, M. A. de Beer, B. N. G. Giepmans, I. S. Zuhorn, Endocytosis of extracellular vesicles and release of their cargo from endosomes, ACS Nano 14(4) (2020) 4444-4455.
[3] X. Chen, Current and future technological advances in transdermal gene delivery, Advanced Drug Delivery Reviews 127(1) (2018) 85-105.
[4] M. T. Vitor, S. Sart, A. Barizien, L. G. Torre, C. N. Baroud, Tracking the evolution of transiently transfected individual cells in a microfluidic platform, Scientific Reports 8(1) (2018) 1225.
[5] C. E. Dunbar, K. A. High, J. K. Joung, D. B. Kohn, K. Ozawa, M. Sadelain, Gene therapy comes of age, Science 359(6372) (2018) eaan4672.
[6] G. J. Doherty, H. T. McMahon, Mechanisms of endocytosis, Annual Review of Biochemistry 78(1) (2009) 857-902.
[7] J. M. Besterman, R. B. Low, Endocytosis: a review of mechanisms and plasma membrane dynamics, Biochemical Journal 210(1) (1983) 1-13.
[8] H. J. Vaughan, J. J. Green, S. Y. Tzeng, Cancer-targeting nanoparticles for combinatorial nucleic acid delivery, Advanced Materials 32(13) (2020) 1901081.
[9] K. Sugano, M. Kansy, P. Artursson, A. Avdeef, S. Bendels, L. Di, G. F. Ecker, B. Faller, H. Fischer, G. Gerebtzoff, H. Lennernaes, F. Senner, Coexistence of passive and carrier-mediated processes in drug transport, Nature Reviews Drug Discovery 9(8) (2010) 597-614.
[10] M. Drechsler, F. Giavazzi, R. Cerbino, I. M. Palacios, Active diffusion and advection in drosophila oocytes result from the interplay of actin and microtubules, Nature Communications 8(1) (2017) 1520.
[11] M. Mittasch, P. Gross, M. Nestler, A. W. Fritsch, C. Iserman, M. Kar, M. Munder, A. Voigt, S. Alberti, S. W. Grill, M. Kreysing, Non-invasive perturbations of intracellular flow reveal physical principles of cell organization, Nature Cell Biology 20(3) (2018) 344-351.
[12] T. M. Fyles, Synthetic ion channels in bilayer membranes, Chemical Society Reviews 36(2) (2007) 335-347.
[13] E. Yuba, Y. Nakajima, K. Tsukamoto, S. Iwashita, C. Kojima, A. Harada, K. Kono, Effect of unsaturated alkyl chains on transfection activity of poly(amidoamine) dendron-bearing lipids, Journal of Controlled Release 160(3) (2012) 552-560.
[14] S. Huang, J. Li, L. Han, S. Liu, H. Ma, R. Huang, C. Jiang, Dual targeting effect of Angiopep-2-modified, DNA-loaded nanoparticles for glioma, Biomaterials 32(28) (2011) 6832-6838.

[15] K. Sandvig, S. Pust, T. Skotland, B. Deurs, Clathrin-independent endocytosis: mechanisms and function, Current Opinion in Cell Biology 23(4) (2011) 413-420.
[16] J. S. Wadia, R. V. Stan, S. F. Dowdy, Transducible TAT-HA fusogenic peptide enhances escape of TAT-fusion proteins after lipid raft macropinocytosis, Nature Medicine 10(3) (2004) 310-315.
[17] A. Y. Lee, M. H. Cho, S. Kim, Recent advances in aerosol gene delivery systems using non-viral vectors for lung cancer therapy, Expert Opinion on Drug Delivery 16(7) (2019) 757-772.
[18] C. T. Ilarduya, Y. Sun, N. Düzgüneş, Gene delivery by lipoplexes and polyplexes, European Journal of Pharmaceutical Sciences 40(3) (2010) 159-170.
[19] W. Song, Z. Ma, Y. Zhang, C. Yang, Autophagy plays a dual role during intracellular siRNA delivery by lipoplex and polyplex nanoparticles, Acta Biomaterialia 58 (2017) 196-204.
[20] Y. Yang, X. Wang, X. Hu, N. Kawazoe, Y. Yang, G. Chen, Influence of cell morphology on mesenchymal stem cell transfection, ACS Applied Materials & Interfaces 11(2) (2019) 1932-1941.
[21] L. H. Wang, D. C. Wu, H. X. Xu, Y. Z. You, High DNA-binding affinity and gene-transfection efficacy of bioreducible cationic nanomicelles with a fluorinated core, Angewandte Chemie International Edition 55(2) (2016) 755-759.
[22] M. Wang, H. Liu, L. Li, Y. Cheng, A fluorinated dendrimer achieves excellent gene transfection efficacy at extremely low nitrogen to phosphorus ratios, Nature Communications 5(1) (2014) 3053.
[23] J. Buck, P. Grossen, P. R. Cullis, J. Huwyler, D. Witzigmann, Lipid-based DNA therapeutics: hallmarks of non-viral gene delivery, ACS Nano 13(4) (2019) 3754-3782.
[24] R. Sheng, T. Luo, Y. Zhu, H. Li, J. Sun, S. Chen, W. Sun, A. Cao, The intracellular plasmid DNA localization of cationic reducible cholesterol-disulfide lipids, Biomaterials 32(13) (2011) 3507-3519.
[25] J. Lee, Y. J. Cho, J. W. Lee, H. J. Ahn, KSP siRNA/paclitaxel-loaded PEGylated cationic liposomes for overcoming resistance to KSP inhibitors: synergistic antitumor effects in drug-resistant ovarian cancer, Journal of Controlled Release 321(10) (2020) 184-197.
[26] Y. Zhao, A. Liu, Y. Du, Y. Cao, E. Zhang, Q. Zhou, H. Hai, Y. Zhen, S. Zhang, Effects of sucrose ester structures on liposome-mediated gene delivery, Acta Biomaterialia 72 (2018) 278-286.
[27] S. Guan, A. Munder, S. Hedtfeld, P. Braubach, S. Glage, L. Zhang, S. Lienenklaus, A. Schultze, G. Hasenpusch, W. Garrels, F. Stanke, C. Miskey, S. M. Johler, Y. Kumar, B. Tümmler, C. Rudolph, Z. Ivics, J. Rosenecker, Self-assembled peptide-poloxamine nanoparticles enable in vitro and in vivo genome restoration for cystic fibrosis, Nature Nanotechnology 14 (2019) 287-297.
[28] I. A. Khalil, K. Kogure, H. Akita, H. Harashima, Uptake pathways and subsequent intracellular trafficking in nonviral gene delivery, Pharmacological Reviews 58(1) (2006) 32-45.
[29] M. Bao, J. Xie, W. T. S. Huck, Recent advances in engineering the stem cell microniche in 3D, Advanced Science 5(8) (2018) 1800448.
[30] Y. Yang, X. Wang, T. C. Huang, X. Hu, N. Kawazoe, W. B. Tsai, Y. Yang, G. Chen, Regulation of mesenchymal stem cell functions by micro-nano hybrid patterned surfaces, Journal of Materials Chemistry B 6(34) (2018) 5424-5434.
[31] X. Wang, W. Song, N. Kawazoe, G. Chen, The osteogenic differentiation of mesenchymal stem cells by controlled cell-cell interaction on micropatterned surfaces, Journal of Biomedical Materials Research Part A 101(12) (2013) 3388-3395.
[32] X. Wang, N. R. Bolanos, B. Jiang, G. A. Ameer, Advanced functional biomaterials for stem cell delivery in regenerative engineering and medicine, Advanced Functional Materials 29(23) (2019) 1809009.
[33] Y. Yang, X. Wang, Y. Wang, X. Hu, N. Kawazoe, Y. Yang, G. Chen, Influence of cell spreading area on the osteogenic commitment and phenotype maintenance of mesenchymal stem cells, Scientific Reports 9(1) (2019) 6891.

[34] M. Bao, J. Xie, A. Piruska, W. T. S. Huck, 3D microniches reveal the importance of cell size and shape, Nature Communications 8 (2017) 1962.
[35] G. Nardone, J. O. Cruz, J. Vrbsky, C. Martini, J. Pribyl, P. Skládal, M. Pešl, G. Caluori, S. Pagliari, F. Martino, Z. Maceckova, M. Hajduch, A. S. Garcia, N. M. Pugno, G. B. Stokin, G. Forte, YAP regulates cell mechanics by controlling focal adhesion assembly, Nature Communications 8(1) (2017) 15321.
[36] Z. Lia, H. Lee, C. Zhu, Molecular mechanisms of mechanotransduction in integrin-mediated cell-matrix adhesion, Experimental Cell Research 349(1) (2016) 85-94.
[37] J. M. Kalappurakkal, A. A. Anilkumar, C. Patra, T. S. Zanten, M. P. Sheetz, S. Mayor, Integrin mechano-chemical signaling generates plasma membrane nanodomains that promote cell spreading, Cell 177(7) (2019) 1738-1756.
[38] W. Song, H. Lu, N. Kawazoe, G. Chen, Gradient patterning and differentiation of mesenchymal stem cells on micropatterned polymer surface, Journal of Bioactive and Compatible Polymers 26(3) (2011) 242-256.
[39] U. Horzum, B. Ozdil, D. P. Okvur, Step-by-step quantitative analysis of focal adhesions, MethodsX 1 (2014) 56-59.
[40] E. K. F. Yim, E. M. Darling, K. Kulangara, F. Guilak, K. W. Leong, Nanotopography-induced changes in focal adhesions, cytoskeletal organization, and mechanical properties of human mesenchymal stem cells, Biomaterials 31(6) (2010) 1299-1306.
[41] L. T. Nguyen, K. Atobe, J. M. Barichello, T. Ishida, H. Kiwada, Complex formation with plasmid DNA increases the cytotoxicity of cationic liposomes, Biological and Pharmaceutical Bulletin 30(4) (2007) 751-757.
[42] Y. Li, K. A. Kilian, Bridging the gap: from 2D cell culture to 3D microengineered extracellular matrices, Advanced Healthcare Materials 4(18) (2015) 2780-2796.
[43] X. Wang, X. Hu, N. Kawazoe, Y. Yang, G. Chen, Manipulating cell nanomechanics using micropatterns, Advanced Functional Materials 26(42) (2016) 7634-7643.
[44] J. Stricker, T. Falzone, M. L. Gardel, Mechanics of the F-actin cytoskeleton, Journal of Biomechanics 43(1) (2010) 9-14.
[45] X. Wang, X. Hu, I. D. Molak, N. Kawazoe, Y. Yang, G. Chen, Discriminating the independent influence of cell adhesion and spreading area on stem cell fate determination using micropatterned surfaces, Scientific Reports 6(1) (2016) 28708.
[46] C. S. Hill, L. F. Lemanski, Immunoelectron microscopic localization of alpha-actinin and actin in embryonic hamster heart cells, European Journal of Cell Biology 39(2) (1986) 300-312.
[47] K. Burridge, J. R. Feramisco, Non-muscle α-actinins are calcium-sensitive actin-binding proteins, Nature 294(5841) (1981) 565-567.
[48] C. G. Hansen, T. Moroishi, K. L. Guan, YAP and TAZ: a nexus for Hippo signaling and beyond, Trends in Cell Biology 25(9) (2015) 499-513.
[49] S. Dupont, L. Morsut, M. Aragona, E. Enzo, S. Giulitti, M. Cordenonsi, F. Zanconato, J. L. Digabel, M. Forcato, S. Bicciato, N. Elvassore, S. Piccolo, Role of YAP/TAZ in mechanotransduction, Nature 474(7350) (2011) 179-183.
[50] X. Wang, T. Nakamoto, I. D. Molak, N. Kawazoe, G. Chen, Regulating the stemness of mesenchymal stem cells by tuning micropattern features, Journal of Materials Chemistry B 4(1) (2016) 37-45.
[51] G. L. Saux, M. C. Wu, E. Toledo, Y. Q. Chen, Y. J. Fan, J. C. Kuo, M. Schvartzman, Cell-cell adhesion-driven contact guidance and its effect on human mesenchymal stem cell differentiation, ACS Applied Materials & Interfaces 12(20) (2020) 22399-22409.
[52] Y. K. Wang, C. S. Chen, Cell adhesion and mechanical stimulation in the regulation of mesenchymal

stem cell differentiation, Journal of Cellular and Molecular Medicine 17(7) (2013) 823-832.
[53] T. D. Pollard, E. D. Korn, Acanthamoeba myosin I. isolation from acanthamoeba castellanii of an enzyme similar to muscle myosin, Journal of Biological Chemistry 248(13) (1973) 4682-4690.
[54] X. Wang, X. Hu, J. Li, A. C. M. Russe, N. Kawazoe, Y. Yang, G. Chen, Influence of cell size on cellular uptake of gold nanoparticles, Biomaterials Science 4(6) (2016) 970-978.
[55] T. C. Erlach, S. Bertazzo, M. A. Wozniak, C. M. Horejs, S. A. Maynard, S. Attwood, B. K. Robinson, H. Autefage, C. Kallepitis, A. R. Hernández, C. S. Chen, S. Goldoni, M. M. Stevens, Cell-geometry-dependent changes in plasma membrane order direct stem cell signalling and fate, Nature Materials 17(3) (2018) 237-242.
[56] B. K. K. Teo, S. H. Goh, T. S. Kustandi, W. W. Loh, H. Y. Low, E. K. F. Yim, The effect of micro and nanotopography on endocytosis in drug and gene delivery systems, Biomaterials 32(36) (2011) 9866-9875.
[57] L. B. Case, C. M. Waterman, Integration of actin dynamics and cell adhesion by a three-dimensional, mechanosensitive molecular clutch, Nature Cell Biology 17(8) (2015) 955-963.
[58] I. Eke, N. Cordes, Focal adhesion signaling and therapy resistance in cancer, Seminars in Cancer Biology 31 (2015) 65-75.
[59] M. Maurer, J. Lammerding, The driving force: nuclear mechanotransduction in cellular function, fate, and disease, Annual Review of Biomedical Engineering 21(1) (2019) 443-468.

.

Chapter 5

Chirality of focal adhesions and cytoskeletons controlled by micropatterns and their influences on gene transfection of mesenchymal stem cells

5.1 Abstract

Cell chirality has been demonstrated to be important for controlling cell functions. However, it is not clear how the chirality of the extracellular microenvironment regulates cell adhesion and cytoskeletal structures and therefore affects gene transfection. In this study, the chirality of focal adhesions and the cytoskeleton of single hMSCs was controlled by specially designed micropatterns, and its influence on gene transfection was investigated. Micropatterns with different cell adhesion areas and swirling stripe lines were prepared by micropatterning fibronectin on polystyrene surfaces. The chiral micropatterns induced the formation of chiral focal adhesions and chiral cytoskeletal structures. Gene transfection efficiency was enhanced with increasing adhesion area, while hMSCs on left-handed and right-handed swirling micropatterns showed the same level of gene transfection. When the swirling angle was changed from 0°, 30°, and 60° to 90°, the gene transfection efficiency at a swirling angle of 60° was the lowest. The influence of cell chirality on gene transfection was strongly associated with cellular uptake capacity, DNA synthesis and cytoskeletal mechanics. The results demonstrated that cytoskeletal swirling had a significant influence on gene transfection.

5.2 Introduction

Chirality is a general phenomenon in nature. Cell chirality is important for the left-right asymmetric development of organisms, and breaking chirality may result in mortality or diseases [1-6]. Molecular chirality and structures with nano and microchirality have been designed to regulate cell chirality and functions [7-11]. A variety of cells have been shown to sense enantiomorphous structures with different responses [12, 13]. Chiral preference of cell adhesion has been reported for the enantiomers of calcium tetrahydrate crystals [14]. Rat embryonic cerebral cells showed better adhesion on poly-L-lysine-coated surfaces than on poly-D-lysine-coated surfaces [15]. Human neutrophils preferred to adhere on an L-(N-isobutyryl cysteine) surface rather than on a D-(N-isobutyryl cysteine) surface [16]. In addition to cell

adhesion, the differentiation of stem cells can also be affected by chiral surfaces. Rat bone marrow-derived mesenchymal stem cells under confluent conditions showed preferential osteogenic differentiation on a D-cysteine monolayer and adipogenic differentiation on an L-cysteine monolayer [17]. In addition to chirality of 2D surface structures, chirality in 3D extracellular matrices has been recently reported to affect cell functions [18]. Chiral 3D nanofiber scaffolds prepared from enantiomers of left-handed 4-benzenedicarboxamide phenylalanine (L-ph) and right-handed D-ph derivatives showed different effects on stem cell differentiation. The left-handed nanofiber scaffold facilitated osteogenic differentiation and in vivo osteogenesis, while the right-handed nanofiber scaffold facilitated adipogenic differentiation and in vivo adipogenesis [18].

Cells interact with surfaces and interfaces through adsorbed proteins. Chiral surface structures can affect protein adsorption, which has been considered one of the prominent causes of the effect of chirality on cell functions [19-26]. Preferable adsorption of proteins on an L-cysteine monolayer was shown to result in enhanced cell spreading [27]. L929 fibroblasts in serum-free medium showed no preference for chiral surfaces of self-assembled L-cysteine or D-cysteine. However, L929 fibroblasts in serum medium preferred to adhere to the self-assembled L-cysteine surface due to the enhanced protein adsorption on the L-cysteine surface [27]. It has been reported that left-handed nanofibers can promote the adsorption of ligands such as fibronectin, therefore facilitating integrin α5 binding and enhancing focal adhesion formation to regulate downstream mechanoresponses for osteogenesis [18]. Human serum albumin showed preferable adsorption on self-assembled nanofibers of gelators bearing amphiphilic L-glutamide and D-pantolactone than on those bearing amphiphilic L-glutamide and L-pantolactone [28].

Although cells can sense chiral structures and demonstrate differential behaviors on chiral surfaces or scaffolds through adsorbed proteins, it is not clear how the adsorbed proteins on chiral surface structures affect the cytoskeleton and therefore regulate cell functions. Directly controlled chirality of adsorbed proteins on micropatterned surfaces can be used to investigate the effect of chirality on cytoskeletal organization and cell functions. In addition to cell adhesion and differentiation, transfection of exogenous genes is an important process for gene therapy, protein production and stem cell establishment. The influence of cell chirality on gene transfection has not been investigated. Therefore, in this study, we prepared chiral fibronectin micropatterns to determine the cell interactions with chiral protein micropatterns and their influence on gene transfection efficiency. The chiral micropatterns of fibronectin induced the formation of chiral focal adhesions and the chiral organization of actin filaments. The influence of cytoskeletal chirality on mesenchymal stem cell gene transfection was disclosed.

5.3 Materials and methods

5.3.1 Preparation and characterization of micropatterns

Micropatterns with alternate stripes of PVA and polystyrene were prepared by micropatterning PVA stripes on TCPS discs through photolithography (Figure 5.1). A photoreactive derivative of PVA was synthesized by introducing the azidophenyl group of 4-azidobenzoic acid to PVA as mentioned in 2.3.2. An aqueous solution of AzPhPVA was coated onto the central area of TCPS discs that were cut from TCPS flasks. After air-drying in the dark for 12 h, a PVA thin layer was formed on the TCPS discs. The AzPhPVA-coated polystyrene discs were covered with a predesigned photomask with alternate stripes of UV-transparent and nontransparent regions. The width of the nontransparent stripes was 2 μm. The swirling angle of the stripes was 0°, 30°, 60° and 90°, and the swirling direction was left- or right-handed. After

exposure to UV light, the discs were ultrasonically rinsed in Milli-Q water to absolutely remove uncreated AzPhPVA. After washing, the micropatterns were obtained.

Images of the micropatterns were captured by a phase-contrast microscope. Atomic force microscopy with a commercial cantilever was used to characterize the micropatterns. The parameters of micropatterns were calculated by analyzing the cross section of each type of micropattern. Every three micropatterns were analyzed and used to calculate the mean and standard deviation (SD).

Fibronectin was allowed to adsorb on the micropatterns. The absorbed fibronectin was visualized by immunological staining. The fibronectin-absorbed micropatterns were incubated with mouse anti-fibronectin antibody for 1.5 h. The micropatterns were incubated in Alexa Fluor-488-labeled donkey anti-mouse IgG antibody for 1 h. The stained micropatterns were observed by a fluorescence microscope.

5.3.2 Cell culture

Fibronectin micropatterns were used for culture of hMSCs as mentioned in 2.3.3. hMSCs at passage 4 were dropped onto the micropatterns. After incubation for 6 h, the glass rings were removed, and the cells were further cultured at 37°C in a 5% CO_2 incubator for 18 h. Cell morphology was observed and captured by a phase-contrast microscope with a DP-70 CCD camera.

5.3.3 Immunological staining of vinculin and cytoskeleton

After incubation at 37°C in a 5% CO_2 incubator for 24 h, the micropatterned cells were fixed with 4% paraformaldehyde for 10 min and permeabilized with Triton X-100 for 10 min. For vinculin staining, the cells were incubated with mouse anti-vinculin antibody and Alexa Fluor-488-labeled donkey anti-mouse IgG antibody, as mentioned in 4.3.3. The stained cells were captured by a confocal laser scanning microscope (Zeiss LSM 510, Germany). The fluorescent images were converted to 16 bit images, and peripheral vinculin length was analyzed. The peripheral vinculin orientation angle was measured by using ImageJ software. For cytoskeleton staining, the fixed cells were blocked with 2% BSA for 30 min. Actin filaments were stained with Alexa Fluor-488 phalloidin (1:40 in PBS) in the dark for 20 min, followed by 3 PBS washes. The samples were dried in the dark and mounted with Vectashield®. The stained cytoskeleton was observed by a fluorescence microscope with a DP-70 CCD camera. The cell spreading area was analyzed based on actin cytoskeleton staining. Five independent experiments (five cells from each independent experiment) were performed to calculate the mean and SD.

5.3.4 Measurement of cellular stiffness

AFM with a point-contact nanoindentation system was used to measure the cellular stiffness of the micropatterned hMSCs, as mentioned in 3.3.3. The living cells were directly measured by nanoindentation to analyze cellular stiffness. The highest point of cells was observed by a phase-contrast microscope and connected with the silica sphere of the cantilever with a diameter of 600 nm. All samples were measured within 2 h to maintain cellular viability. After measurement, Young's modulus was analyzed from force-distance curves. Ten cells were measured for each type of micropattern, and 20 force-distance curves for each cell were analyzed. The average Young's modulus of 10 cells was calculated as the mean and SD.

To investigate the influence of actin disturbance on actin filaments and cell mechanics, we incubated micropatterned hMSCs with an actin inhibitor. After the cells were cultured on the micropatterns for 6 h, the

micropatterned hMSCs were treated with 0.2 μg mL^{-1} cytochalasin D (Cyto D) and further cultured in DMEM growth medium for 18 h. Actin filament staining and measurement of the cellular stiffness of the cytochalasin D-treated cells were conducted as described above.

5.3.5 Gene transfection

Gene transfection experiments were performed by using Lipofectamine™ 2000 transfection reagent as a plasmid transmembrane vector, as mentioned in 2.3.5. The fluorescence intensity of GFP was analyzed using ImageJ software. The percentage of GFP-positive cells to the total number of cells was regarded as the transfection efficiency. Five independent experiments (cell number ≥ 200) were carried out to calculate the mean and SD. The micropatterned cells after treatment with cytochalasin D were also used for the gene transfection experiment by the same procedures.

5.3.6 Cellular uptake of FITC-labeled microspheres

Cellular uptake was investigated by using Fluoresbrite carboxylate microspheres with a diameter of 500 nm. The cellular uptake experiment was performed, as mentioned in 2.3.6. The fluorescence intensity per unit area was calculated and further normalized to that of the cells on A3. Five independent experiments (25 cells) were performed to evaluate the normalized fluorescence intensity per unit area and averaged to calculate the mean and SD. The micropatterned cells after treatment with cytochalasin D were also used for cellular uptake of FITC-labeled microspheres by the same procedures.

5.3.7 DNA synthesis evaluation by BrdU staining

DNA synthesis was analyzed by BrdU staining, as mentioned in 2.3.7. After BrdU and nuclei staining, the stained cells were observed by a fluorescence microscope. The fluorescent images were used to analyze the percentage of BrdU-positive cells to the total cells. Five independent experiments (cell number ≥ 200 cells) were carried out to calculate the mean and SD. The micropatterned cells after treatment with cytochalasin D were also used for BrdU staining by the same procedures.

5.3.8 Statistical analysis

The data were analyzed in Microsoft Excel and are presented as the mean ± SD. Significant differences in the quantitative or fluorescent results were determined by one-way ANOVAs with Tukey's post-test for multiple variables, and the confidence level was defined as 0.05 for all statistical results by using KyPlot 5.0 software. A significant difference was considered when $p < 0.05$.

5.4 Results

5.4.1 Preparation and characterization of micropatterns and cell morphology

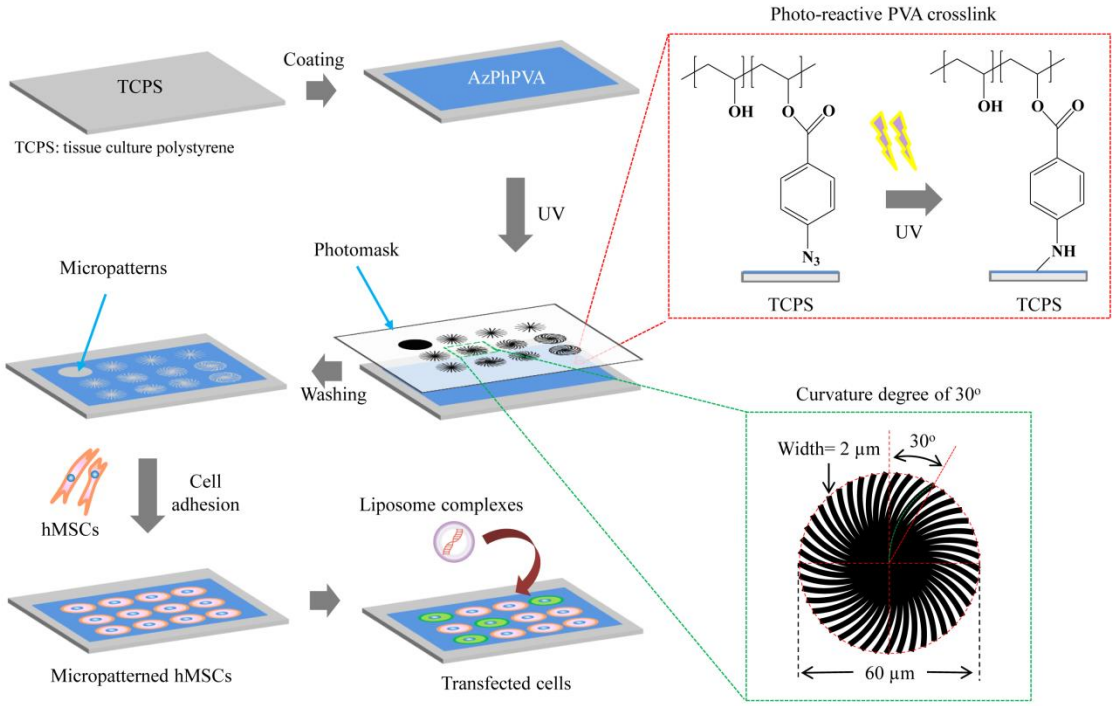

Figure 5.1 Flowchart for preparation of micropatterns with vertical, right-handed and left-handed swirling stripes of fibronectin on TCPS substrate and gene transfection of cationic liposome/plasmid complexes into hMSCs.

The preparation scheme of micropatterns and application of the micropatterns for cell culture and gene transfection are shown in Figure 5.1. Micropatterns with alternate stripes of PVA and polystyrene were prepared by micropatterning PVA on TCPS discs. The stripes of PVA and polystyrene were straight, left-handed swirling or right-handed swirling. Ten types of photomask patterns were used for micropatterning (Figure 5.2a). The photomask patterns of A1, A2 and A3 had alternate UV-transparent and nontransparent dark stripes that were straight. The width of nontransparent dark stripes was 2 μm. The number of nontransparent dark stripes in A1, A2 and A3 was 30, 36 and 45, respectively. A4 was a dark circle pattern with a diameter of 60 μm. The photomask patterns of R1, R2 and R3 had alternate UV-transparent and nontransparent dark swirling stripes with right-handed swirling angles of 30°, 60° and 90°, respectively. The counter photomask patterns (L1, L2 and L3) had the same parameters but were left-handed. The total area of nontransparent dark regions increased from A1, A2, A3 to A4. The total area of nontransparent dark regions in A3, R1-R3 and L1-L3 was the same. The nontransparent dark regions in the photomask reflected polystyrene regions allowing adsorption of fibronectin, which supported cell adhesion. Based on the design, the A1, A2, A3 and A4 micropatterns had an increase in the cell adhesion area. A3, R1-R3 and L1-L3 had the same cell adhesion area but different swirling angles and directions. R1-R3 were the enantiomorphous micropatterns of L1-L3. The size (outermost circle) of all the A1-A4, R1-R3 and L1-L3 photomask patterns was 60 μm. Therefore, cell spreading could be controlled by the micropattern size,

suggesting that cell size could be controlled at the same level of 60 μm diameter. These micropatterns could be used to control cells with the same chirality but different adhesion areas (A1-A4), the same adhesion area but different swirling angles (A3 and R1-R3; A3 and L1-L3) or the same adhesion area and swirling angle but different swirling directions (R1 and L1, R2 and L2, R3 and L3).

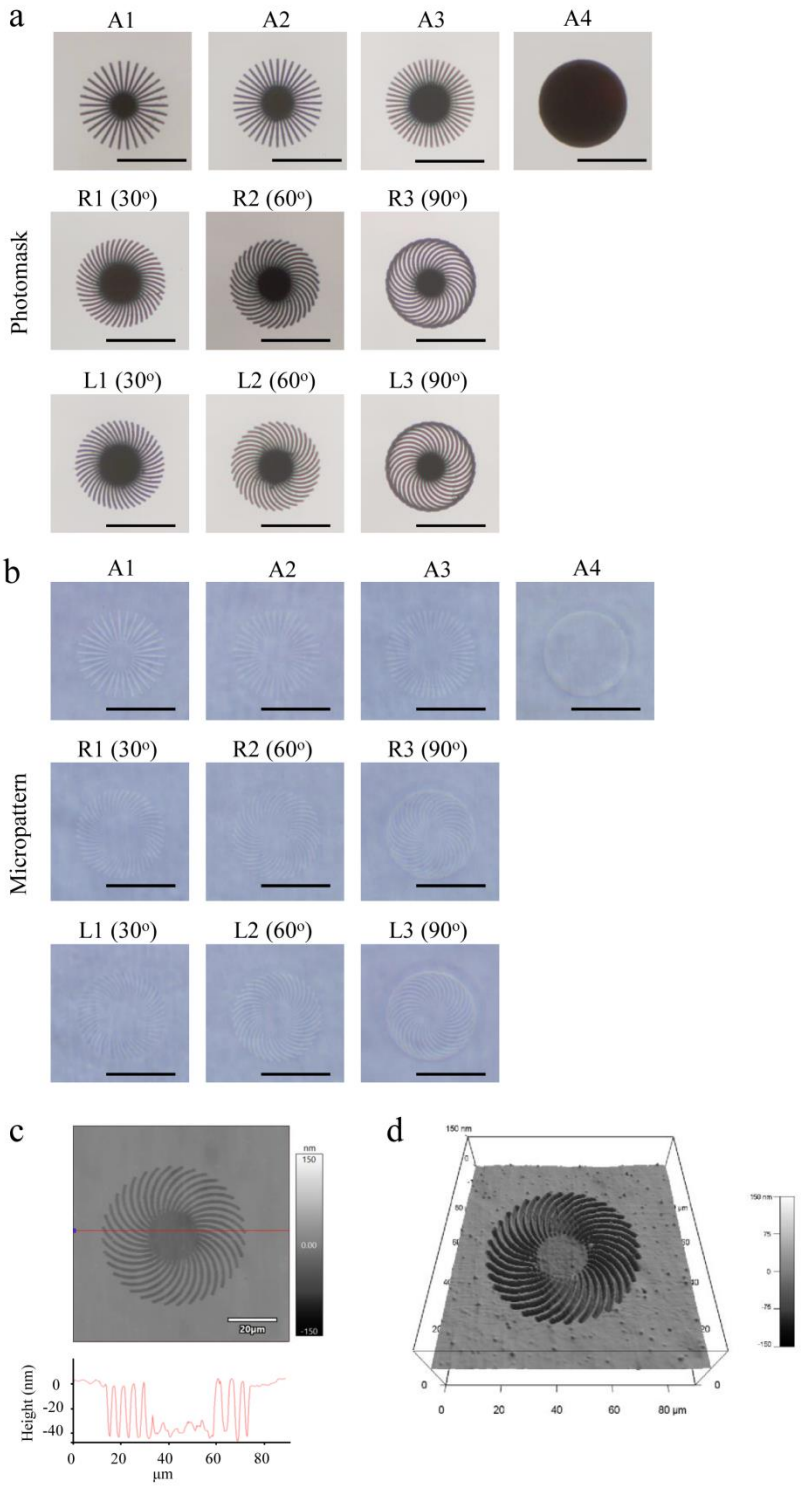

Figure 5.2 Characterization of photomasks and micropatterns. (a) Phase-contrast images of photomasks with different numbers of vertical, right-handed and left-hand swirling stripes. (b) Phase-contrast images of as-prepared micropatterns. Scale bar: 50 μm. (c) Height images (top) and section view (bottom) and (d) 3D images of the micropattern with a right-handed swirling angle of 60°.

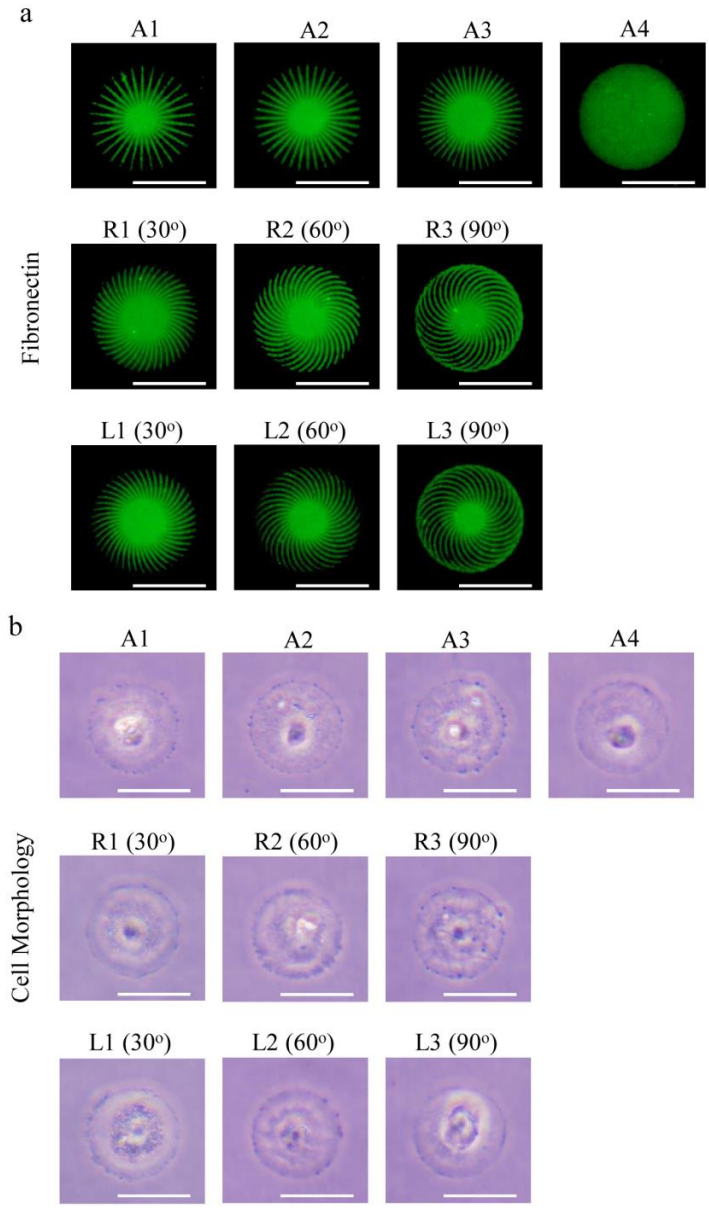

Figure 5.3 (a) Immunofluorescence staining images of fibronectin micropatterns. (b) Phase-contrast micrographs of micropatterned hMSCs. Scale bar: 50 μm.

The photoreactive AzPhPVA molecules were grafted onto the TCPS through UV irradiation. The unreacted AzPhPVA molecules under the nontransparent dark photomask stripes were removed after washing. Microscopy observations showed the formation of micropatterns on polystyrene disc surfaces (Figure 5.2b). The white stripes were polystyrene micropatterns surrounded by a grafted PVA layer. Each type of micropattern was further characterized by AFM. The height view and 3D view of AFM scanning images clearly showed the structures of micropatterns (Figure 5.2c, d). The dark stripes in the AFM height and 3D images were polystyrene stripes, while the gray regions were PVA-grafted layers. The diameter of the outermost circles, width of polystyrene stripes and height (thickness) of the PVA-grafted layer were analyzed from the AFM images (Table 5.1). The diameter of the outermost circles and width of the polystyrene stripes were very close to those of the designed patterns of the photomask. The height of the PVA-grafted layer was between 38.5 and 41.1 nm. These results indicated that micropatterns were successfully prepared and had almost the same parameters as those of the photomask.

Table 5.1 Diameters, gap width of PVA stripes and height of PVA layer of the micropatterns. Data represent the mean ± SD, n = 3.

Pattern types		Number of cell adhesion stripes	Diameter of large circle (μm)		Gap width of PVA stripes (μm)		Height of PVA layer (nm)
			Designed	Measured	Designed	Measured	
Adhesion area	A1	30	60	59.3±0.3	2	2.4±0.3	40.1±1.6
	A2	36	60	60.2±0.8	2	2.1±0.2	38.5±1.5
	A3	45	60	60.4±0.9	2	2.2±0.1	38.6±0.6
	A4	full	60	61.7±1.8			41.1±2.1
Right rotating	R1 (30°)	45	60	61.2±0.5	2	2.1±0.2	39.7±1.3
	R2 (60°)	36	60	60.9±0.5	2	2.0±0.1	40.1±1.3
	R3 (90°)	30	60	61.4±0.4	2	2.2±0.4	38.9±0.5
Left rotating	L1 (30°)	45	60	59.5±0.7	2	2.1±0.2	40.9±0.9
	L2 (60°)	36	60	60.2±1.4	2	2.0±0.1	40.7±0.8
	L3 (90°)	30	60	60.7±1.0	2	2.2±0.3	38.9±1.1

Fibronectin was adsorbed on the micropatterned surfaces. Immunological staining showed that the adsorbed fibronectin showed exactly the same micropattern structures as the underlying micropatterns (Figure 5.3a). Fibronectin was absorbed on the polystyrene stripes, other than the PVA regions. It has been reported that polystyrene surfaces can support protein adsorption, while PVA can protect protein adsorption [33, 34]. The hMSCs were seeded on the fibronectin micropatterns. After incubation for 24 h, the cells attached to the micropatterns and spread along the micropatterns (Figure 5.3b). The cells occupied the micropatterns and had the same size as that of the micropatterns, suggesting that the morphology of hMSCs could be controlled by the micropatterns.

5.4.2 Focal adhesion, cytoskeletal structure and cell stiffness on micropatterns

Cells adhere to matrices through interactions between integrin and their ligands in the matrices by forming focal adhesions (FAs) [35, 36]. Upon adhesion, the cytoskeleton is reorganized to transfer signals from the matrix to the nucleus and therefore trigger a variety of cellular activities [37-40]. Vinculin is a dominant component of focal adhesion [41]. To investigate the formation of FAs and cytoskeletal structure, we immunologically stained vinculin and actin filaments in hMSCs cultured on micropatterns for 24 h. The formation of FAs was confirmed in all micropatterned cells (Figure 5.4a). In particular, fiber-like vinculin assembly structures were obviously observed along the adhesive stripes at the periphery of micropatterns. Furthermore, the peripheral vinculin length of micropatterned cells was measured (Figure 5.4b). The peripheral vinculin length significantly increased with increasing adhesive area from A1 to A4, while the cells showed the shortest peripheral vinculin length on R2 or L2 micropatterns. The left-handed and right-handed micropatterns did not significantly affect vinculin length.

The FAs showed straightforward, right-handed and left-handed orientations on the A1-A3, R1-R3 and L1-L3 micropatterns, respectively. The peripheral vinculin orientation angle was analyzed from the stained images (Figure 5.4c). The vinculin orientation angle was 0.7° ± 6.1°, -1.3° ± 6.5°, -1.7° ± 8.0° and 0.4° ± 6.5° on the straightforward adhesion stripes (A1-A3) and A4, respectively. It was 32.1° ± 8.0° and 61.0° ± 6.7° on

R1 and R2 and -32.7° ± 6.9° and -58.4° ± 10.6° on L1 and L2, respectively. However, the angle changed to 1.7° ± 8.9° and 0.0° ± 7.2° on R3 and L3, respectively. The results indicated that vinculin orientation followed the swirling lines on all the micropatterns except R3 and L3. On the R3 and L3 micropatterns, the peripheral points of the swirling lines were interconnected to form a circle, and vinculin was vertically oriented. The results indicated that FA chirality could be controlled by the absorbed fibronectin chirality on the micropatterns.

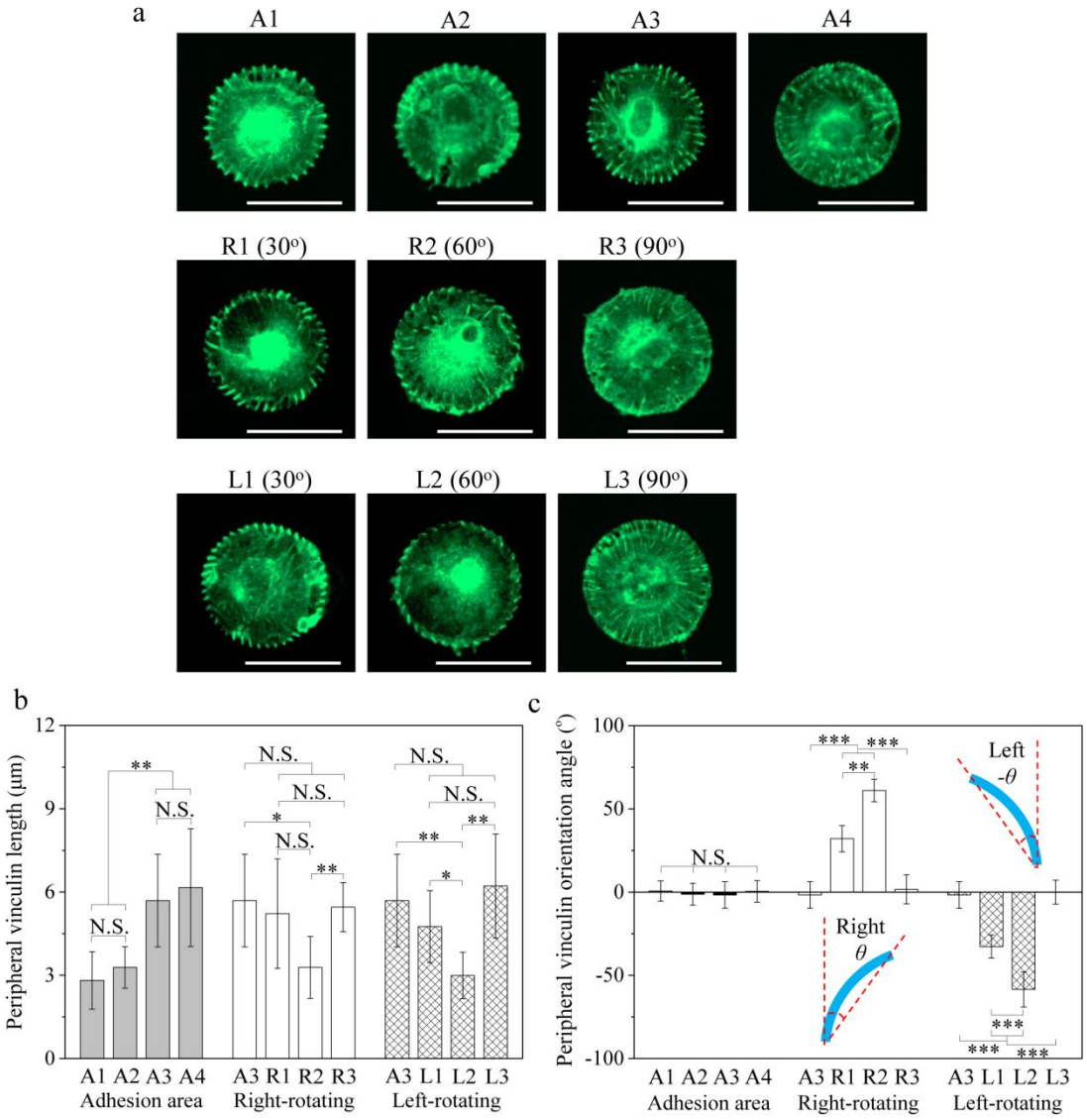

Figure 5.4 Formation of focal adhesions in micropatterned hMSCs. (a) Representative vinculin staining images (green). Scale bar: 50 μm. (b) Peripheral vinculin length. (c) Peripheral vinculin orientation angles. Inserts show that right-handed vinculin is regarded as a positive angle, while left-handed vinculin is regarded as a negative angle. Data represent the mean ± SD (n = 10), N.S. represents no significant difference, *p < 0.05, **p < 0.01, ***p < 0.001.

Actin filaments, one of the major cytoskeletal components, have critical roles in mechanosensing and mechanotransduction processes [42, 43]. The actin filament structure of the micropatterned cells was investigated by immunological staining and observed by a fluorescence microscope (Figure 5.5a). The hMSCs cultured on the micropatterns developed cytoskeletal structures in both radial and concentric directions. The radial actin filaments were assembled in a straightforward, right-handed and left-handed

pattern along the underlying stripe swirling direction. Accompanying the increase in adhesion area from A1 to A4, the assembly of actin filaments became more evident, both radially and concentrically. When the swirling angle was 0°, 30° and 90° (A3, R1, R3, L1 and L3), the cells showed intensive assembly of actin filaments. The cells on micropatterns with a swirling angle of 60° (R2 and L2) showed the weakest level of actin filament assembly. The hMSCs on the enantiomorphous micropatterns (either right-handed or left-handed) showed similar levels of actin filament assembly. Compared to those on the micropattern without stripes (A4), the cells on the micropatterns with stripes showed stronger assembly of actin filaments along the swirling stripes at the micropattern periphery. After treatment with an actin inhibitor (cytochalasin D), the assembled actin filaments disappeared in all micropatterned cells (Figure 5.5c).

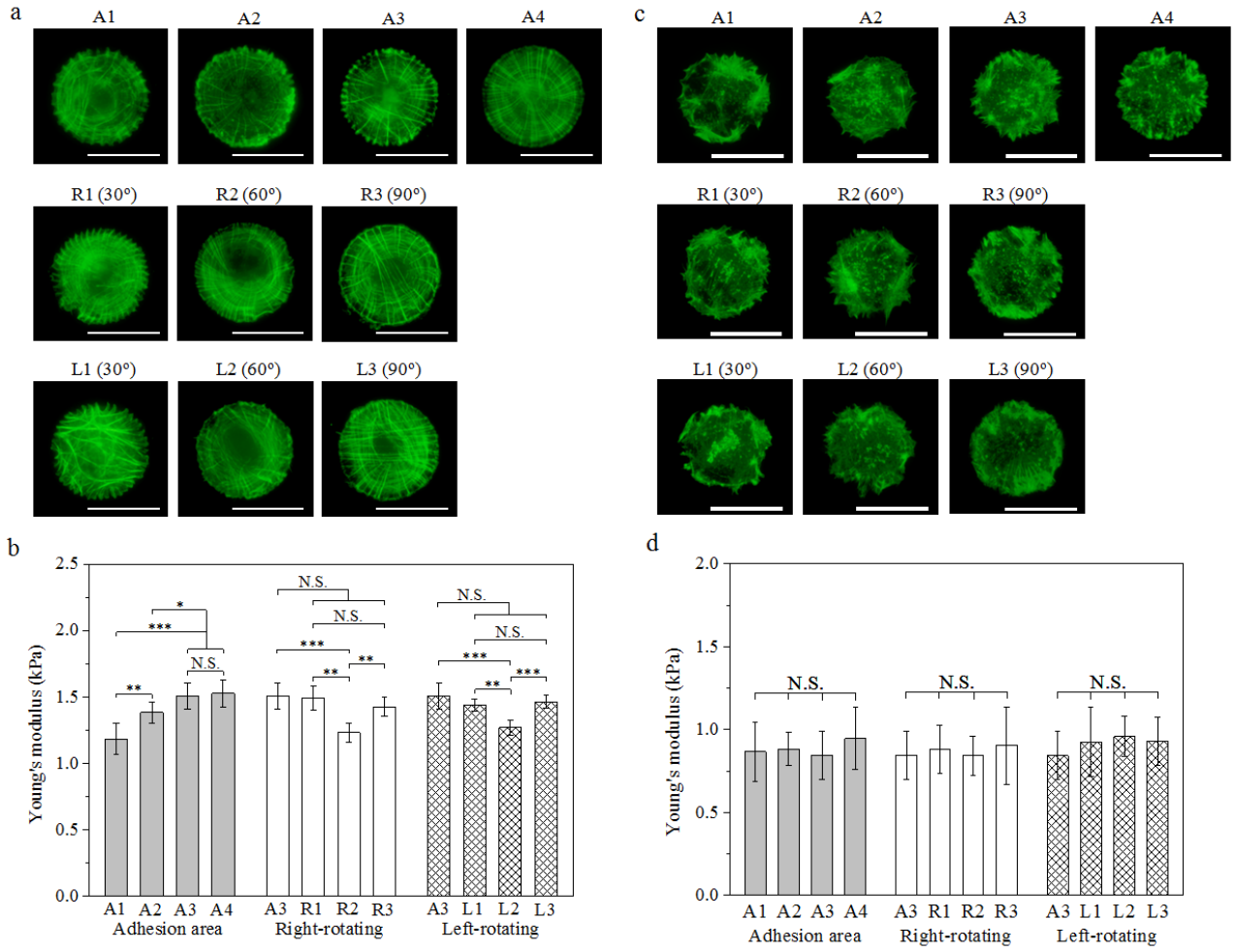

Figure 5.5 Influence of chiral micropatterns and swirling angles on cytoskeletal organization. (a) Representative fluorescence images of actin filament (green) staining of hMSCs cultured on micropatterns before (a) and after (c) the disturbance of actin inhibitor (cytochalasin D). Scale bar: 50 μm. (b) Young's modulus of hMSCs cultured on micropatterns before (b) and after (d) the disturbance of actin inhibitor (cytochalasin D). Data represent the mean ± SD (n = 10), N.S. represents no significant difference, *$p < 0.05$, **$p < 0.01$, ***$p < 0.001$.

Cytoskeletal structures are related to cell stiffness [44-46]. Cells with a highly organized cytoskeleton have high stiffness [30]. Therefore, the Young's modulus of micropatterned hMSCs was measured by AFM nanoindentation (Figure 5.5b). The Young's modulus of the micropatterned hMSCs increased with increasing cell adhesion area. The Young's modulus of A3 and A4 cells was almost the same, which indicated that the A3 micropattern had a sufficient cell adhesion area for assembly of actin filaments to reach the same level as the A4 micropattern. When the chiral micropatterns were compared, the cells showed the lowest Young's

modulus on R2 and L2 micropatterns that had a swirling angle of 60°. The Young's modulus was most similar for the cells on the A3, R1, R3, L1 and L3 micropatterns. The stripe swirling direction did not affect the cellular Young's modulus. After disturbance of the actin cytoskeleton with an actin inhibitor, the cellular Young's modulus of all the micropatterned cells decreased to the same level (Figure 5.5d). The results indicated a close correlation between the actin cytoskeleton and cell stiffness.

5.4.3 Influence of chirality and swirling angle on gene transfection

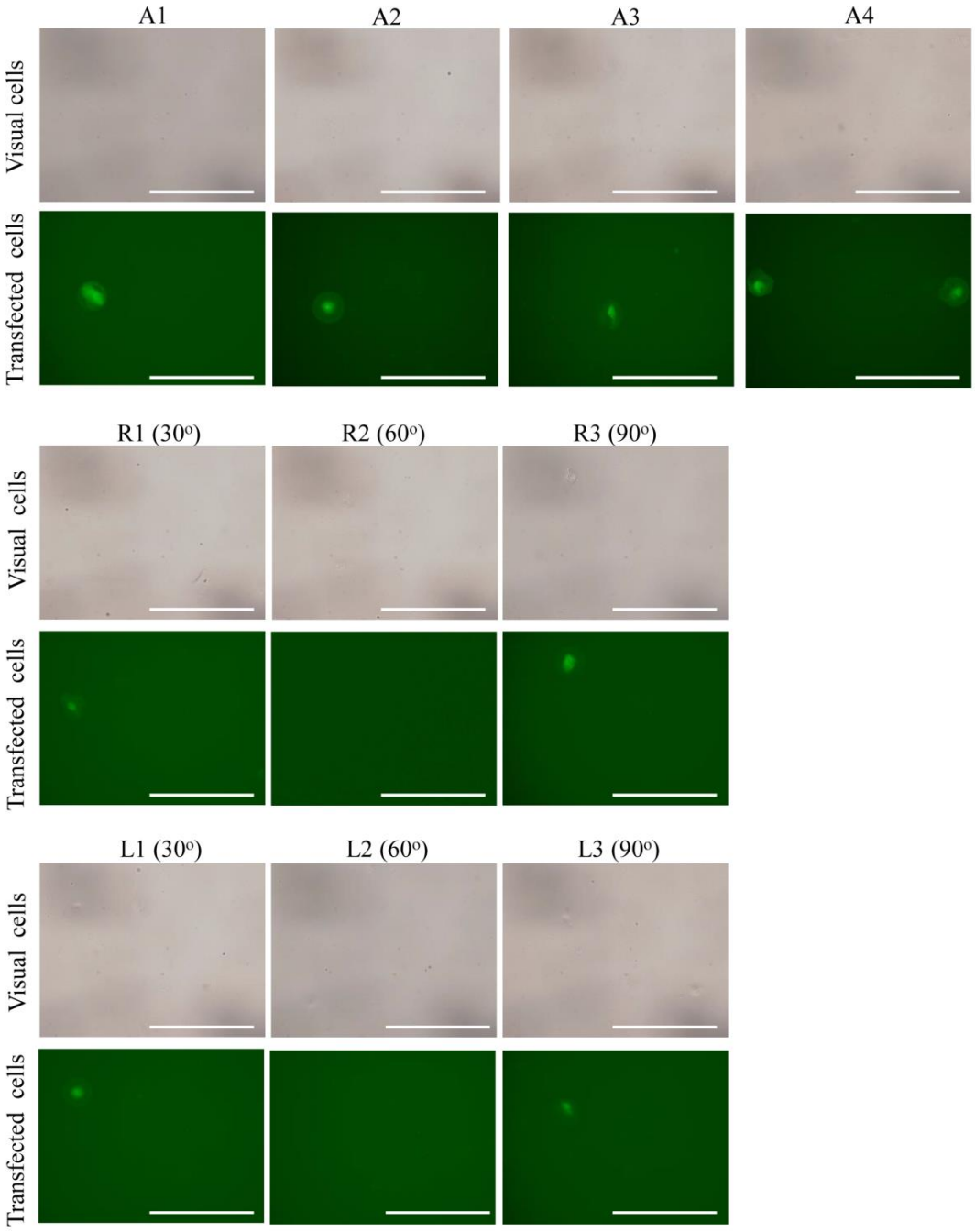

Figure 5.6 Representative phase-contrast (top) and fluorescence (bottom) images of hMSCs cultured on the micropatterns. Scale bar: 200 μm.

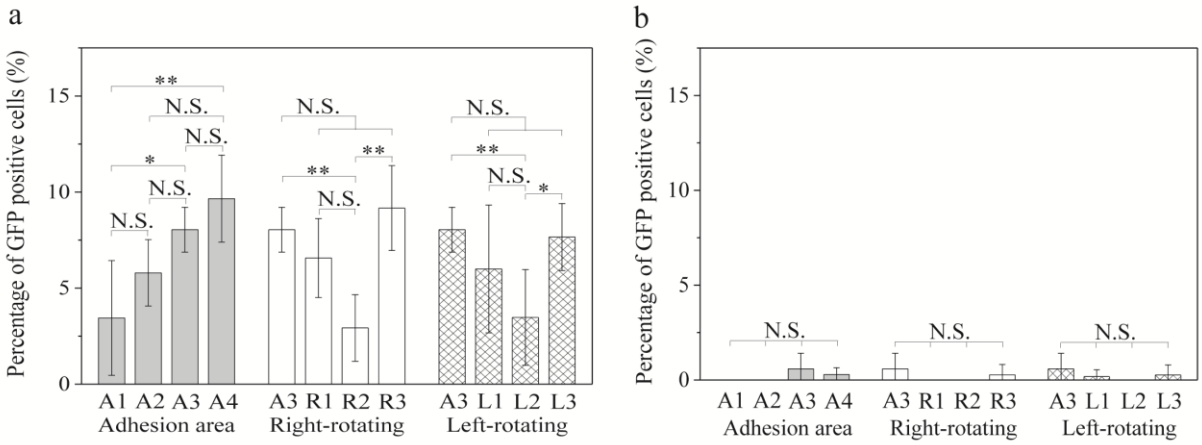

Figure 5.7 Influence of chiral micropatterns and swirling angle on gene transfection. (a) Percentage of GFP-positive cells in all examined cells to show the gene transfection efficiency of micropatterned hMSCs. (b) Percentage of GFP-positive cells after treatment with actin inhibitor. Data represent the mean ± SD (n = 5), N.S. represents no significant difference, *$p < 0.05$, **$p < 0.01$.

hMSCs cultured on micropatterns were transfected with the pAcGFP1-N1 plasmid. The successfully transfected cells expressed green fluorescence proteins and were observed by a fluorescence microscope (Figure 5.6). Transfection efficiency was evaluated by calculating the percentage of GFP-positive cells in the total cell number (Figure 5.7a). The percentage of GFP-positive cells increased with increasing adhesion area (from A1 to A4). When the cell adhesion area was controlled at the same level (A3, R1-R3 and L1-L3), the gene transfection efficiency decreased at first and then increased as the swirling angle of the stripes changed from 0° to 90°. The hMSCs on the micropatterns with a swirling angle of 60° had the lowest transfection efficiency. The hMSCs on the micropatterns with swirling angles of 0°, 30°, and 90° had the same level of transfection efficiency. When the hMSCs on micropatterns with right-handed or left-handed swirling stripes were compared, the gene transfection efficiency was almost the same. These results indicated that the cell adhesion area and swirling angle could affect gene transfection efficiency. A large cell adhesion area was beneficial for gene transfection. A swirling angle of 60° had a little inhibitory effect on gene transfection. However, the swirling direction (right-handed or left-handed) had no effect on gene transfection. The gene transfection efficiency of micropatterned cells treated with actin inhibitor was significantly decreased (Figure 5.7b).

5.4.4 Influence of chirality and the swirling angle on the cellular uptake capacity of FITC-labeled microspheres

Gene transfection efficiency depends on the cellular uptake of exogenous genes and DNA synthesis [47]. To examine the influence of chiral micropatterns on cellular uptake capacity, we used FITC-labeled microspheres for the same experiment as that of gene transfection. Green fluorescence-labeled microspheres in hMSCs were confirmed by a fluorescence microscope (Figure 5.8a). Nuclei and actin filaments were counterstained blue and red for observation. Quantitative fluorescence analysis revealed that the normalized fluorescence intensity per unit area increased significantly with increasing cell adhesion area, while the fluorescence intensity showed a first-decreasing and then-increasing tendency when the stripe swirling angle

changed from 0° to 90° (Figure 5.8b). The fluorescence intensity of hMSCs on the A3, R1, R3, L1 and L3 micropatterns was not significantly different, while that on the R2 and L2 micropatterns was the lowest. However, the fluorescence intensity was not significantly different between the micropatterns with right-handed or left-handed swirling stripes. The fluorescence intensity of the micropatterned cells treated with actin inhibitor decreased to the same level (Figure 5.8c). Cellular uptake of microspheres showed a similar trend as that of gene transfection efficiency, suggesting that cellular uptake of exogenous genes should be one of the dominant factors affecting gene transfection.

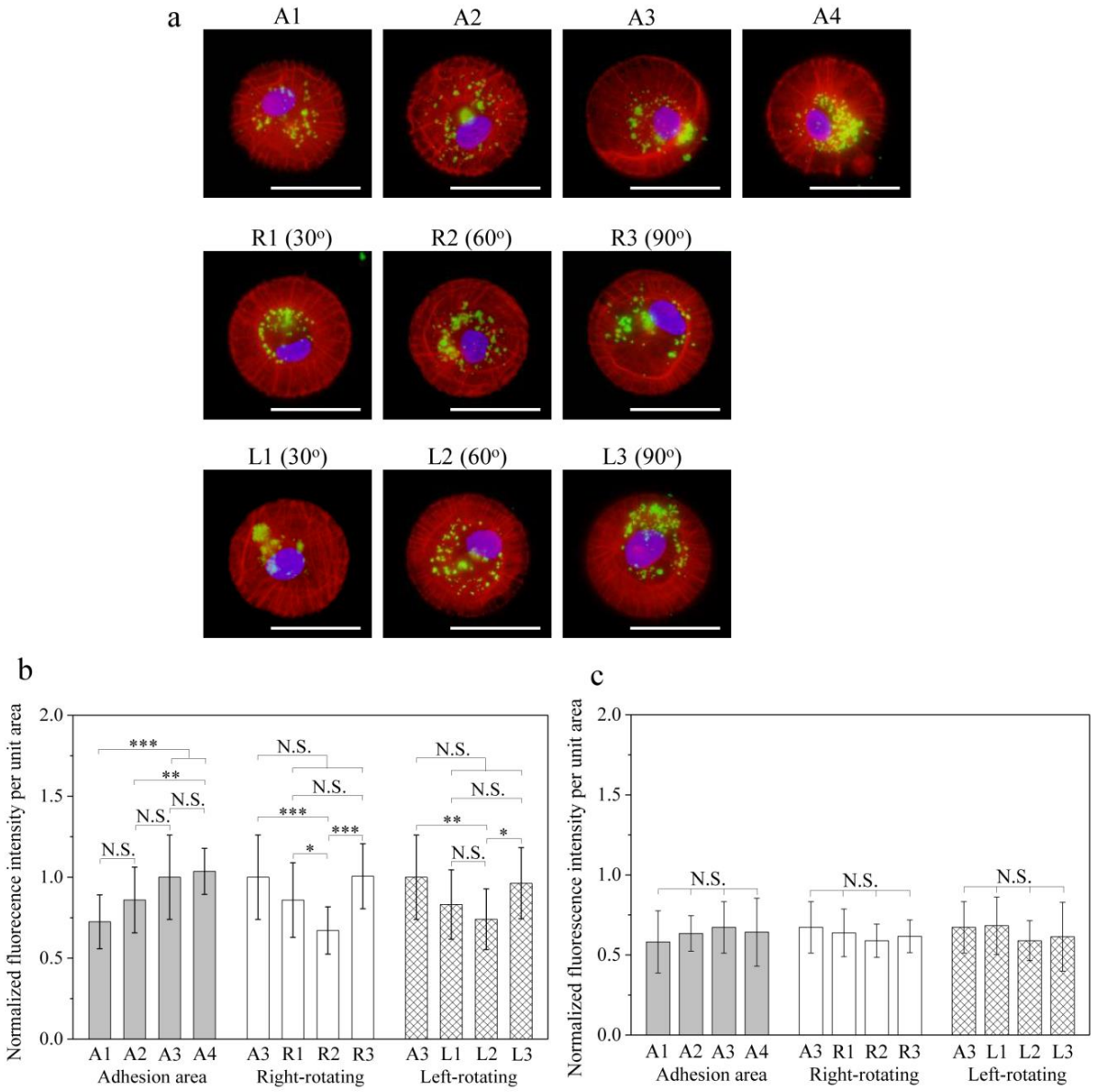

Figure 5.8 Influence of chiral micropatterns and swirling angles on cell uptake capacity. (a) Representative fluorescence images of micropatterned hMSCs showing cellular uptake of cationic FITC-labeled microspheres (green). Nuclei and actin filaments were stained blue and red, respectively. Scale bar: 50 μm. Normalized fluorescence intensity per unit area of FITC-labeled microspheres in hMSCs cultured on micropatterns before (b) and after (c) treatment with actin inhibitor. The fluorescence intensity per unit area was normalized to that of the cells on A3. Data represent the mean ± SD (n = 25), N.S. represents no significant difference, *$p < 0.05$, **$p < 0.01$, ***$p < 0.001$.

5.4.5 Influence of chirality and the swirling angle on the DNA synthesis of hMSCs

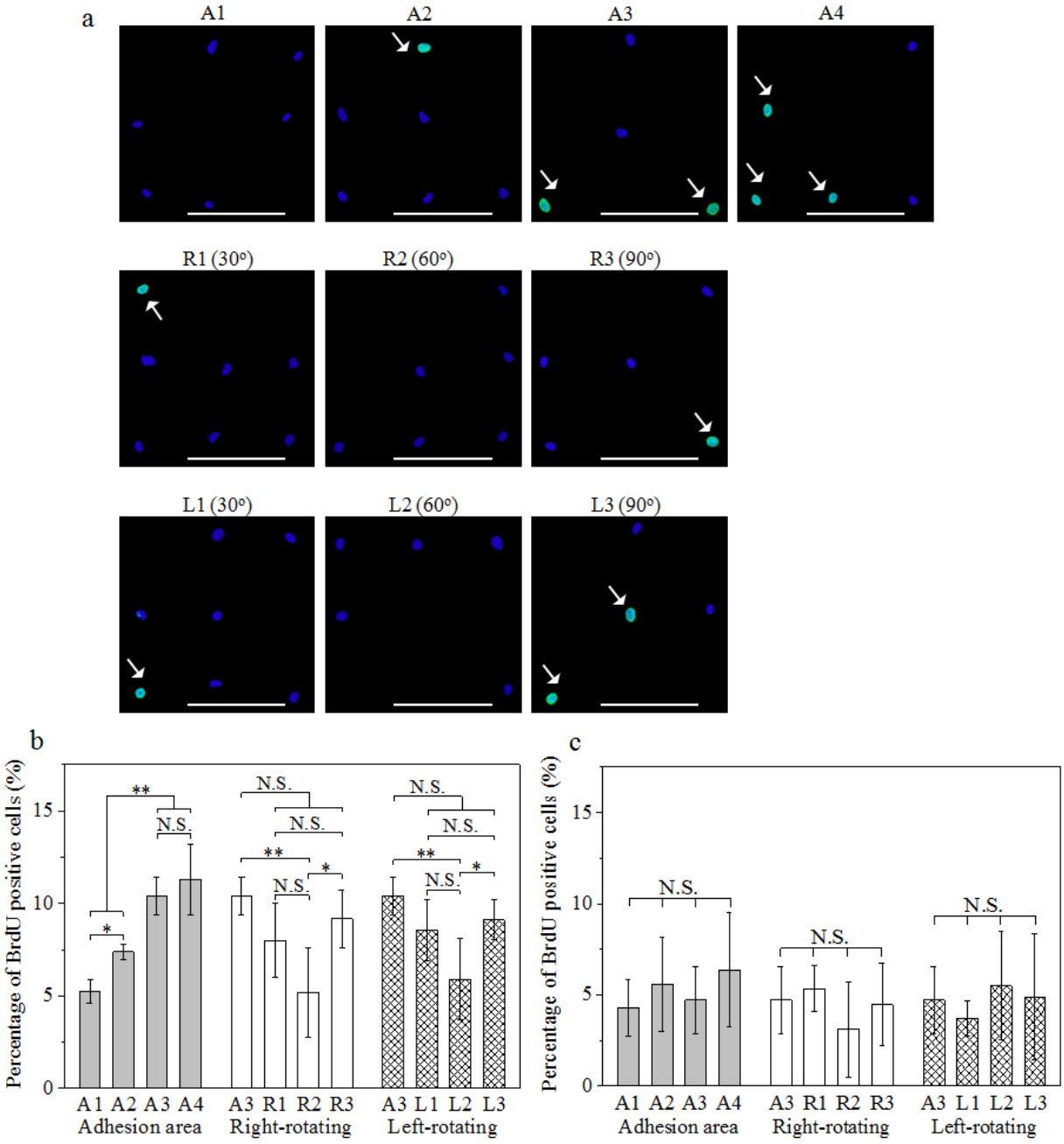

Figure 5.9 (a) Representative fluorescence images of nuclei (blue) and BrdU (green, white arrow indicated) staining of the micropatterned hMSCs. Scale bar: 200 μm. Percentage of BrdU-positive cells in all assessed cells to show the influence of chiral micropatterns and swirling angles on DNA synthesis before (b) and after (c) the cells were treated with actin inhibitor. Data represent the mean ± SD (n = 5), N.S. represents no significant difference, *$p < 0.05$, **$p < 0.01$.

The DNA synthesis of hMSCs cultured on micropatterns should be another important factor regulating the transfection and expression capacity of exogenous genes. BrdU staining was used to evaluate DNA synthesis activity. The staining images of BrdU-positive cells were observed by a fluorescence microscope (Figure 5.9a). The number of BrdU-positive hMSCs was counted, and the percentage relative to the total cell

number was calculated (Figure 5.9b). The percentage of BrdU-positive cells increased significantly with increasing cell adhesion area (from A1 to A4). The cells cultured on the micropattern with a stripe swirling angle of 60° had the lowest percentage of BrdU-positive cells. There was no significant difference among the A3, R1, R3, L1 and L3 micropatterns. When the cell adhesion area and stripe swirling angle were the same, the cells on the right-handed or left-handed swirling stripe micropatterns showed the same level of DNA synthesis. After treatment with an actin inhibitor, the DNA synthesis of all the micropatterned cells decreased to the same level (Figure 5.9c). The DNA synthesis activity of the micropatterned hMSCs showed the same trend as that of gene transfection efficiency, suggesting a correlation between DNA synthesis and gene transfection efficiency.

5.5 Discussion

Cell chirality was controlled by chiral micropatterns of fibronectin, and its effect on gene transfection was investigated. The swirling angle, direction and total area of fibronectin stripes were controlled by the micropatterns (Figure 5.3a). When the area of total straight stripes increased, the gene transfection efficiency increased. The swirling angle of fibronectin micropattern stripes could affect gene transfection efficiency. The gene transfection efficiency at a swirling angle of 60° was lower than that of 0°, 30° and 90° (Figure 5.7). The uptake capacity of the FITC-labeled microspheres (Figure 5.8) and the DNA synthesis (Figure 5.9) of the hMSCs cultured on the micropatterns showed the same trend as that of gene transfection efficiency. The results suggested that cellular uptake of exogenous genes and DNA synthesis should account for the gene transfection efficiency. Higher cellular uptake and higher DNA activity could result in high gene transfection efficiency.

It has been reported that cells form FAs and organize their cytoskeletal structures upon interactions with the proteins adsorbed on cell culture substrate surfaces, which can induce a variety of cell responses [35-40, 48]. The formation of FAs of hMSCs on the chiral micropatterns was confirmed by vinculin staining (Figure 5.4). Intensive staining of vinculin was observed at the central regions of micropatterns, which was due to the fusion of swirling stripes at the centers of each micropattern. Fiber-like FAs were formed along the adhesive stripes at the periphery of micropattern circles. The staining images of vinculin were similar to those of fibronectin, suggesting that FA formation was regulated by coated fibronectin. FA formation showed the same chirality as that of the fibronectin micropatterns. FAs were elongated when the adhesion area increased from A1 to A4. FAs on R1, L1, R3 and L3 were still long, while the length of FAs on R2 and L2 decreased. Chirality did not affect the length of the FAs. The origin of the FAs followed the swirling direction of the micropatterns except R3 and L3, in which vertically oriented FAs were formed.

Furthermore, cytoskeletal organization was confirmed by staining actin filaments (Figure 5.5a). Actin filaments were assembled radially and concentrically on the micropatterns. The radial actin filaments connected nuclear regions with the cell peripheral regions. When the curvature angle was 0° or 30°, the assembled actin filaments were very clearly observed along the swirling stripes. However, when the swirling angle increased to 60°, the assembled actin filaments became vague at the peripheral regions. When the swirling angle further increased to 90°, the assembled actin filaments at the peripheral regions were almost connected and formed a large circle assembly, which could strengthen the assembly. Variation in actin filaments on different micropatterns can be explained by the maturation of FAs in micropatterned hMSCs. Actin filaments are connected to FAs and assemble in the radial and concentric directions when cells are cultured in circular micropatterns [49, 50]. The

mature FAs on straightforward micropatterns (A1-A4) became larger when the adhesion area increased from A1 to A4. The length of the mature FAs was high when the swirling angle was 30° and 90°. However, the length of mature FAs decreased when the swirling angle was 60°. The decreased length of FAs could explain the vague assembly of actin filaments at the peripheral regions when the swirling angle was 60°.

Young's modulus reflected the assembled structures of actin filaments. A stronger assembly of cytoskeletal structures showed a higher Young's modulus (Figure 5.5b). The hMSCs on micropatterns with a swirling angle of 60° had lower assembly of the cytoskeleton and a lower Young's modulus than other micropatterns. However, the cells on the micropatterns had the same cell adhesion areas and swirling angles, while different rotation directions resulted in the same FA formation, cytoskeletal structure and Young's modulus. Disturbance of actin filament assembly and a decrease in the Young's modulus of the micropatterned cells treated with actin inhibitor suggested a strong correlation between cytoskeletal structures and cell stiffness.

In the process of cellular uptake, the cell membrane serves as a natural boundary to hinder the endocytosis and exocytosis of exotic particles [51]. The cell membrane will allow uptake of cationic liposome/microparticle complexes [52]. In this study, FITC-labeled microspheres were used to replace exogenous DNA and to determine the cellular uptake capacity of micropattern-induced chiral cells. The results strongly agreed with those of gene transfection. Several studies have revealed the close relationship between cytoskeletal structures and cellular uptake capacity [53-55]. It is hypothesized that the nonspecific but high-efficiency internalization of microspheres may be partially affected by clathrin-mediated vesicles due to the unique cytoskeletal distribution [56, 57]. The formation of the cytoskeleton is tightly related to the internalization of exogenous particles. The cells on micropatterns with good organization of actin filaments showed high uptake of exogenous microparticles, therefore increasing the uptake of exogenous genes for transfection.

DNA synthesis is another important factor for efficient gene transfection [58, 59]. Extracellular signals through FAs, the cytoskeleton and related pathways are transduced to the cell nucleus for DNA synthesis [60]. Some studies have reported that cells can translate their cytoskeletal mechanics into nuclei to control the expression of genes through actin-induced mechanotransduction pathways [61-65]. The well-organized structures of actin filaments of hMSCs on the large adhesion area micropatterns and micropatterns with swirling angles of 30° and 90° could transduce strong signals to induce high DNA synthesis activity and therefore the expression of transfected exogenous genes. Disturbance of actin filament assembly decreased the cellular uptake capacity and DNA synthesis, therefore decreasing gene transfection efficiency (Figure 5.10).

Through the use of the chiral micropatterns of fibronectin, chiral FAs were formed, and the cells organized chiral cytoskeletons. The right-handed or left-handed chirality of hMSCs did not show a significant influence on the transfection of exogeneous genes. However, the swirling angle of the fibronectin stripes had some effect on gene transfection. Furthermore, the total fibronectin area had a major effect on gene transfection efficiency. The influence of adhesion area (total fibronectin area), chirality and swirling angle on gene transfection should be correlated with the formation and maturation of FAs, interactions between FAs and actin filaments and activation of mechanotransduction signals. The cytoskeletal structure affects cellular uptake, and activation of mechanotransduction signals could increase DNA synthesis. The synergistic effects of cellular uptake and DNA synthesis should result in high efficiency gene transfection.

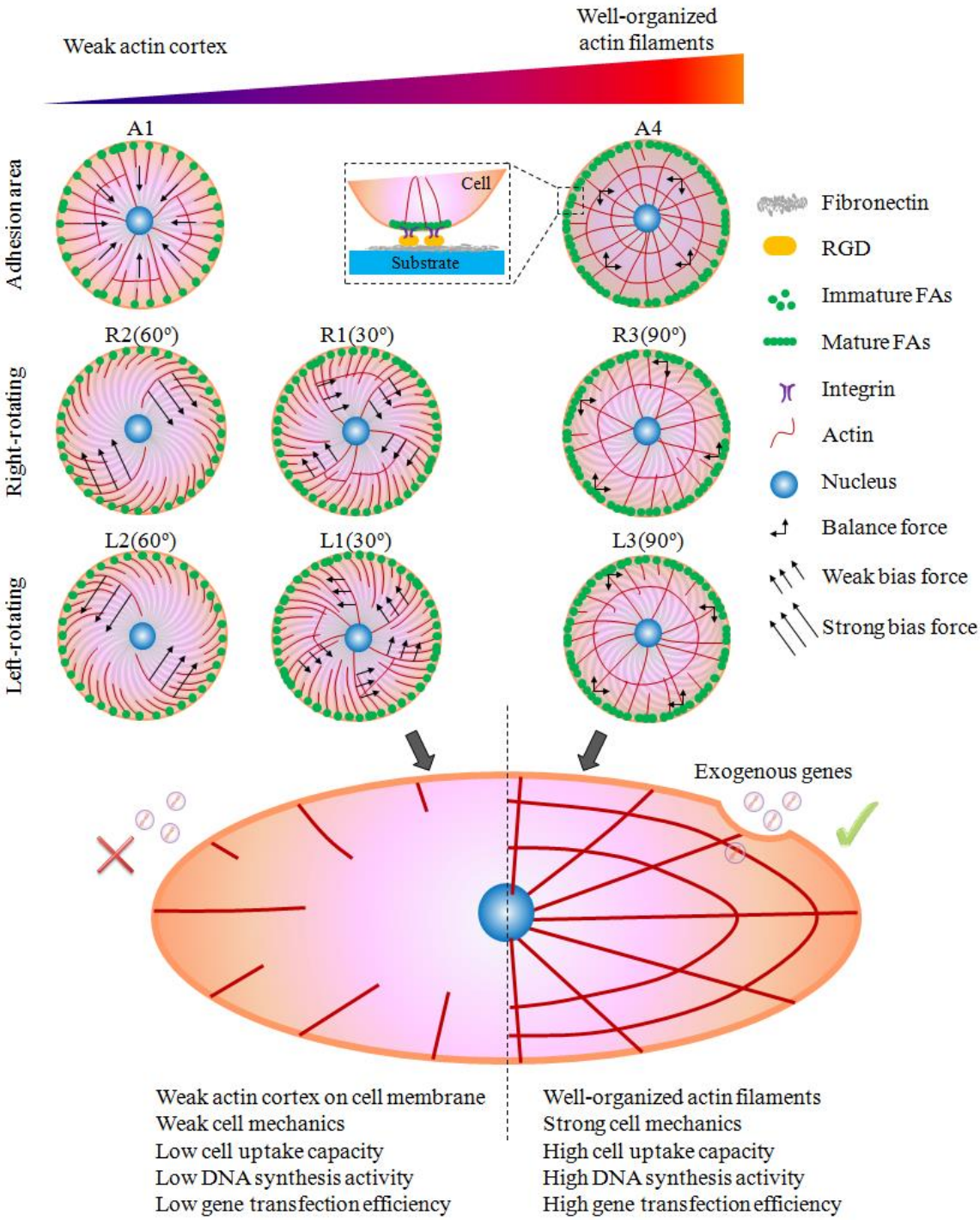

Figure 5.10 Potential mechanism of straightforward, right-handed and left-handed swirling stripes to affect gene transfection in micropatterned cells. hMSCs on fibronectin-coated vertical stripes (A1-A3) and right/left rotating stripes (R1 and R2, L1 and L2) formed immature FAs and weak actin cortex to induce radially bias force on vertical stripes and right/left bias force on right/left rotating stripes. These bias forces induced weak cell stiffness, low cell uptake capacity and low DNA synthesis activity, therefore resulting in low gene transfection efficiency. On the other hand, the cells on A4 micropatterns and R3/L3 micropatterns with swirling angle of 90° formed mature FAs and well-organized actin filaments to induce balance force. Therefore, the balance force stimulated strong cell stiffness, high cell uptake capacity and high DNA synthesis activity to generate high gene transfection efficiency.

5.6 Conclusions

Chiral micropatterns of fibronectin with straight stripes but different cell adhesion areas or the same adhesion areas but different swirling angles were prepared and used to control the chirality of hMSCs. The influence of cell chirality on exogenous gene transfection was investigated on the micropatterns. The transfection efficiency was enhanced with increasing cell adhesion area. The gene transfection efficiency of hMSCs on micropatterns with swirling angles of 0°, 30° and 90° was at the same level, which was significantly higher than that on micropatterns with swirling angles of 60°. The swirling direction did not affect the gene transfection efficiency. The different transfection efficiencies were associated with FA formation, cytoskeletal mechanics, cellular uptake of exogenous genes and DNA synthesis. The results may help elucidate the relationship of cell chirality and cell functions and provide useful information for gene therapy.

5.7 References

[1] M. Inaki, T. Sasamura, K. Matsuno, Cell chirality drives left-right asymmetric morphogenesis, Frontiers in Cell and Developmental Biology 6 (2018) 24.
[2] P. Ray, A. S. Chin, K. E. Worley, E. W. Kathryn, J. Fan, G. Kaur, M. Wu, L.Q. Wan, Intrinsic cellular chirality regulates left-right symmetry breaking during cardiac looping, Proceedings of the National Academy of Sciences of the United States of America 115 (2018) E11568-E11577.
[3] L. Q. Wan, K. Ronaldson, M. Guirguis, G. Vunjak-Novakovic, Micropatterning of cells reveals chiral morphogenesis, Stem Cell Research & Therapy 4 (2013) 24.
[4] M. Inaki, J. Liu, K. Matsuno, Cell chirality: its origin and roles in left-right asymmetric development, Philosophical Transactions of the Royal Society B 371 (2016) 20150403.
[5] L. Q. Wan, A. S. Chin, K. E. Worley, P. Ray, Cell chirality: emergence of asymmetry from cell culture, Philosophical Transactions of the Royal Society B 371 (2016) 20150413.
[6] K. Taniguchi, R. Maeda, T. Ando, T. Okumura, N. Nakazawa, R. Hatori, M. Nakamura, S. Hozumi, H. Fujiwara, K. Matsuno, Chirality in planar cell shape contributes to left-right asymmetric epithelial morphogenesis, Science 333 (2011) 339-341.
[7] H. Shi, D. A. Quint, G. M. Grason, A. Gopinathan, K. C. Huang, Chiral twisting in a bacterial cytoskeletal polymer affects filament size and orientation, Nature Communications 11 (2020) 1408.
[8] M. M. C. Tortora, G. Mishra, D. Prešern, J. P. K. Doye, Chiral shape fluctuations and the origin of chirality in cholesteric phases of DNA origamis, Science Advances 6 (2020) eaaw8331.
[9] X. Zhao, L. Xu, M. Sun, W. Ma, X. Wu, C. Xu, H. Kuang, Tuning the interactions between chiral plasmonic films and living cells, Nature Communications 8 (2017) 2007.
[10] Y. H. Tee, T. Shemesh, V. Thiagarajan, R. F. Hariadi, K. L. Anderson, C. Page, N. Volkmann, D. Hanein, S. Sivaramakrishnan, M. M. Kozlov, A. D. Bershadsky, Cellular chirality arising from the self-organization of the actin cytoskeleton, Nature Cell Biology 17 (2015) 445-457.
[11] J. Fan, P. Ray, Y. W. Lu, G. Kaur, J. J. Schwarz, L. Q. Wan, Cell chirality regulates intercellular junctions and endothelial permeability, Science Advances 4 (2018) eaat2111.
[12] X. Yao, J. Ding, Effects of microstripe geometry on guided cell migration, ACS Applied Materials & Interfaces 12 (2020) 27971-27983.
[13] A. S. Chin, K. E. Worley, P. Ray, G. Kaur, J. Fan, L. Q. Wan, Epithelial cell chirality revealed by three-dimensional spontaneous rotation, Proceedings of the National Academy of Sciences of the United

States of America 115 (2018) 12188-12193.
[14] E. Yavin, Z. Yavin, Attachment and culture of dissociated cells from rat embryo cerebral hemispheres on polylysine-coated surface, Journal of Cell Biology 62 (1974) 540-546.
[15] D. Hanein, B. Geiger, L. Addadi, Differential adhesion of cells to enantiomorphous crystal surfaces, Science 263 (1994) 1413-1416.
[16] T. L. Sun, D. Han, K. Rhemann, L. F. Chi, H. Fuchs, Stereospecific interaction between immune cells and chiral surfaces, Journal of the American Chemical Society 129 (2007) 1496-1497.
[17] X. Yao, Y. Hu, B. Cao, R. Peng, J. Ding, Effects of surface molecular chirality on adhesion and differentiation of stem cells, Biomaterials 34 (2013) 9001-9009.
[18] Y. Wei, S. Jiang, M. Si, X. Zhang, J. Liu, Z. Wang, C. Cao, J. Huang, H. Huang, L. Chen, S. Wang, C. Feng, X. Deng, L. Jiang, Chirality controls mesenchymal stem cell lineage diversification through mechanoresponses, Advanced Materials 31 (2019) e1900582.
[19] X. Zhao, S. Q. Zang, X. Chen, Stereospecific interactions between chiral inorganic nanomaterials and biological systems, Chemical Society Reviews 49 (2020) 2481-2503.
[20] Y. Ma, L. Shi, M. Zhou, B. Li, Z. Chen, L. Wu, Cell adhesion and proliferation in chiral pores triggered by polyoxometalates, Chemical Communications 55 (2019) 7001-7004.
[21] X. Wang, H. Gan, T. L. Sun, Chiral design for polymeric biointerface: the influence of surface chirality on protein adsorption, Advanced Functional Materials 21 (2011) 3276-3281.
[22] M. Zhang, G. Y. Qing, T. L. Sun, Chiral biointerface materials, Chemical Society Reviews 41 (2012) 1972-1984.
[23] Q. Chen, J. Zhou, Q. Han, Y. H. Wang, Y. Z. Fu, The selective adsorption of human serum albumin on N-isobutyryl-cysteine enantiomers modified chiral surfaces, Biochemical Engineering Journal 69 (2012) 155-158.
[24] F. Zhou, L. Yuan, D. Li, H. Huang, T. L. Sun, H. Chen, Cell adhesion on chiral surface: the role of protein adsorption, Colloids and Surfaces B: Biointerfaces 90 (2012) 97-101.
[25] L. Zhang, Q. Jin, K. Lv, L. Qin, M. Liu, Enantioselective recognition of a fluorescence-labeled phenylalanine by self-assembled chiral nanostructures, Chemical Communications 51 (2015) 4234-4236.
[26] G. Nardone, J. O. L. Cruz, J. Vrbsky, C. Martini, J. Pribyl, P. Skládal, M. Pešl, G. Caluori, S. Pagliari, F. Martino, Z. Maceckova, M. Hajduch, A. Sanz-Garcia, N. M. Pugno, G. B. Stokin, G. Forte, YAP regulates cell mechanics by controlling focal adhesion assembly, Nature Communications 8 (2017) 15321.
[27] S. Utsunomiya, S. Sakamura, T. Sasamura, T. Ishibashi, C. Maeda, M. Inaki, K. Matsuno, Cells with broken left-right symmetry: roles of intrinsic cell chirality in left-right asymmetric epithelial morphogenesis, Symmetry 11 (2019) 505.
[28] K. Lv, L. Zhang, W. Lu, M. Liu, Control of supramolecular chirality of nanofibers and its effect on protein adhesion, ACS Applied Materials & Interfaces 6 (2014) 18878-18884.
[29] W. Song, H. Lu, N. Kawazoe, G. Chen, Gradient patterning and differentiation of mesenchymal stem cells on micropatterned polymer surface, Journal of Bioactive and Compatible Polymers 26 (2011) 242-256.
[30] X. Wang, X. Hu, N. Kawazoe, Y. Yang, G. Chen, Manipulating cell nanomechanics using micropatterns, Advanced Functional Materials 26 (2016) 7634-7643.
[31] X. Wang, T. Nakamoto, I. D. Molak, N. Kawazoe, G. Chen, Regulating the stemness of mesenchymal stem cells by tuning micropattern features, Journal of Materials Chemistry B 4 (2016) 37-45.
[32] L. Li, H. Clevers, Coexistence of quiescent and active adult stem cells in mammals, Science 327 (2010) 542-545.
[33] D. Falconnet, G. Csucs, H. M. Grandin, M. Textor, Surface engineering approaches to micropattern surfaces for cell-based assays, Biomaterials 27 (2006) 3044-3063.

[34] Y. Yang, X. Wang, Y. Wang, X. Hu, N. Kawazoe, Y. Yang, G. Chen, Influence of cell spreading area on the osteogenic commitment and phenotype maintenance of mesenchymal stem cells, Scientific Reports 9 (2019) 6891.
[35] Y. Yang, X. Wang, T. C. Huang, X. Hu, N. Kawazoe, W. B. Tsai, Y. Yang, G. Chen, Regulation of mesenchymal stem cell functions by micro-nano hybrid patterned surfaces, Journal of Materials Chemistry B 6 (2018) 5424-5434.
[36] B. Stutchbury, P. Atherton, R. Tsang, D. Y. Wang, Distinct focal adhesion protein modules control different aspects of mechanotransduction, Journal of Cell Science 130 (2017) 1612-1624.
[37]A. Elosegui-Artola, R. Oria, Y. Chen, A. Kosmalska, C. Pérez-González, N. Castro, C. Zhu, X. Trepat, P. Roca-Cusachs, Mechanical regulation of a molecular clutch defines force transmission and transduction in response to matrix rigidity, Nature Cell Biolohy 18 (2016) 540-548.
[38] D. W. Dumbauld, T. T. Lee, A. Singh, J. Scrimgeour, C. A. Gersbach, E. A. Zamir, J. Fu, C. S. Chen, J. E. Curtis, S. W. Craig, A. J. García, How vinculin regulates force transmission, Proceedings of the National Academy of Sciences of the United States of America 110 (2013) 9788-9793.
[39] J. K. Kim, A. Louhghalam, G. Lee, B. W. Schafer, D. Wirtz, D. H. Kim, Nuclear lamin A/C harnesses the perinuclear apical actin cables to protect nuclear morphology, Nature Communications 8 (2017) 2123.
[40] S. K. Mitra, D. A. Hanson, D. D. Schlaepfer, Focal adhesion kinase: in command and control of cell motility, Nature Reviews Molecular Cell Biology 6 (2005) 56-68.
[41] Q. Zhou, J. Chen, Y. Luan, P. A. Vainikka, S. Thallmair, S. J. Marrink, B. L. Feringa, P. Rijn, Unidirectional rotating molecular motors dynamically interact with adsorbed proteins to direct the fate of mesenchymal stem cells, Science Advances 6 (2020) eaay2756.
[42] L. B. Case, M. A. Baird, G. Shtengel, S. L. Campbell, H. F. Hess, M. W. Davidson, C. M. Waterman, Molecular mechanism of vinculin activation and nanoscale spatial organization in focal adhesions, Nature Cell Biology 17 (2015) 880-892.
[43] D. A. Fletcher, R. D. Mullins, Cell mechanics and the cytoskeleton, Nature 463 (2010) 485-492.
[44] N. Mandriota, C. Friedsam, J. A. Jones-Molina, K. V. Tatem, D. E. Ingber, O. Sahin, Cellular nanoscale stiffness patterns governed by intracellular forces, Nature Materials 18 (2019) 1071-1077.
[45] R. P. Martins, J. D. Finan, F. Guilak, D. A. Lee, Mechanical regulation of nuclear structure and function, Annual Review of Biomedical Engineering 14 (2012) 431-455.
[46] K. Bhadriraju, L. K. Hansen, Extracellular matrix- and cytoskeleton-dependent changes in cell shape and stiffness, Experimental Cell Research 278 (2002) 92-100.
[47] Y. Yang, X. Wang, X. Hu, N. Kawazoe, Y. Yang, G. Chen, Influence of cell morphology on mesenchymal stem cell transfection, ACS Applied Materials & Interfaces 11 (2019) 1932-1941.
[48] T. Hohmann, F. Dehghani, The cytoskeleton-a complex interacting meshwork, Cells 8 (2019) 362.
[49] T. Vallenius, Actin stress fibers subtypes in mesenchymal-migrating cells, Open Biology 3 (2013) 130001.
[50] C. Y. Tay, Y. L. Wu, P. Cai, N. S. Tan, S. S. Venkatraman, X. Chen, L. P. Tan, Bio-inspired micropatterned hydrogel to direct and deconstruct hierarchical processing of geometry-force signals by human mesenchymal stem cells during smooth muscle cell differentiation, NPG Asia Materials 7 (2015) e199.
[51] G. J. Doherty, H. T. McMahon, Mechanisms of endocytosis, Annual Review of Biochemistry 78 (2009) 857-902.
[52] J. Lin, A. Alexander-Katz, Cell membranes open “doors” for cationic nanoparticles/biomolecules: insights into uptake kinetics, ACS Nano 7 (2013) 10799-10808.
[53] F. Zhao, Y. Zhao, Y. Liu, X. Chang, C. Chen, Y. Zhao, Cellular uptake, intracellular trafficking, and

cytotoxicity of nanomaterials, Small 7 (2011) 1322-1337.
[54] X. Wang, X. Hu, J. Li, A. C. M. Russe, N. Kawazoe, Y. Yang, G. Chen, Influence of cell size on cellular uptake of gold nanoparticles, Biomaterials Science 4 (2016) 970-978.
[55] X. Lin, N. Zhao, P. Yan, H. Hu, F. J. Xu, The shape and size effects of polycation functionalized silica nanoparticles on gene transfection, Acta Biomaterialia 11 (2015) 381-392.
[56] M. Gupta, B. R. Sarangi, J. Deschamps, Y. Nematbakhsh, A. Callan-Jones, F. Margadant, R. M. Mège, C. T. Lim, R. Voituriez, B. Ladoux, Adaptive rheology and ordering of cell cytoskeleton govern matrix rigidity sensing, Nature Communications 6 (2015) 7525.
[57] M. Kaksonen, C. P. Toret, D. G. Drubin, Harnessing actin dynamics for clathrin-mediated endocytosis, Nature Reviews Molecular Cell Biology 7 (2006) 404-414.
[58] S. K. Misra, P. Moitra, P. Kondaiah, S. Bhattachary, Co-liposomes having anisamide tagged lipid and cholesteryl tryptophan trigger enhanced gene transfection in sigma receptor positive cells, Colloids and Surfaces B: Biointerfaces 142 (2016) 130-140.
[59] Y. Gluzman, SV40-transformed simian cells support the replication of early SV40 mutants, Cell 23 (1981) 175-182.
[60] C. Uhler, G. V. Shivashankar, Regulation of genome organization and gene expression by nuclear mechanotransduction, Nature Reviews Molecular Cell Biology 18 (2017) 717-727.
[61] A. R. Harris, P. Jreij, D. A. Fletcher, Mechanotransduction by the actin cytoskeleton: converting mechanical stimuli into biochemical signals, Annual Review of Biophysics 47 (2018) 617-631.
[62] G. Halder, S. Dupont, S. Piccolo, Transduction of mechanical and cytoskeletal cues by YAP and TAZ, Nature Reviews Molecular Cell Biology 13 (2012) 591-600.
[63] K. Anselme, N. T. Wakhloo, P. Rougerie, L. Pieuchot, Role of the nucleus as a sensor of cell environment topography, Advanced Healthcare Materials 7 (2018) 1701154.
[64] E. Infante, A. Stannard, S. J. Board, P. Rico-Lastres, E. Rostkova, A. E. M. Beedle, A. Lezamiz, Y. J. Wang, S. G. Breen, F. Panagaki, V. S. Rajan, C. Shanahan, P. Roca-Cusachs, S. Garcia-Manyes, The mechanical stability of proteins regulates their translocation rate into the cell nucleus, Nature Physics 15 (2019) 973-981.
[65] A. J. Ridley, M. A. Schwartz, K. Burridge, R. A. Firtel, M. H. Ginsberg, G. Borisy, J. T. Parsons, A. R. Horwitz, Cell migration: integrating signals from front to back, Science 302 (2003) 1704-1709.

Chapter 6

Conclusions

This dissertation describes the influence of cell morphology on gene transfection of hMSCs by using micropatterned surfaces. The micropatterns were prepared by micropatterning the photoreactive PVA on TCPS plates through photolithography. hMSCs were cultured on the micropatterns to precisely control their various cell morphologies, including cell density, cell-cell interaction, cell size, cell shape, cell elongation, cell adhesion area, spreading area and cytoskeleton chirality. Their influences on transfection of exogenous genes were investigated. Furthermore, the correlations between gene transfection and cellular uptake, DNA synthesis, focal adhesion formation, cytoskeletal mechanics and mechanotranduction signal activation was elucidated.

In chapter 1, a general introduction is stated to introduce cellular uptake pathways of gene transfection and gene expression in cells. Current factors including different cell lines, various gene carrier materials and cellular microenvironment are presented to disclose the influence of these factors on gene transfection. In addition, applications of micropatterning techniques in gene transfection are also summarized. Finally, the motivation, objectives and outline are made clear.

In chapter 2, the micropatterned surfaces with different square densities were prepared on TCPS discs through photolithography. Cell density was controlled by the micropatterns to study the influence of cell density on gene transfection of hMSCs. Transfection efficiency showed a first-increasing and then-decreasing tendency with increasing cell density. The different influence of cell density on transfection efficiency was correlated with its influence on cellular uptake capacity and DNA synthesis. Insufficient cell-cell interaction at a low cell density and too strong cell-cell interaction at a high cell density was not preferable for gene transfection. A moderate cell density had appropriate cell-cell interaction to facilitate gene transfection.

In chapter 3, the influences of cell size, shape and elongation on gene transfection were elucidated. Transfection efficiency was enhanced in well-spread and elongated cells. Cell size had a dominant influence on gene transfection, independent of cell shape. Elongation could increase the transfection efficiency in large cells but not small cells. High transfection efficiency was strongly correlated with high cellular uptake and DNA synthesis through the regulation of cytoskeletal structures and cell mechanics.

In chapter 4, the influence of cell adhesion and spreading areas on gene transfection was investigated. Cell adhesion area showed dominant influence on gene transfection, while cell spreading area did not affect

gene transfection. Uptake of microparticles and BrdU staining showed that both cellular uptake capacity and DNA synthesis increased with cell adhesion area, but were not affected by cell spreading area. The high transfection efficiency of cells with large adhesion area should be due to their high uptake capacity and DNA synthesis activity through FAs formation, cytoskeletal mechanics and YAP/TAZ nuclear localization.

In chapter 5, the chirality of focal adhesions and cytoskeleton on gene transfection was investigated. The chiral micropatterns induced the formation of chiral focal adhesions and chiral cytoskeletal structures. Gene transfection efficiency was enhanced with increasing adhesion area, while hMSCs on left-handed and right-handed swirling micropatterns showed the same level of gene transfection. When the swirling angle was changed from 0°, 30°, and 60° to 90°, the gene transfection efficiency at a swirling angle of 60° was the lowest. The influence of cell chirality on gene transfection was associated with cellular uptake capacity, DNA synthesis and cytoskeletal mechanics.

In conclusion, the various micropatterns were prepared to disclose the relationship between cell morphology and exogenous gene transfection. Cell morphology, including cell density, cell-cell interaction, cell size, cell shape, cell elongation, cell adhesion and spreading area and cytoskeleton chirality was well controlled. Gene transfection efficiency was enhanced in moderate cell density and in single cells with large adhesion area and elongation, while not affected by cell shape, spreading area and chirality. The different influence was due to the regulation of cellular uptake, DNA synthesis, focal adhesion (FA) formation, cytoskeletal mechanics (actin, actinin and myosin) and mechanotranduction signal activation (YAP/TAZ). These results suggest the importance of cell density and morphology in exogenous gene transfection and should provide useful information for manipulation of cell functions in gene therapy, protein modification and cell reprogramming.

List of publications

1. **Yongtao Wang**, Yingjun Yang, Xinlong Wang, Toru Yoshitomi, Naoki Kawazoe, Yingnan Yang, Guoping Chen. Micropattern-controlled chirality of focal adhesions regulates the cytoskeletal arrangement and gene transfection of mesenchymal stem cells. Biomaterials, 2021, 271, 120751.

2. **Yongtao Wang**, Yingjun Yang, Xinlong Wang, Naoki Kawazoe, Yingnan Yang, Guoping Chen. The varied influences of cell adhesion and spreading on gene transfection of mesenchymal stem cells on a micropatterned substrate. Acta Biomaterialia, 2021, 125, 100-111.

3. **Yongtao Wang**, Yingjun Yang, Toru Yoshitomi, Naoki Kawazoe, Yingnan Yang, Guoping Chen. Regulation of gene transfection by cell size, shape and elongation on micropatterned surfaces. Journal of Materials Chemistry B, 2021, 9, 4329-4339.

4. Yingjun Yang, Xinlong Wang, **Yongtao Wang**, Xiaohong Hu, Naoki Kawazoe, Yingnan Yang, Guoping Chen. Influence of cell spreading area on the osteogenic commitment and phenotype maintenance of mesenchymal stem cells. Scientific Reports, 2019, 9(1), 1-11.

5. Kyubae Lee, Yazhou Chen, Xiaomeng Li, **Yongtao Wang**, Naoki Kawazoe, Yingnan Yang, Guoping Chen. Solution viscosity regulates chondrocyte proliferation and phenotype during 3D culture. Journal of Materials Chemistry B, 2019, 7(48), 7713-7722.

6. **Yongtao Wang**, Toru Yoshitomi, Naoki Kawazoe, Yingnan Yang, Guoping Chen. Cell density and interaction controlled by micropatterned surfaces and their influences on gene transfection of mesenchymal stem cells. To be submitted.

Acknowledgements

At the end of my PhD dissertation, I sincerecely give my appreciations to all those who have supported and helped me during my doctoral project.

First, I would like to give my great gratitude to Professor Guoping Chen. As my PhD supervisor, Professor Chen always guided me selflessly. He guided my research activity with his extensive knowledge and kind patience. His insightful feedback and knowledge always inspired me to improve myself to reach a higher research level. Under his kind guidance, I learnt how to exquisitely choose the research topics, how to reasonably design the experiments and how to logically write scientific research papers. Professor Chen also supported me to attend some international conferences. He really wanted to enhance my research level. Professor Chen helped me a lot not only in my research activity but also in my daily life. He always took care of my health and safety. He helped us to stay safe and healthy from some disasters, in particular, COVID-19, typhoons and earthquakes in Japan. It is my great honor to complete my PhD thesis under the guidance of Professor Chen.

I also want to give my sincere appreciations to Dr. Naoki Kawazoe sensei and Dr. Toru Yoshitomi sensei for their kind guidance and help during my PhD project. Their professional research knowledge and skills helped me a lot. At the beginning, I spoke with Kawazoe sensei to improve my English skills and discussed my research topic with him. He always gave me some valuable suggestions. I also discussed some new research ideas with Yoshitomi sensei. His positive attitudes and knowledge always promoted me a lot. I really thank them for their suggestions and comments in my research.

I would like to thank our former group members for their help. They are Dr. Xinlong Wang, Dr. Yingjun Yang, Dr. Xiuhui Wang, Dr. Yazhou Chen and Dr. Kyubae Lee. Furthermore, I want to give my thanks to all members in Tissue Regeneration Materials Group for their patient support and help. They are Ms. Yan Xie, Ms. Linawati Sutrisno, Mr. Huajian Chen, Mr. Jing Zheng and Mr. Rui Sun.

I would like to give my sincere appreciation to Mrs. Haruyo Akiyama and Mrs. Akiko Ito. Akiyama san helped me to finish many documents related with University of Tsukuba and NIMS. Ito san always assisted me to manage our lab and order some reagents. They made my life in Japan easier and enjoyable.

I also want to thank the professors of my thesis committee. They are Professor Yukio Nagasaki, Professor Kohsaku Kawakami and Professor Tetsushi Taguchi. During my PhD defense, their valuable comments, great encouragement and meaningful suggestions helped me to improve my research and thesis.

Finally, I give my thanks and love to my family members. Their supports and love let my life more meaningful.

Thank you very much.